2011-04-26

Simultaneous Measurement of Oxygen and Carbon Monoxide Saturation using Pulse Oximeters

Shanthi Vasudevan
Worcester Polytechnic Institute

Simultaneous Measurement of Oxygen and Carbon Monoxide Saturation using Pulse Oximeters

A thesis

Submitted to the Faculty

of the

WORCESTER POLYTECHNIC INSTITUTE

in partial fulfillment of the requirements for the

Degree of Master of Science

By

Shanthi Vasudevan

Shanthi Vasudevan

Date: April 22, 2011

Approved:

Professor Yitzhak Mendelson, Major Advisor
Department of Biomedical Engineering

Professor Christopher Lambert, Committee Member
Bioengineering Institute

Professor Ki Chon, Committee Member
Department of Biomedical Engineering

Abstract

The ability of pulse oximeters to measure carboxyhemoglobin (HbCO) in blood or measure accurate values of oxygen saturation (SpO_2) in the presence of elevated levels of HbCO is an important advantage because high exposure to carbon monoxide (CO) can be fatal or results in permanent neurological damage. The aim of my research was to develop an algorithm that would measure SpO_2 and SpCO simultaneously using a pulse oximeter. Several specific wavelengths at which changes in SpCO and SpO_2 can be measured with high sensitivity and specificity were identified. The choice of these wavelengths was experimentally verified utilizing an *in-vitro* set up. Preliminary results using our algorithm showed an accuracy of -1.1 to +2.7% [±1.96 SD] for SpO_2 ranging between 70-100%, and -2 to 3.3% [±1.96 SD] for SpCO ranging between 30% with a specificity of 83.3% and a sensitivity of 100% for SpO_2 and SpCO, respectively.

Acknowledgements

I wish to convey my deepest appreciation to Prof. Mendelson for his expertise and assistance throughout the course of my work.

I would like to thank Prof. Lambert and Prof. Chon for their valuable suggestions and many helpful discussions.

I also wish to express my deepest gratitude to my family for their constant support and love.

This work was supported by the U.S. Army Medical Research and Material Command under Contracts No. W81XWH-07-2-0106 and W81XWH-10-1-0529. The views, opinions and/or findings are those of the author and should not be construed as an official Department of the Army position, policy or decision unless so designated by other documentation.

Table of contents

List of figures

List of tables

List of abbreviations

Hb	Hemoglobin
HbO_2	Oxyhemoglobin
HbCO	Carboxyhemoglobin
MetHb	Methemoglobin
THb	Total Hemoglobin
SpO_2	Oxygen saturation
SpCO	Carbon monoxide saturation
O_2	Oxygen
CO	Carbon monoxide
PPG	Photoplethysmogram
AVF	Armored fighting vehicle
LED	Light emitting diode

Chapter 1. Physiological and clinical significance of oxygen and carbon monoxide saturation

1.1. Oxygen saturation and its significance

Oxygen (O_2) is essential to human life. Cells and tissues in the body require oxygen to survive. Any reduction in the supply of this vital nutrient causes irreversible cell damage or even death. O_2 is not particularly soluble in blood [1]. Normally, only about 3% of the total oxygen carried is in a dissolved state while about 97% of the oxygen transported to the tissues is carried by hemoglobin (Hb). Therefore, Hb is solely responsible for the bulk of O_2 transportation to tissues [2].

Hb is an iron-containing protein that is made of amino acids strung together forming polypeptide chains. Each hemoglobin molecule consists of a heme component and a globin component. The globin unit is made up of four polypeptide chains. In commonly occurring forms of adult Hb, two of the polypeptide chains are called alpha chains and the other two are called beta chains. Each of these chains has one heme group which has an iron atom at the center of a porphyrin ring. One polypeptide chain with a heme group is a subunit of Hb. Hb has four such subunits, each with an iron atom [3]. These iron atoms in the heme group are the binding sites for molecules. Each oxygen molecule combines with one iron atom loosely and reversibly. Hence, four O_2 molecules can bind to one molecule of Hb [4]. For one polypeptide chain the reaction between Hb and O_2 can be shown as

$$Hb + O_2 \leftrightarrow HbO_2 \qquad (1.1)$$

Hb with oxygen combined to it is called oxyhemoglobin (HbO_2), while Hb without any oxygen bound to it is called deoxyhemoglobin or reduced Hb (Hb). Normal human blood contains 15 g Hb/ 100 ml blood. Each gram of Hb can bind with about 1.34 ml of O_2 resulting in an oxygen

capacity of 20ml/100 ml of blood [5]. Oxygen saturation in blood is defined as the fraction of Hb molecules that are bound to O_2. Oxygen saturation can be defined in terms of functional oxygen saturation or as fractional oxygen saturation. Fractional oxygen saturation is defined as the ratio of HbO_2 concentration to the total concentration of Hb. Functional oxygen saturation is defined as the ratio of HbO_2 concentration to the sum of the concentrations of Hb and HbO_2. Pulse oximeters measure functional oxygen saturation (SpO_2) given by Eq. 1.2.

$$SpO_2 = \frac{HbO_2}{HbO_2+Hb} \times 100 \qquad (1.2)$$

When the oxygen saturation is at 100%, there are no free binding sites available.

SpO_2 measurement is commonly used in anesthesia, neonatology, pediatric care, cardio-pulmonary resuscitations and intensive care. Using pulse oximeters, desaturation in anesthetized patients can be identified in real time before irreversible tissue death occurs. It is especially useful in preventing hypoxemia that occurs due to diminished alveolar ventilation during anesthesia [6]. Pulse oximeters are also used as a standard diagnostic tool in intensive care and emergency room.

1.2. Physiological and clinical effects of CO

The most important physiological effect of CO exposure is its preferential binding with Hb. The binding affinity of CO is ~230 times the affinity O_2 has for Hb. Hence, when CO exposure occurs, Hb binds preferentially with CO resulting in the formation of carboxyhemoglobin (HbCO) [7]. The effect of this preferential binding is the shift in the Hb dissociation curve to the left (Fig. 1.1) [8].

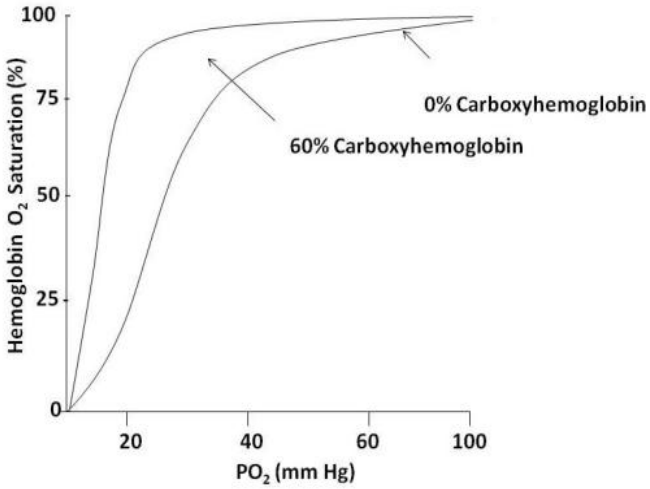

Fig. 1.1. O_2-CO-Hb dissociation curve [7].

From Fig. 1.1, at 0% HbCO, in the region between 0-60 mmHg, a large amount of O_2 can leave the Hb with only a slight decrease in PO_2, thus releasing O_2 to the cells in the body. On the contrary, in the flattened region above 60 mmHg, oxygen saturation is consistently high. This enables Hb to bind to O_2 in the lungs where PO_2 is high [2]. Shifting of the curve to the right indicates a decrease in the affinity of Hb to O_2, whereas shifting of the curve to the left indicates an increase in affinity. In the absence of HbCO, the shifting of the curve to left is due to changes in the molecular structure of Hb caused by Bohr's effect [4]. As mentioned earlier, in the presence of HbCO, the preferential binding of Hb with CO causes the curve to shift to the left. Shifting of the curve towards the left, indicating the increase in the affinity of Hb for O_2, implies that the tissues will have difficulty obtaining O_2 from the blood. Thus, as the concentration of HbCO increases and the concentration of HbO_2 decreases, cells are deprived of normal oxygen delivery resulting in hypoxia. Observations and studies in literature report that 3 parts of CO per 10,000 parts ambient air will cause fatalities within 20 minutes.

In a clinical environment, both oxygen and carbon monoxide saturation in blood are significant parameters. When CO exposure occurs, pulse oximeters are unable to detect the

presence of HbCO and also lose the ability to measure SpO_2 accurately. This is an important limitation because CO, a colorless, odorless gas, is the leading cause of poisoning deaths in the United States. It is believed to be responsible for more than half the poisoning deaths worldwide. Around 5000 to 6000 people die every year in the United States alone due to CO exposure. CO exposures at home or workplaces can occur due to improper maintenance of heaters, indoor air conditioners, gas stoves, and vehicle exhaust. While firefighters are susceptible to CO poisoning due to smoke inhalation, army field exposures commonly occur in tanks, troop compartments of armored vehicles, enclosed communication vans, indoor testing and firing of weapons [7]. Miners are another group of people who are at the risk of CO poisoning. Several accidents resulting in fatalities of miners have been reported due to CO exposure, caused by detonations and explosions in the confines of a narrow shaft [8]. Due to lack of ventilation, the miners will be exposed to high concentrations of CO in within a short span that results in fatalities. There have also been reports of CO poisoning cases in houses constructed near old shaft mines [9]. Apparent health effects of CO exposure is reported to occur at a concentration of approximately 20% and higher. Early cardiovascular effect caused by CO poisoning is tachycardia in response to hypoxia [10-11]. At higher concentrations hypotension, dysrhythmia, ischemia, infarction and cases of cardiac arrest have been reported [7]. Therefore, diagnosing CO poisoning before it causes severe tissue damage becomes critical. If pulse oximeters could monitor HbCO levels noninvasively, patients with CO poisoning may be treated immediately, thus preventing further harm. Also, in case of exposure during combat or fire, medics might be able to perform remote triage from a safe location without being exposed to CO.

Diagnosing CO poisoning at early stages is the key because Hb-CO binding is a reversible chemical reaction. After dissociating from CO, Hb does not exhibit any impairment in its oxygen

carrying capacity [12]. Hence, if patients who have been exposed to CO poisoning can be treated immediately, damage to cells and tissues can be prevented.

Chapter 2. Background on pulse oximetry

Pulse oximeters measure SpO_2 in blood noninvasively using the time-varying photoplethysmographic signal (PPG) caused by variation in the arterial blood volume corresponding to the heart beat [13]. When light is passed through the skin, it is absorbed by venous blood, tissue, hair, skin pigments, pulsating and non-pulsating arterial blood. During systole, when there is more blood in the arteries, there is an increased absorption as the diameter of the arteries increase. During diastole, when blood in the arteries is diminished, the light path length is decreased and hence the absorption decreases. Thus, light absorption pulsates between the maximum and minimum intensity, resulting in a PPG signal as illustrated in Fig. 2.1. The absorption of light through the skin, hair and tissues is constant for a given individual and is denoted as the DC component.

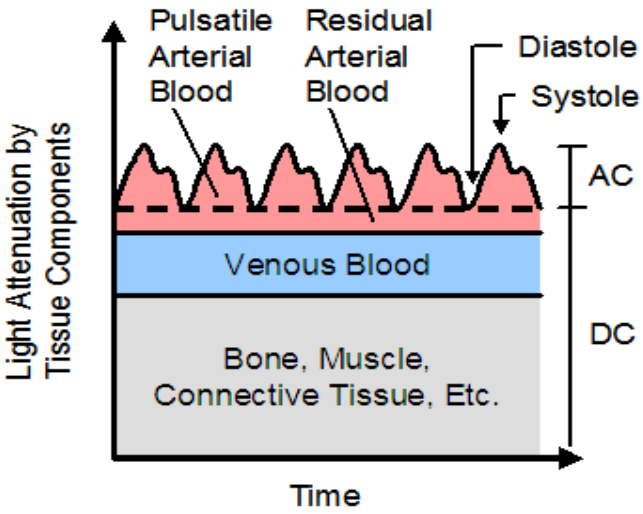

Fig. 2.1. Light absorption through the skin [13].

2.1. SpO_2 measurement using pulse oximetry

At wavelengths used in pulse oximetry, Hb and its derivatives are the main absorbers of light in blood. The most commonly occurring Hb derivatives are HbO_2, HbCO, MetHb and Hb. As

shown in Fig. 2.2, in the red region, the absorption of light by Hb is more than the absorption of HbO_2. Similarly, the absorption of light in the IR region is low for Hb compared to the absorption caused by HbO_2. Assuming that HbCO and MetHb are absent, SpO_2 is measured based on the variation in this absorption of light by HbO_2 and Hb (Fig. 2.2). Two wavelengths, typically from the red and infrared region, are used. The ratios of PPG signals at these two wavelengths are used to calculate SpO_2 [14].

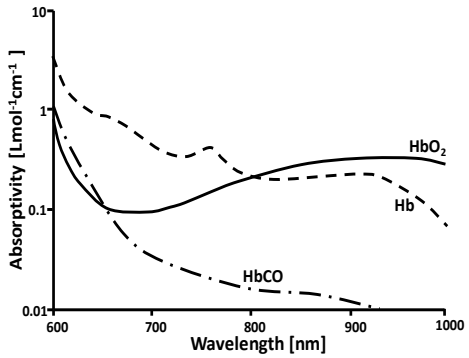

Fig. 2.2. Absorption spectra of Hb and its derivatives [14].

SpO_2 calculation is based on the assumption that HbCO and MetHb are absent. When HbCO or MetHb is present in significant quantities, pulse oximeters give erroneous SpO_2 readings. Apart from the presence of HbCO and MetHb, the variation caused by differences in the absorption of light by the skin can also affect the accuracy of pulse oximeters because, practically, when light is passed through the skin, the DC component varies between individuals and also with wavelengths. This variation also affects the AC component [15-16]. To make the AC absorption independent of the DC absorption, a normalization process is applied (Fig. 2.3). Accordingly, the absorbance of light is calculated using the normalized signals as given below.

$$\text{Normalized Absorbance} = -\ln\frac{(I_L)}{(I_H)} \cong -\ln\frac{AC}{DC} = -\ln\frac{Io\, e^{-\alpha(\lambda)bc}}{I_o} = \alpha\,(\lambda)\,bc \qquad (2.1)$$

where, I_L is the transmitted intensity during systole and I_H is the transmitted intensity during diastole [15]. The ratio of the normalized absorbances at the red and infrared wavelength is calculated as shown in Eq. 2.2

$$R = \frac{A_R}{A_{IR}} = \frac{(\frac{AC}{DC})_R}{(\frac{AC}{DC})_{IR}} \tag{2.2}$$

where, A_R and A_{IR} are the normalized red and infrared absorptions, respectively.

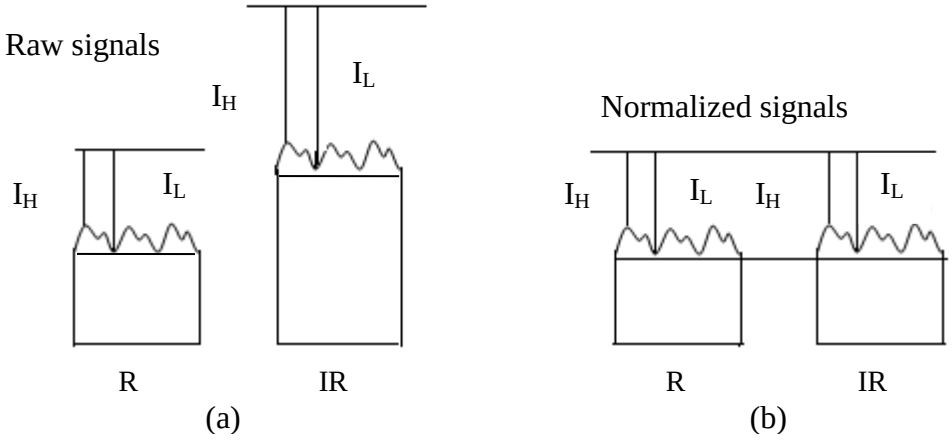

Fig. 2.3. Variation in DC absorption between R and IR wavelengths before (a) and after normalization (b) [14].

Typically, 660 nm (red) and 940 nm (infrared) are the two wavelengths that are commonly used in commercial pulse oximeters to measure SpO_2. Absorption ratios are calculated at these two wavelengths after the PPG signals are amplified, filtered and undergo signal processing. In commercially available pulse oximeters, SpO_2 is calculated using an empirical calibration conducted based on this ratio. As mentioned earlier, calculation and calibration for SpO_2 measurement using pulse oximeters is based on the assumption that HbCO is absent. Hence, during CO exposure the pulse oximeters are unable detect the presence of HbCO in blood. It wrongly reads the additional absorption caused by HbCO as the absorption due to HbO_2, resulting in erroneous computations of SpO_2.

2.2. Current methods available for simultaneous measurement of oxygen and carbon monoxide saturation using pulse oximetry

So far, only one commercially available pulse oximeter, the Masimo Rad-57 (Masimo Inc., Irvine, CA) can measure SpCO and SpO_2 simultaneously, but the algorithms used are not disclosed. The Masimo Rad-57 uses eight wavelengths, but it measures an additional parameter MetHb apart from SpCO and SpO_2 [10]. Hence, the number of wavelengths or the exact wavelengths used to measure SpCO is not known.

As mentioned in Chapter 1, firefighters, miners and army personnel are more susceptible to CO poisoning. In the modern day warfare, nearly 30% of the soldiers would be deployed using armored fighting vehicle (AVF) which not only increases the chances of exposure to CO but also increase the levels of exposure. Even development of better ventilation systems has not eradicated the risk of CO poisoning in AVFs [12]. Similarly, firefighters and miners are constantly exposed to CO in their line of duty [17]. The currently existing Masimo pulse oximeter cannot be used for continuous monitoring of firefighter, army personnel or miners as they carry on their day-to-day activities. A continuous monitoring system which can monitor vital physiological parameters, including HbCO, would enable a clinician or field commanders to remotely monitor the health of these individuals and take immediate and appropriate action to prevent any harm to health.

Our lab has developed a wearable wireless pulse oximeter sensor for non-invasive monitoring of vital signs that can be used by first responders like firefighters or field medics to facilitate rescue and triage operation. The device can be worn around the forehead and is designed to transmit the information wirelessly to a remote location [Fig. 2.4]. Firefighters, army personnel or first responders can go about their activities with the device strapped around their

forehead. The wireless pulse oximeter sensor developed in our laboratory can measure SpO_2, heart rate (HR) and respiratory rate (RR). The aim of this thesis was to develop an algorithm that can be used in this wireless device to simultaneously measure SpO_2 and carbon monoxide saturation (SpCO).

Fig. 2.4. Multiwavelength wireless pulse oximeter device designed in our lab.

Inadequacies of commercial pulse oximeters like low battery life, bulkiness and wires that prohibit the use of the device in field applications have been eliminated in our wireless pulse oximeter. Hence, if the wireless device can simultaneously measure SpO_2 and SpCO, it will find additional potential applications not just for firefighters or first responders, but also in clinical settings where patient mobility is important.

Chapter 3: Specific objectives

The inability of pulse oximeters to measure HbCO in blood, or measure accurate values of SpO_2 in the presence of elevated levels of HbCO, is an important limitation because high exposure to CO can be fatal or result in permanent neurological damage. If pulse oximeters could monitor HbCO levels, CO poisoning can be treated immediately, preventing further harm. Therefore, the aim of this thesis was to develop an algorithm that could simultaneously measure SpO_2 and HbCO in blood using a pulse oximeter. The specific objectives of this thesis were to:

1. Develop a theoretical model for simultaneous measurement of SpCO and SpO_2.
2. Identify the specific wavelengths at which changes in SpCO and SpO_2 can be measured simultaneously.
3. Formulate an algorithm to simultaneously measure SpCO and SpO_2 using pulse oximetry.
4. Verify the algorithm experimentally using an *in-vitro* set up.

Chapter 4. *In-vitro* model for simultaneous measurement of SpO_2 and SpCO

4.1. Need for an *in-vitro* model

Although *in-vivo* measurements can provide information on the impact of different physiological variables, it is not practically possible to desaturate a healthy individual below 80% or elevate SpCO above 12% due to safety and ethical considerations as there is a risk of hypoxic brain damage to the person at SpO_2 values lower than 80% and greater than 12% SpCO. Hence, it is difficult to obtain data from *in-vivo* measurements at low values of SpO_2 or high values of SpCO for initial testing of pulse oximeters [16]. Use of animal models for initial testing of pulse oximeters is possible. But, results from animal studies have suggested that unknown or uncontrollable physiological parameters can cause large variation especially at low SpO_2 values [18]. Similarly, a study comparing an animal model and *in-vivo* calibration reports that differences in skin structure between humans and animals can also affect the calibration of pulse oximeter. Although, piglets are reported to have histologically a skin structure similar to human beings, the effect of skin structure on pulse oximeters has not been completely studied [18]. Hence, in spite of calibration using animal models, as mentioned in chapter 2, pulse oximeters have to be finally calibrated on humans. This is because there is no other accepted standard reference for checking the calibration of pulse oximeter [20]. As shown in Fig. 4.1, *in-vivo* calibration for SpO_2 requires *in-vivo* tests on volunteers after they breathe N_2 gas to decrease the SpO_2 in their blood. Similarly, SpCO calibration required subject to breathe CO to elevate the concentration of HbCO in the blood. These studies are expensive, time consuming and carry a certain risk. Hence, *in-vitro* measurements using a tissue simulator can be a practical and relatively inexpensive method for initial testing and calibration of a new pulse oximeter.

Fig. 4.1. *In-vivo* calibration of a pulse oximeter sensor conducted on a volunteer.

4.2. Description of *in-vitro* models

Various attempts have been made at developing an *in-vitro* model that simulates the optical properties of biological tissues. The interaction of light with tissue is a complicated process. It is not practically possible to simulate the interaction of light with tissue to a great detail. Hence, an *in-vitro* model tries to simulate the relevant optical properties of tissue. Typically, an *in vitro* model consists of a flexible cuvette through which the blood is pulsed. The change in blood channel depth as blood is pulsed through creates the pulsatile signals (PPG) that are used to calculate the ratios required for SpO_2 or SpCO measurement [18]. The true value of oxygen or carbon monoxide saturation can be obtained by simultaneous blood sampling in an *in-vitro* analysis using a CO-Oximeter.

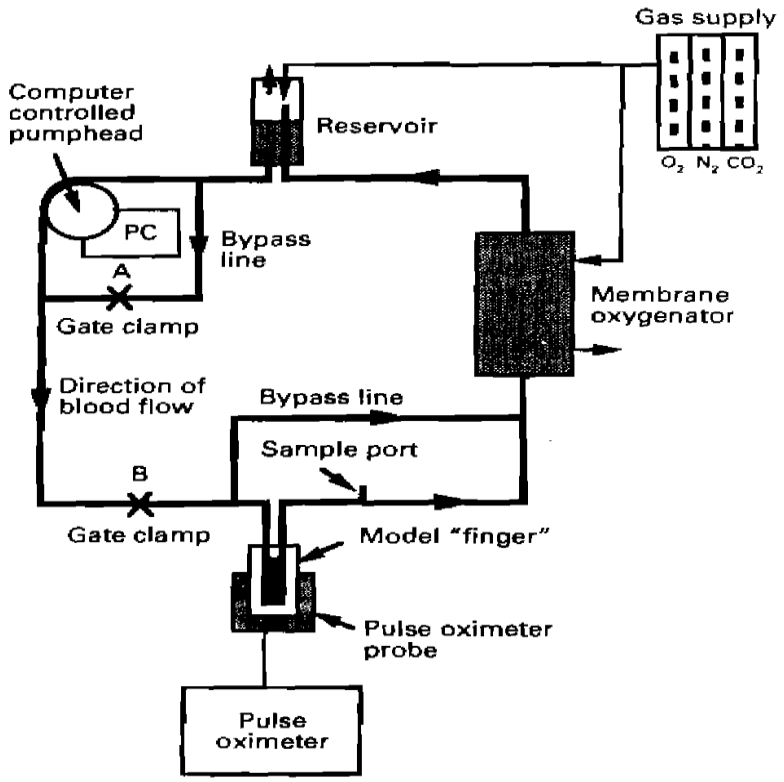

Fig. 4.2. *In-vitro* model developed by Reynolds et al. [22].

The majority of these *in-vitro* models use a phantom finger that can be inserted between the LEDs and the photodiode of a pulse oximeter probe. An i*n-vitro* model developed by Vegfors [21] consists of a cylindrical oxygenator which also acts as blood reservoir and a phantom finger through which blood was pulsed using a peristaltic pump, thereby simulating a finger containing blood surrounded by tissue. While the model used silicone for the phantom fingers, plastic cubes were used to simulate tissues surrounding the blood vessel. Similarly, the system developed by Reynolds [22] consists of a phantom finger made of silicone strips through which the blood can be pulsed by a computer controlled pump. It also consists of an oxygenator controlled by rotameters and a gas mixing pump that is used to control the saturation of the blood (Fig. 4.2).

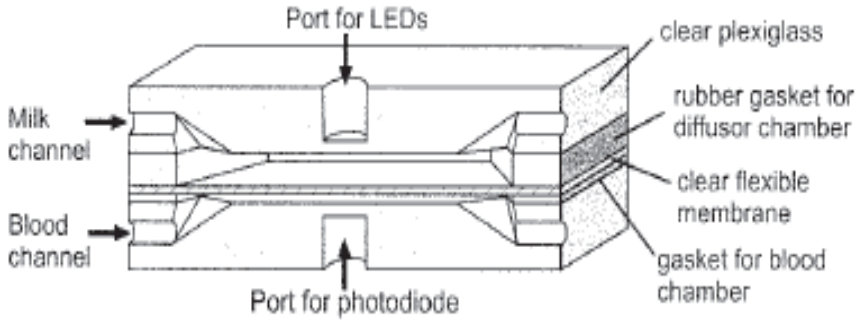

Fig. 4.3. *In-vitro* model developed by Edrich et al. [18].

The *in-vitro* model developed by Edrich et al. [18] also had a similar phantom finger but the model had incorporated additional layers to the phantom finger to mimic the biological tissue more closely. The cuvette was made of two plexiglass slabs, separated from each other by a rubber gasket and flexible membrane, forming two chambers each with separate input and output. While blood was pulsed through one of the chambers of the cuvette, homogenized milk was circulated through the second chamber. Milk was meant to act as a diffuser to simulate the light scattering effect of the bloodless tissue (Fig. 4.3). Oura et al. [23] developed a double – layered model that simulated both arterial and venous circulation that creates a mock circulatory system (Fig 4.4).

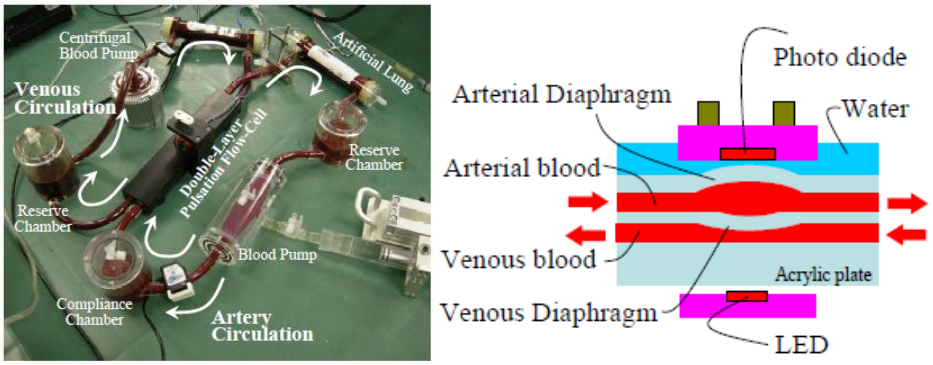

(a) **(b)**

Fig. 4.4. Mock circulatory system developed by Oura et al. (a). Schematic representation of the double layered cuvette (b) [23].

Although all these *in-vitro* models mimic the optical properties of biological tissues, they are not simple and easy to use. As mentioned earlier, in spite of using such complicated models, a final *in-vivo* calibration has to be conducted on the device. Hence, instead of using models that are complicated and difficult to use, a simple *in-vitro* model that had been designed in our lab was used in the experiments [Fig. 4.5].

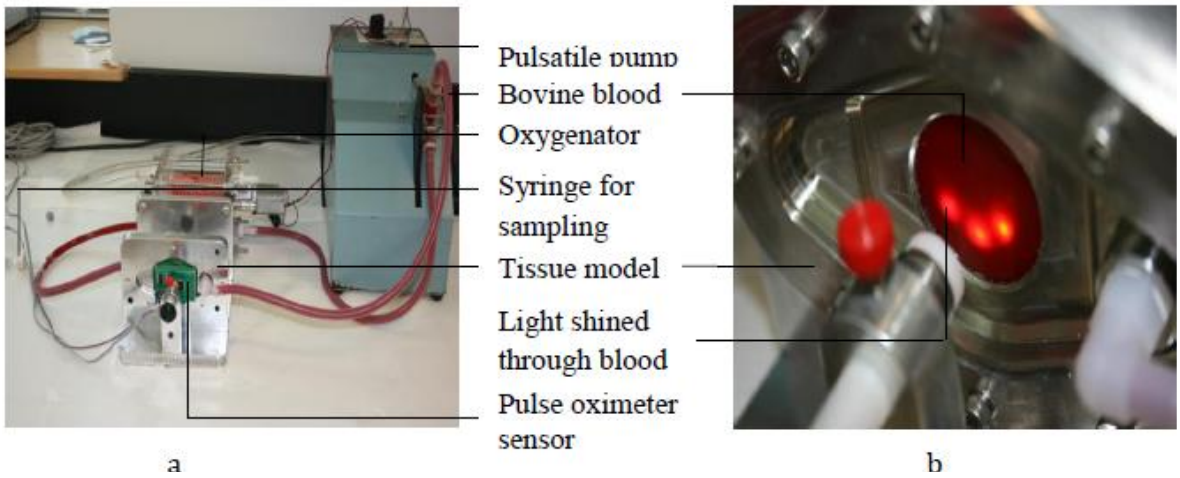

Fig. 4.5. Experimental set up (a) and a close up of the blood compartment in the tissue simulator (b).

The *in*-vitro model that was designed in our lab also has a cuvette through which blood can be pulsed through, using a pulsatile pump, similar to the models described above. An oxygenator was used to change the O_2 or CO content in blood. But, the cuvette was designed for placement of a reflectance sensor which consists of the LEDs and the photo detector on the same plane. Typically reflectance sensors are placed on the forehead and are not as affected by peripheral vasoconstriction as transmission sensors which are placed on fingers. The cuvette in the model designed in our lab, could simulate a thin layer of blood between tissues similar to the blood layer observed in the forehead. A small white substrate is placed on one side of the cuvette to simulate the strong reflection caused by the frontal bones in the forehead. The prototype sensor is designed to be used on the forehead. Measurements from other parts of the body, such as the

arms or legs are feasible, but typically result in poor signal-to-noise ratio because tissue depth in these parts will cause high attenuation which in turn results in poor quality PPG signal.

4.3. Experimental set-up

Data was collected using the tissue simulator, a pulsatile pump, reflectance type pulse oximeter sensor and an oxygenator (Fig.4.5a). The true values of oxygen and carbon monoxide saturation was obtained using a IL 682 CO-oximeter. A sensor with seven LED wavelengths between 600nm to 1000nm that has been previously designed in our laboratory was used in the experiments. The seven wavelengths were chosen for the following reasons:

1. At wavelengths below 600nm the absorption by the blood and tissue is very high. Above 1000nm, the absorption by water in the tissue becomes very high. Therefore, the window of 600nm to 1000nm was chosen.
2. Only LEDs of specific wavelengths are available commercially. Although other sources (e.g. incandescent light) are available at different wavelengths, they increase the expense and complexity of the sensor.
3. Increasing the number of LEDs will increase the size of the sensor and the complexity of the hardware.

   The particular LED's were chosen such that the wavelengths are approximately dispersed evenly as shown in Fig. 4.6.

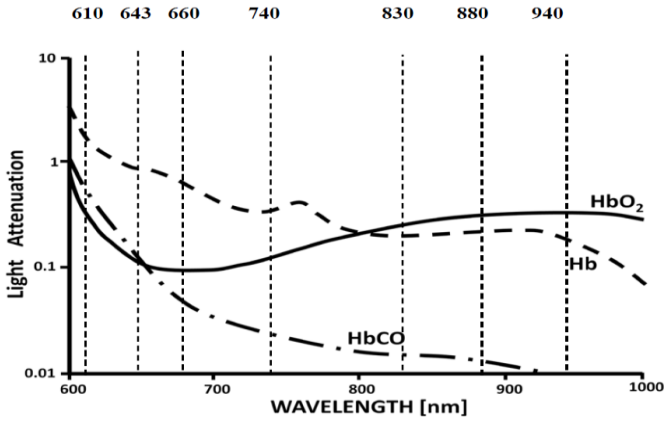

Fig. 4.6. Absorption spectra for Hb and its derivatives. The vertical lines indicate seven wavelengths used in our prototype sensor.

4.4. HbCO measurement using CO-Oximeters

As mentioned earlier, the true values of HbO_2 and HbCO in blood used in experiments was obtained using an IL 682 CO-Oximeter. Blood samples drawn from patients can be analyzed *in-vitro* by a CO-Oximeter to obtain HbO_2, HbCO, Hb and MetHb. CO-Oximeters use four wavelengths to measure light transmission based on Beer-Lambert's law. It uses a hollow cathode lamp as a spectral source to obtain fixed spectral lines at 535nm, 585.2nm, 594.5nm, and 626.6nm using an optical set up that includes lens, a rotating filter wheel and a beam splitter. The coefficients of absorptivity for HbO_2, HbCO, Hb and MetHb are obtained at these wavelengths and are locked into the digital memory. Absorption values are obtained for all the parameters measured after the blood sample is hemolyzed in the instrument. From Fig. 4.7, 535nm and 594.5nm are isobestic for HbCO and HbO_2 and 585.2nm is isobestic for HbO_2 and Hb. Using Beer- Lambert's law, CO-Oximeters simultaneously measure the values of HbCO, HbO_2, Hb and MetHb using these isobestic wavelengths.

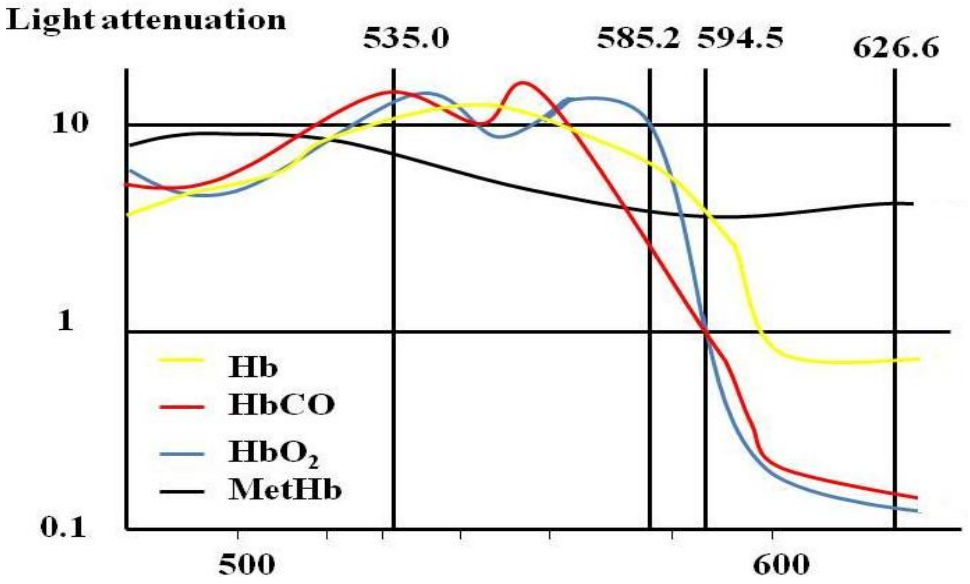

Fig. 4.7. Absorption spectra of Hb, HbCO, HbO_2, MetHb in the visible region. The vertical lines indicate the wavelengths used in an IL 682 CO-oximeter [25].

Using Beer-Lamberts law, the absorption at the four wavelengths can be generalized as

$$A_i = bC_j(\varepsilon)_{ij} \tag{4.1}$$

where, A_i is the absorption at four wavelengths(i=1-4), b is the sample path length, C_j is the concentration of the four Hb species (j=1-4), $(\varepsilon)_{ij}$ is the absorptivity or extinction coefficient at four wavelengths for the four Hb species. From equation (4.1), the device calculates the concentrations of each of the Hb derivatives. Total hemoglobin (THb) is calculated as the sum of concentrations of all four Hb derivatives. $\%HbO_2$ is calculated using the formula for fractional oxygen saturation given by

$$\%HbO_2 = \frac{C_{HbO_2} \times 100}{THb} \tag{4.2}$$

Similarly %HbCO and %MetHb are calculated using the formula shown in Eq. 4.3 and 4.4,

$$\%HbCO = \frac{C_{HbCO} \times 100}{THb} \tag{4.3}$$

$$\%\text{MetHb} = \frac{C_{\text{MetHb}} \times 100}{\text{THb}} \quad (4.4)$$

A microcomputer is used to compute HbO_2, HbCO, Hb and MetHb. The device has an accuracy of ±1% for all the parameters it measures [24]. The wavelengths used in CO-Oximetry are in the visible range (500nm-650nm) where absorption by blood is very high (Fig. 4.7). The same wavelengths cannot be used in pulse oximeters because the incident light absorbed by the tissue and the thickness of blood in the tissues is high in the visible region.

Chapter 5: Preliminary research to validate the sensor and *in-vitro* model

Preliminary experiments were conducted to validate the data collected from our *in-vitro* model. The goals of the preliminary experiments were to verify if the optical properties of blood, with varying HbO_2 and HbCO, observed from our sensor and model follow the trend suggested by the standard absorption plot obtained using the coefficients of absorptivities derived from spectrophotometric measurements on human blood as published in the literature [25]. For testing, the pulse oximeter probe was attached to the model and HbO_2 or HbCO concentrations were varied by varying the amount of N_2 or CO gas introduced into the set up, respectively. Readings from the pulse oximeter were simultaneously obtained with blood sampled using an IL 682 CO-Oximeter as a reference. The *in-vitro* testing was repeated at different concentrations of SpO_2 and SpCO.

5.1. Methodology

5.1.1. SpO_2 experiments

Since HbO_2 in the blood varies according to variation in HbCO, understanding and verifying the optical properties of blood with varying concentrations of HbO_2 was necessary. HbO_2 concentrations in the blood were varied from 50-100% and the absorption readings corresponding to different concentrations were obtained at all wavelengths from the sensor. Experiments were repeated thrice and the results were averaged and plotted (Fig. 5.1). These averaged results were then compared to the plot obtained using the standard absorptivity values, for concentrations similar to the values obtained in the preliminary experiments (Fig. 5.2). When results from our *in-vitro* experiments follow the same general trend observed in human blood, it implies that the results that will be obtained for simultaneous measurement of SpO_2 and SpCO

from our *in-vitro* set up will follow a general trend that will be observed in *in-vivo* measurements.

5.1.2. SpCO experiment

Similarly, preliminary SpCO experiments were performed with the addition of CO to the blood. HbCO in the blood was varied from 0-35% and the results are plotted in Fig. 5.3. Similar to the SpO_2 analysis, the results from our experiments were then compared to the plot obtained using the standard absorptivity values found in the literature, at concentrations similar to the values obtained in the preliminary experiments (Fig. 5.4).

5.1.3. Assessing the validity of the tissue simulator

In an *in-vitro* set up, in addition to the optical properties of blood, light absorption and scattering is also dependent on the optical properties of the tissue simulator. To validate our tissue simulator, a set of experiments were conducted with a commercially available Masimo reflectance pulse oximeter. SpO_2 levels were varied between 50-100%. The blood was simultaneously sampled using the IL 682 CO-oximeter as a reference. The *in-vitro* model was validated by comparing the results from the Masimo pulse oximeter and the true values obtained from the IL 682 CO-Oximeter.

5.2. Results

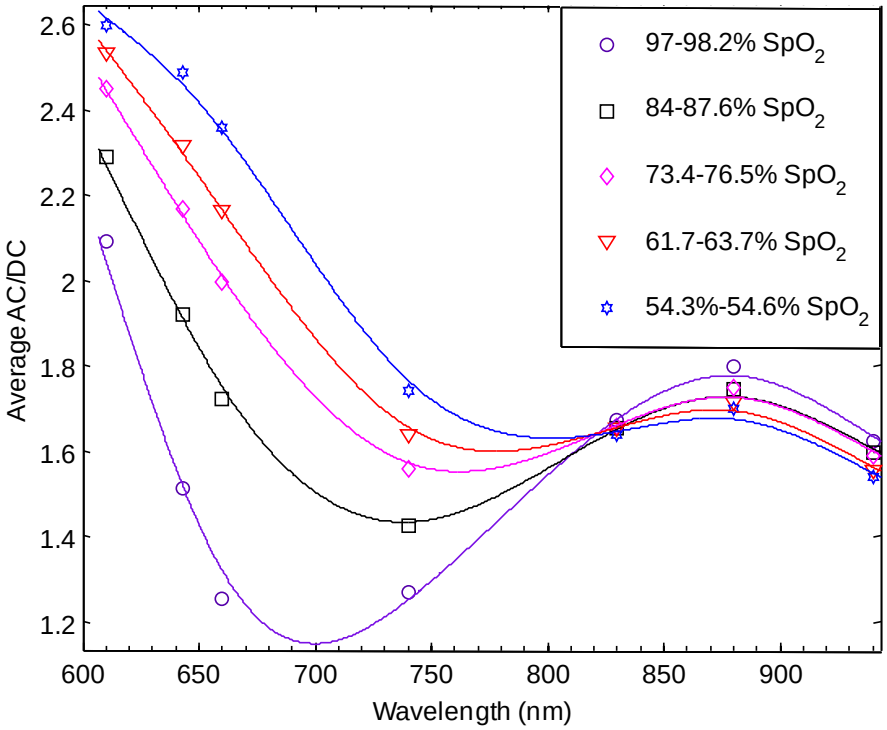

Fig.5.1. Mean AC/DC plots obtained from three sets of SpO_2 experiments.

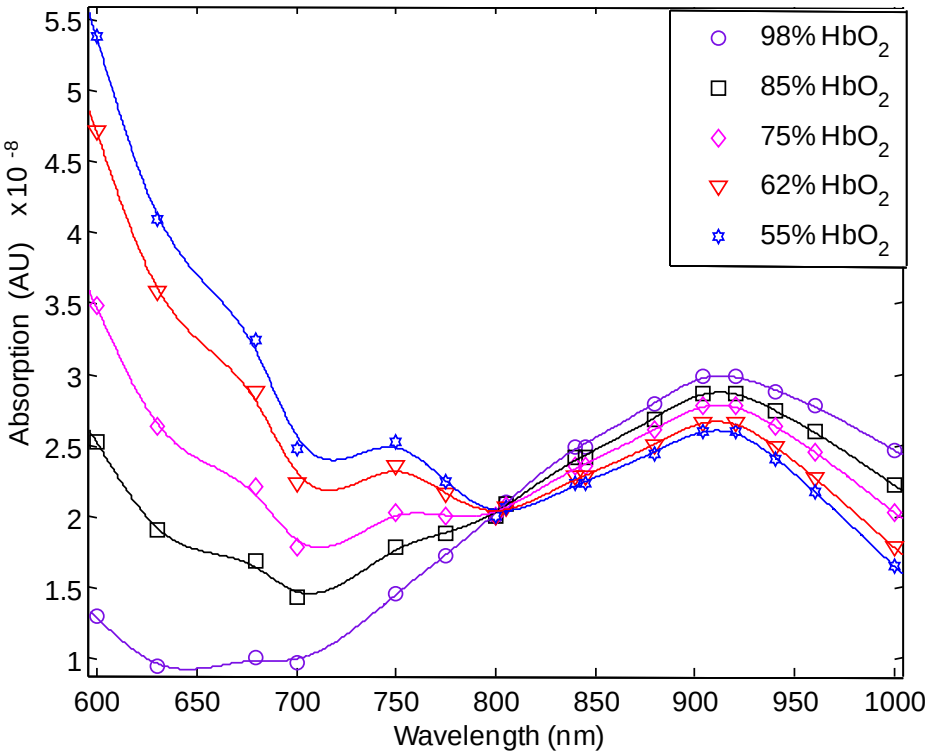

Fig. 5.2. Absorption spectra of HbO_2 obtained from the literature [25].

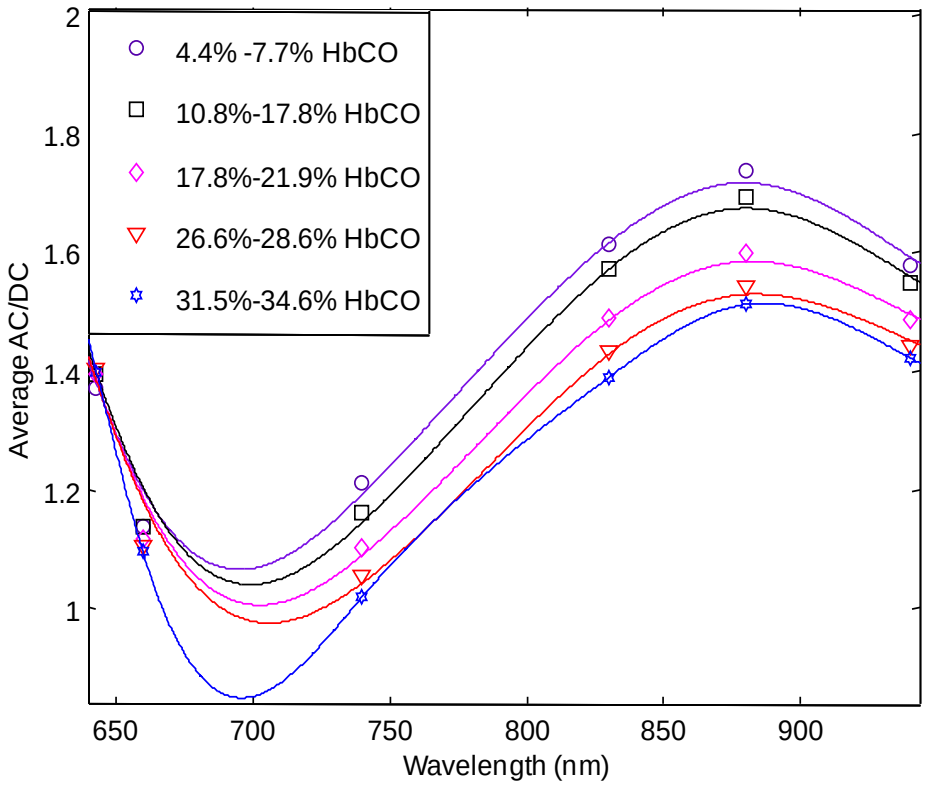

Fig. 5.3. Mean AC/DC plots obtained for three sets of SpCO experiments.

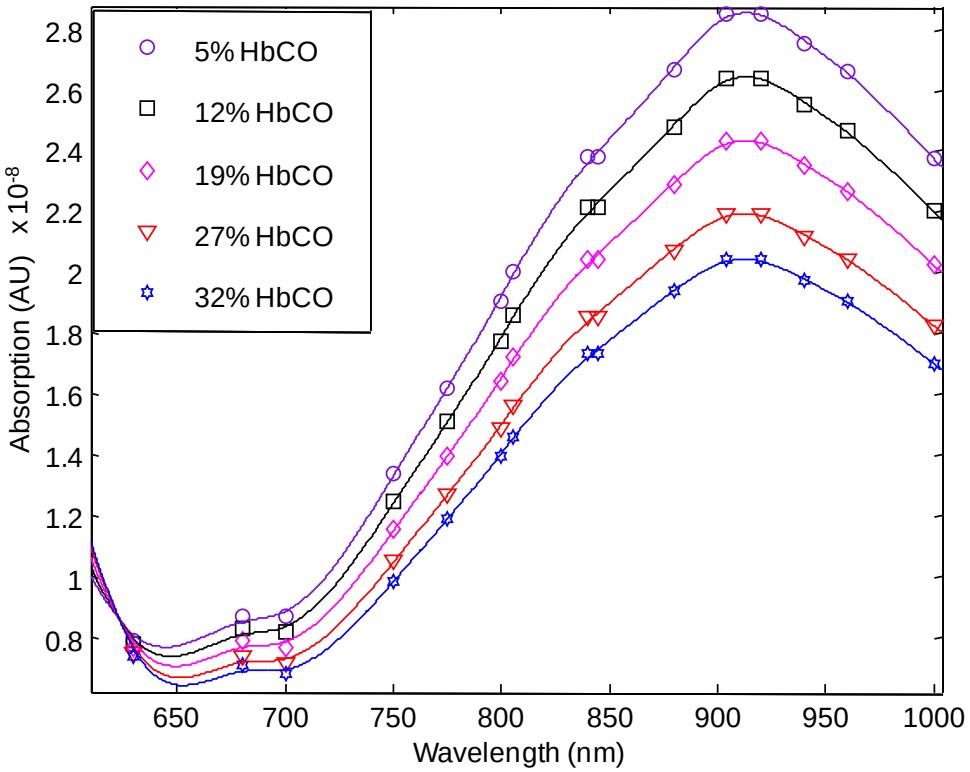

Fig. 5.4. Absorption spectra of HbCO obtained from the literature [25].

5.3. Discussion

5.3.1. SpO_2 experiments

The results from our SpO_2 experiments (Fig. 5.1) were found to follow the same trend suggested by Fig. 5.2 which was obtained from hemolysed blood using a collimated, monochromatic light source. Results from our experiments, on the contrary, were obtained from an *in-vitro* model using whole blood and a reflectance sensor which uses LEDs that are neither monochromatic nor collimated sources. Hence, although the curves from Fig. 5.1 and Fig. 5.2 follow the same trend, they are not identical. To check for reproducibility, the mean and standard deviation from three SpO_2 experiments were calculated and tabled in Table 5.1.

Table 5.1: AC/DC ratios (mean ±standard deviation) for three sets of experiments with varying SpO_2.

	SpO_2 (%)				
Wavelength (nm)	97 - 98.2	84 - 87.6	73.4 - 76.5	61.7 - 63.7	54.3 - 54.6
610	2.09 ± 0.00	2.28 ± 0.19	2.44 ± 0.20	2.53 ± 0.19	2.59 ± 0.16
643	1.51 ± 0.04	1.92 ± 0.19	2.16 ± 0.17	2.31 ± 0.19	2.48 ± 0.23
660	1.25 ± 0.07	1.72 ± 0.10	1.99 ± 0.11	2.16 ± 0.13	2.35 ± 0.21
740	1.26 ± 0.04	1.42 ± 0.01	1.55 ± 0.01	1.63 ± 0.02	1.73 ± 0.05
830	1.67 ± 0.02	1.65 ± 0.04	1.65 ± 0.03	1.65 ± 0.05	1.63 ± 0.02
880	1.79 ± 0.05	1.74 ± 0.07	1.74 ± 0.07	1.71 ± 0.08	1.69 ± 0.06
940	1.61 ± 0.05	1.59 ± 0.10	1.58 ± 0.08	1.55 ± 0.07	1.53 ± 0.07

From Table 5.1, at 610 nm, 643 nm and 660 nm, the absorption by Hb is high for lower values of SpO_2. This results in a weak signal, thereby, decreasing the signal-to-noise ratio. Hence, the variation is higher for low values of SpO_2 but low at higher ranges of SpO_2. Since the variation between the three sets of readings is less than 1% for all the ranges of SpO_2 and wavelength tested, the results obtained using our sensor and *in-vitro* model can be considered to be reproducible within experimental errors.

5.3.2. SpCO experiments

The results from our SpCO experiments were also found to follow the same trend suggested by Fig. 5.4. As mentioned previously, the results from our *in-vitro* model are not identical to the absorption plot obtained from measurements conducted on hemolysed blood (Fig. 5.4). Mean and standard deviation between the three SpCO experiments were calculated to check for reproducibility.

Table 5.2: AC/DC ratios (mean ±standard deviation) for three sets of experiments with varying SpCO.

	SpCO (%)				
Wavelength (nm)	4.4 – 7.7	10.8 – 17.8	17.8 – 21.9	26.6-28.8	31.5-34.6
610	1.94 ± 0.12	1.92 ± 0.12	1.92 ± 0.11	1.92 ± 0.11	1.91 ± 0.12
643	1.39 ± 0.10	1.39 ± 0.10	1.39 ± 0.10	1.39 ± 0.09	1.37 ± 0.11
660	1.13 ± 0.06	1.13 ± 0.06	1.11 ± 0.05	1.09 ± 0.04	1.13 ± 0.11
740	1.15 ± 0.03	1.15 ± 0.03	1.10 ± 0.03	1.01 ± 0.06	1.20 ± 0.02
830	1.57 ± 0.07	1.57 ± 0.07	1.48 ± 0.08	1.38 ± 0.11	1.61 ± 0.05
880	1.69 ± 0.09	1.69 ± 0.09	1.59 ± 0.09	1.51 ± 0.12	1.73 ± 0.08
940	1.54 ± 0.10	1.54 ± 0.10	1.48 ± 0.08	1.42 ± 0.11	1.57 ± 0.09

Table 5.2 shows that the standard deviation between the absorption values for three sets of experiments is low at all wavelengths and concentration ranges considered. At 610nm, the absorption by HbCO is high. This results in a weak signal that decreases the signal-to-noise ratio. Hence, the variation is relatively higher for all ranges of SpCO at this wavelength. The standard deviation between the readings is less than 1% for all wavelengths at all ranges of SpCO. Hence, these results can be considered to be reproducible within experimental errors.

5.3.3. Assessing the validity of the tissue simulator

As mentioned in Section 5.1.3, experiments were conducted using the commercial Masimo pulse oximeter on our *in-vitro* simulator with simultaneous blood sampling using IL 682 CO-Oximeter. Standard deviation was calculated between IL 682 data and the data from the Masimo pulse oximeter obtained from our *in-vitro* model. The mean standard deviation between the two data sets was found to be ±2.9% for SpO_2 between 50-100%. This error is acceptable because commercially available pulse oximeters are calibrated on humans and not on *in-vitro* models. Thus, the model can be used for the HbCO determination.

Hence from these preliminary experiments, it is shown that the results obtained from our model and our sensor can be used for measurement of both SpO_2 and SpCO.

Chapter 6: Theoretical modeling for simultaneous measurement of SpO_2 and SpCO

6.1. Need for a theoretical model

The wavelengths required for accurate monitoring of SpO_2 can be identified based on Fig. 2.2. Assuming, HbCO is absent, SpO_2 measurement involves two unknowns, the concentration of HbO_2 and Hb. To calculate these two unknowns, we would need a minimum of two wavelengths. One wavelength can be chosen from the region of maximum sensitivity to changes in SpO_2 and the other wavelength can be chosen from an isobestic wavelength region. The ratio of absorption at those two wavelengths can be used to calculate SpO_2. However, to determine the effect different factors would have on SpO_2 measurements, like temperature induced changes in LED peak wavelengths, time consuming and expensive experiments have to be conducted. Alternatively, the sensitivity at different wavelengths can be found using a theoretical model. The need for a theoretical model is more pronounced in the case of SpCO measurement because, in the presence of HbCO, there are three unknown variables (concentrations of HbO_2, Hb and HbCO) involved in SpO_2 and SpCO measurement. A minimum of three wavelengths are required to calculate these variables simultaneously. Identifying experimentally three wavelengths that would have good sensitivity to changes in both SpO_2 and SpCO solely based on Fig. 2.2 will be time consuming and expensive. Hence, a theoretical model becomes a practical and effective means to identify the wavelengths for simultaneous measurement of SpO_2 and SpCO.

The laws that can be used to obtain a theoretical model should simulate the effects of light interaction with blood and tissue. Twerky's multiple scattering theory has so far been the most successful for modeling whole blood for *in-vitro* oximetry [26-27]. Similarly, a model based on 3-D photon diffusion theory has been used to effectively simulate light propagation through

biological tissues [27-28]. However, the mathematical models that are based on these theories are more complex. In spite of using these complex theories to model light interaction with blood and tissue, a pulse oximeter must be finally calibrated on humans. This is because there is no standard to validate the results that will be obtained from these models [29]. Although Beer-Lamberts law is not applicable to pulse oximetry, the final empirical calibration performed on the device based on *in*-vivo measurements compensates for the simplifications made in the theoretical model [30]. Therefore, Beer-Lamberts law was used to develop a theoretical formulation to facilitate the development of a simple algorithm for simultaneous measurement of SpO_2 and SpCO.

6.2. Beer-Lambert's Law

According to Beer-Lambert's law, when a monochromatic, collimated light I_o is incident on an absorbing medium, part of the light is transmitted while the other part is absorbed. It is based on the property that the sum of the transmitted and absorbed light intensities are equal to I_o. Thus, I_o will decrease exponentially with distance (Fig. 6.1) [7].

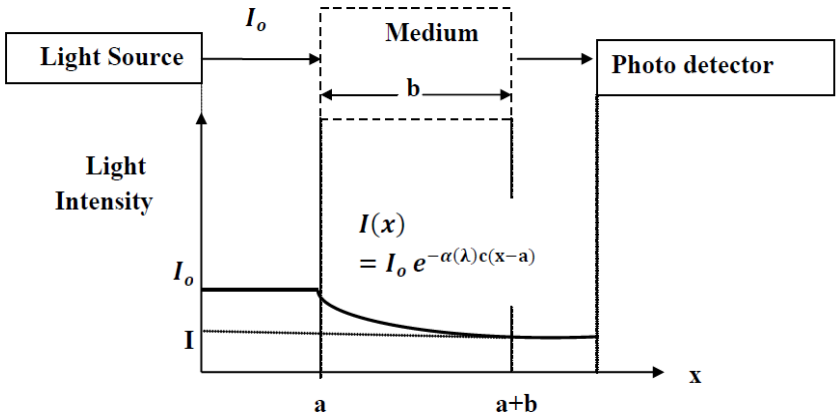

Fig. 6.1. Exponential decrease in light intensity as it passes through an absorbing medium [7].

According to Beer- Lambert's law, the absorption through a medium (A) is given as

$$A = -\log\left(e^{-\alpha bc}\right) = \alpha(\lambda)bc \qquad (6.1)$$

where, $\alpha(\lambda)$ is the absorptivity for a given wavelength

b is the path length

c is the concentration of the absorbing substance

If there are multiple absorbers in the medium, each absorbing substance contributes to the total absorbance corresponding to its concentration and absorptivity. Thus, the total absorbance for n absorbing substance is

$$A_t = \alpha_1(\lambda)b_1c_1 + \alpha_2(\lambda)b_2c_2 + \alpha_3(\lambda)b_3c_3 + \alpha_n(\lambda)b_nc_n = \sum_{i=1}^{n} \alpha_i(\lambda)\, b_ic_i \quad (6.2)$$

where, $\alpha_i(\lambda)$ represent the absorptivity, b_i represent the path length and c_i is the concentration of the absorbing substance i, respectively.

Strictly, Beer-Lambert's law does not account for light scattering or specular light reflection at the surface of a biological medium. In reflectance pulse oximetry, as in the case of transmission mode, the principle quantity measured is the change in light absorption. The theoretical model developed based on Beer-Lambert's law was used to estimate the relative change in the absorption ratio corresponding to the change in SpO_2 or SpCO. By quantifying this relative change in ratio, the sensitivity of different wavelengths to changes in SpO_2 or SpCO can be identified. To avoid inaccuracies associated with any attempt to utilize a theoretical formulation to describe light propagation through biological tissues and obtain a quantitatively accurate algorithm to determine SpO_2 or SpCO, commercial pulse oximeters rely on empirical calibration [15].

A study evaluating the relationship between SaO_2 and the R/IR ac-dc ratio, used in pulse oximeters under a variety of physiological conditions, like different blood volumes, hematocrit, pigmentation and finger thickness, show that in pulse oximeters using fixed calibration curves

based on empirical measurements, errors introduced by interfering variables should be less than a few percent in the clinically significant range of 70-100% [28]. Hence empirical calibration of the device has been successfully employed for SpO_2 measurement in commercially available pulse oximeters. Similarly such calibration can be employed for simultaneous measurement of SpO_2 and SpCO.

6.3. Derivation of the theoretical model

As mentioned in Chapter 2, at wavelengths used in pulse oximetry, Hb and its derivatives are the main absorbers of light in blood. The most dominant Hb derivatives are HbO_2, Hb, HbCO and MetHb. The measurement of SpO_2 by a pulse oximeter is based on the assumption that the concentration of HbCO or MetHb in blood is negligible. For the purpose of this thesis, we will assume that the concentration of MetHb is negligible. The blood that was used in our experiments had negligible concentrations of MetHb. Hence, concentrations of HbO_2, HbCO and Hb are the three unknowns that need to be calculated and hence a minimum of three wavelengths were required to calculate these unknowns.

Literature search on simultaneous measurement of SpCO and SpO_2 yielded only two results. Lee et al. [31] developed two theoretical models, one based on Beer-Lambert's law and the other based on photon diffusion theory. Using the theoretical model based on Beer-Lambert's law, the sensitivity of different combinations of three wavelengths to changes in SpCO and SpO_2 were determined. The wavelengths used by Lee were reported to be between 600-940 nm. Then, using an *in-vitro* model which mimics the absorption properties of the tissue, absorption values were obtained from blood samples with a known concentration of HbCO and HbO_2 at these wavelength combinations and the sensitivity of the wavelength ratios to changes in SpO_2 and SpCO were verified experimentally. The paper reports good accuracy for simultaneous *in-vitro*

measurement of SpCO and SpO_2 at 630 nm, 660 nm and 950 nm, but it does not discuss the sensitivity of other wavelength combinations to changes in SpCO and SpO_2. Pieralli et al. [32] developed a theoretical model for SpO_2 and SpCO measurement also based on Beer-Lambert's law. Three laser diodes (660 nm, 830 nm and 1060 nm) were used in a prototype sensor. The paper discusses the results of a series of *in-vivo* SpO_2 and SpCO experiments where SpCO was varied from 3.5%-8%. Discrepancies were reported in 3 out of 440 human tests. Since there are no LED's available at 1060 nm, the use of laser diodes makes the hardware more complicated, bulky and expensive. Hence, the use of this specific wavelength is not practical in a pulse oximeter sensor. Although both papers do not discuss the sensitivity of other wavelength combinations to changes in SpCO and SpO_2, they suggest that the use of a three wavelength combination is sufficient for simultaneous measurements of SpCO and SpO_2 using pulse oximeters. Despite these developments in identifying potential wavelengths, a pulse oximeter that would simultaneously measure SpO_2 and SpCO was not commercially available until Masimo Rad-57 was commercialized. As mentioned previously, a minimum of three wavelengths are required to measure SpO_2 and SpCO simultaneously. Based on this assumption, a theoretical model was be established by applying Beer-Lambert's law.

According to Beer-Lambert's law, the total absorbance for n absorbing substances is the sum of absorbance of each substance corresponding to its concentration, absorptivity and path length. For simultaneous measurement of SpCO and SpO_2, the total absorbance for three homogenously mixed absorbing substances (HbO_2, RHb and HbCO) at each wavelength is given as

$$A(\lambda_1) = a_{11}(HbO_2)b + a_{21}(Hb)b + a_{31}(HbCO)b \quad (6.3)$$

$$A(\lambda_2) = a_{12}(HbO_2)b + a_{22}(Hb)b + a_{32}(HbCO)b \quad (6.4)$$

$$A(\lambda_3) = a_{13}(HbO_2)b + a_{23}(Hb)b + a_{33}(HbCO) \quad (6.5)$$

where,

a_{11}, a_{21}, a_{31} are the absorptivities of HbO_2, Hb and HbCO at wavelength λ_1, respectively,

a_{12}, a_{22}, a_{32} are the absorptivities of HbO_2, Hb and HbCO at wavelength λ_2, respectively,

a_{13}, a_{23}, a_{33} are the absorptivities of HbO_2, Hb and HbCO at wavelength λ_3, respectively,

λ_1, λ_2, λ_3 are the chosen wavelengths,

b is the optical path length.

Dividing equations (Eq. 6.3), (Eq. 6.4), (Eq. 6.5) by HbO_2, we get

$$\frac{A(\lambda_1)}{HbO_2} = a_{11}b + a_{21}(c_2)b + a_{31}(c_1)b \quad (6.6)$$

$$\frac{A(\lambda_2)}{HbO_2} = a_{12}b + a_{22}(c_2)b + a_{32}(c_1)b \quad (6.7)$$

$$\frac{A(\lambda_3)}{HbO_2} = a_{13}b + a_{23}(c_2)b + a_{33}(c_1)b \quad (6.8)$$

where,

c_2= Hb/HbO_2

c_1= $HbCO/HbO_2$

Let $$r_1 = \frac{A(\lambda_1)}{A(\lambda_2)} = \frac{[a_{11} + a_{21}(c_2) + a_{31}(c_1)]b}{[a_{12} + a_{22}(c_2) + a_{32}(c_1)]b} \quad (6.9)$$

and $$r_2 = \frac{A(\lambda_3)}{A(\lambda_2)} = \frac{[a_{13} + a_{23}(c_2) + a_{33}(c_1)]b}{[a_{12} + a_{22}(c_2) + a_{32}(c_1)]b} \quad (6.10)$$

From Eq. 6.9 and Eq. 6.10, we get

$$r_1 [a_{12} + a_{22}(c_2) + a_{32}(c_1)] = a_{11} + a_{21}(c_2) + a_{31}(c_1) \quad (6.11)$$

$$r_2 [a_{12} + a_{22}(c_2) + a_{32}(c_1)] = a_{13} + a_{23}(c_2) + a_{33}(c_1) \quad (6.12)$$

Grouping the c_1 and c_2 terms in Eq. 6.11 and Eq. 6.12,

$$r_1a_{12} - (a_{11}) = (a_{21} - r_1a_{22})c_2 + (a_{31} - r_1a_{32})c_1 \quad (6.13)$$

$$r_2a_{12} - (a_{13}) = (a_{23} - r_2a_{22})c_2 + (a_{33} - r_2a_{32})c_1 \quad (6.14)$$

Simultaneous equations (Eq. 6.13- Eq. 6.14) can be solved for c_1 and c_2 using Cramer's rule as shown below.

$$\Delta = \begin{bmatrix}(a_{21} - r_1a_{22}) & (a_{31} - r_1a_{32})\\ (a_{23} - r_2a_{22}) & (a_{33} - r_2a_{32})\end{bmatrix} \quad (6.15)$$

$$c_1 = \frac{1}{\Delta}\begin{bmatrix}(a_{21} - r_1a_{22}) & r_1a_{12} - (a_{11})\\ (a_{23} - r_2a_{22}) & r_2a_{12} - (a_{13})\end{bmatrix} \quad (6.16)$$

$$c_2 = \frac{1}{\Delta}\begin{bmatrix}r_1a_{12} - (a_{11}) & (a_{31} - r_1a_{32})\\ r_2a_{12} - (a_{13}) & (a_{33} - r_2a_{32})\end{bmatrix} \quad (6.17)$$

Solving for Δ using Eq. 6.15,

$$\Delta=(a_{21} - r_1a_{22})(a_{33} - r_2a_{32}) - (a_{31} - r_1a_{32})(a_{23} - r_2a_{22})$$

$$= a_{21}a_{33} - r_2a_{32}a_{21} - r_1a_{22}a_{33} + r_1r_2a_{22}a_{32} - a_{31}a_{23} + r_2a_{31}a_{22} + r_1a_{32}a_{23} - r_1r_2a_{32}a_{22}$$

Simplification yields,

$$\Delta= r_1(a_{32}a_{23} - a_{22}a_{33}) + r_2(a_{31}a_{22} - a_{32}a_{21}) + r_1r_2(a_{22}a_{32} - a_{32}a_{22}) + (a_{21}a_{33} - a_{31}a_{23})$$

$$= r_1(a_{32}a_{23} - a_{22}a_{33}) + r_2(a_{31}a_{22} - a_{32}a_{21}) + (a_{21}a_{33} - a_{31}a_{23}) \quad (6.18)$$

Solving for c_1 using Eq. 6.16,

$$c_1 = \frac{1}{\Delta}[(a_{21} - r_1a_{22})(r_2a_{12} - a_{13}) - (r_1a_{12} - a_{11})(a_{23} - r_2a_{22})]$$

$$= \frac{1}{\Delta}[r_2 a_{21} a_{12} - a_{21} a_{13} - r_1 r_2 a_{22} a_{12} + r_1 a_{22} a_{13} - r_1 a_{12} a_{23} + r_1 r_2 a_{12} a_{22} + a_{11} a_{23} - r_2 a_{11} a_{22}]$$

Simplification yields,

$$c_1 = \frac{1}{\Delta}[\, r_1(a_{22} a_{13} - a_{12} a_{23}) + r_2(a_{21} a_{12} - a_{11} a_{22}) + r_1 r_2(a_{12} a_{22} - a_{22} a_{12}) + (a_{11} a_{23} - a_{21} a_{13})]$$

$$c_1 = \frac{1}{\Delta}[r_1(a_{22} a_{13} - a_{12} a_{23}) + r_2(a_{21} a_{12} - a_{11} a_{22}) + (a_{11} a_{23} - a_{21} a_{13})] \quad (6.19)$$

Solving for c_2 using Eq. 6.17,

$$c_2 = \frac{1}{\Delta}[\, (r_1 a_{12} - a_{11})(a_{33} - r_2 a_{32}) - (a_{31} - r_1 a_{32})(r_2 a_{12} - a_{13})]$$

$$= \frac{1}{\Delta}[r_1 a_{12} a_{33} - r_1 r_2 a_{12} a_{32} - a_{11} a_{33} + r_2 a_{11} a_{32} - r_2 a_{31} a_{12} + a_{31} a_{13} + r_1 r_2 a_{32} a_{12} - r_1 a_{32} a_{13}]$$

Simplification yields,

$$c_2 = \frac{1}{\Delta}[r_1(a_{12} a_{33} - a_{32} a_{13}) + r_2(a_{11} a_{32} - a_{31} a_{12}) + r_1 r_2(a_{32} a_{12} - a_{12} a_{32}) + (a_{31} a_{13} - a_{11} a_{33})]$$

$$c_2 = \frac{1}{\Delta}[r_1(a_{12} a_{33} - a_{32} a_{13}) + r_2(a_{11} a_{32} - a_{31} a_{12}) + (a_{31} a_{13} - a_{11} a_{33})] \quad (6.20)$$

The formula for SpO_2 and SpCO is given by Eq. 6.21 and Eq. 6.22.

$$SpO_2 = \frac{[HbO_2]}{[HbCO]+[HbO_2]+[RHb]} = \frac{1}{1+c_2+c_1} \quad (6.21)$$

$$SpCO = \frac{[HbCO]}{[HbCO]+[HbO_2]+[RHb]} = \frac{c_1}{1+c_2+c_1} \quad (6.22)$$

Substituting the values of Δ, c_1 and c_2 in Eq. 6.21,

$$SpO_2 = \frac{1}{1 + \frac{1}{\Delta}[r_1(a_{22} a_{13} - a_{12} a_{23}) + r_2(a_{21} a_{12} - a_{11} a_{22}) + (a_{11} a_{23} - a_{21} a_{13})]} =$$

$$= \frac{1}{+\frac{1}{\Delta}[r_1(a_{12} a_{33} - a_{32} a_{13}) + r_2(a_{11} a_{32} - a_{31} a_{12}) + (a_{31} a_{13} - a_{11} a_{33})]}$$

$$SpO_2 = \frac{\Delta}{\Delta + [r_1(a_{22}a_{13} - a_{12}a_{23}) + r_2(a_{21}a_{12} - a_{11}a_{22}) + (a_{11}a_{23} - a_{21}a_{13})]} =$$

$$= \frac{\Delta}{+ [r_1(a_{12}a_{33} - a_{32}a_{13}) + r_2(a_{11}a_{32} - a_{31}a_{12}) + (a_{31}a_{13} - a_{11}a_{33})]}$$

$$SpO_2 =$$

$$\frac{r_1(a_{32}a_{23} - a_{22}a_{33}) + r_2(a_{31}a_{22} - a_{32}a_{21}) + (a_{21}a_{33} - a_{31}a_{23})}{r_1(a_{32}a_{23} - a_{22}a_{33} + a_{22}a_{13} - a_{12}a_{23} + a_{12}a_{33} - a_{32}a_{13}) + r_2(a_{31}a_{22} - a_{32}a_{21} + a_{21}a_{12} - a_{11}a_{22} + a_{11}a_{32} - a_{31}a_{12})} =$$

$$= \frac{r_1(a_{32}a_{23} - a_{22}a_{33}) + r_2(a_{31}a_{22} - a_{32}a_{21}) + (a_{21}a_{33} - a_{31}a_{23})}{+(a_{21}a_{33} - a_{31}a_{23} + a_{11}a_{23} - a_{21}a_{13}a_{31}a_{13} - a_{11}a_{33}} \quad (6.23)$$

Eq. 6.23 can be written as

$$SpO_2 = \frac{Ar_1 + Br_2 + C}{Dr_1 + Er_2 + F} \quad (6.24)$$

where,

$A = (a_{32}a_{23} - a_{22}a_{33})$

$B = (a_{31}a_{22} - a_{32}a_{21})$

$C = (a_{21}a_{33} - a_{31}a_{23})$

$D = (a_{32}a_{23} - a_{22}a_{33} + a_{22}a_{13} - a_{12}a_{23} + a_{12}a_{33} - a_{32}a_{13})$

$E = (a_{31}a_{22} - a_{32}a_{21} + a_{21}a_{12} - a_{11}a_{22} + a_{11}a_{32} - a_{31}a_{12})$

$F = (a_{21}a_{33} - a_{31}a_{23} + a_{11}a_{23} - a_{21}a_{13}a_{31}a_{13} - a_{11}a_{33})$

Similarly, substituting for c_1, c_2 and Δ, in Eq. 6.22,

SpCO=

$$\frac{[r_1(a_{22}a_{13} - a_{12}a_{23}) + r_2(a_{21}a_{12} - a_{11}a_{22}) + (a_{11}a_{23} - a_{21}a_{13})]}{r_1(a_{32}a_{23} - a_{22}a_{33} + a_{22}a_{13} - a_{12}a_{23} + a_{12}a_{33} - a_{32}a_{13}) + r_2(a_{31}a_{22} - a_{32}a_{21} + a_{21}a_{12} - a_{11}a_{22} + a_{11}a_{32} - a_{31}a_{12})} =$$

$$= \frac{[r_1(a_{22}a_{13} - a_{12}a_{23}) + r_2(a_{21}a_{12} - a_{11}a_{22}) + (a_{11}a_{23} - a_{21}a_{13})]}{+(a_{21}a_{33} - a_{31}a_{23} + a_{11}a_{23} - a_{21}a_{13}a_{31}a_{13} - a_{11}a_{33}} \quad (6.25)$$

Eq. 6.25 can be written as shown in Eq. 6.26.

$$SpCO = \frac{A'r_1 + B'r_2 + C'}{D'r_1 + E'r_2 + F'} \tag{6.26}$$

where,

$$A' = (a_{22}a_{13} - a_{12}a_{23})$$

$$B' = (a_{21}a_{12} - a_{11}a_{22})$$

$$C' = (a_{11}a_{23} - a_{21}a_{13})$$

$$D' = (a_{32}a_{23} - a_{22}a_{33} + a_{22}a_{13} - a_{12}a_{23} + a_{12}a_{33} - a_{32}a_{13})$$

$$E' = (a_{31}a_{22} - a_{32}a_{21} + a_{21}a_{12} - a_{11}a_{22} + a_{11}a_{32} - a_{31}a_{12})$$

$$F' = (a_{21}a_{33} - a_{31}a_{23} + a_{11}a_{23} - a_{21}a_{13}a_{31}a_{13} - a_{11}a_{33})$$

Thus, the values of SpO_2 and SpCO when $r_1 = A(\lambda_1)/A(\lambda_2)$ and $r_2 = A(\lambda_3)/A(\lambda_2)$ can be calculated from Eq. 6.24 and Eq. 6.26 using the absorption ratios obtained at desired wavelengths. Since, the wavelengths that would have high sensitivity to changes in SpO_2 and SpCO measurements were not known a priory, models were developed for different possible ratio as follows.

$r_1 = A(\lambda_1)/A(\lambda_2)$ and $r_2 = A(\lambda_1)/A(\lambda_3)$;

$r_1 = A(\lambda_1)/A(\lambda_2)$ and $r_2 = A(\lambda_3)/A(\lambda_1)$;

$r_1 = A(\lambda_1)/A(\lambda_2)$ and $r_2 = A(\lambda_2)/A(\lambda_3)$.

The models obtained for these ratios are shown in the table below.

Table 6.1. Theoretical models derived for different ratio.

$r_1 = A(\lambda_1)/A(\lambda_2)$ and $r_2 = A(\lambda_1)/A(\lambda_3)$

$SpO_2 =$

$$\frac{r_1 (a_{32}a_{21} - a_{22}a_{31}) + r_2(a_{31}a_{23} - a_{21}a_{33}) + r_1r_2(a_{22}a_{33} - a_{32}a_{23})}{r_1 (a_{32}a_{21} - a_{22}a_{31} + a_{12}a_{31} - a_{11}a_{32} + a_{11}a_{22} - a_{12}a_{21}) + r_2(a_{31}a_{23} - a_{21}a_{33} + a_{11}a_{33} - a_{31}a_{13} + a_{21}a_{13} - a_{23}a_{11})} =$$

$$= \frac{r_1 (a_{32}a_{21} - a_{22}a_{31}) + r_2(a_{31}a_{23} - a_{21}a_{33}) + r_1r_2(a_{22}a_{33} - a_{32}a_{23})}{+ r_1r_2(a_{22}a_{33} - a_{32}a_{23} + a_{32}a_{13} - a_{12}a_{33} + a_{12}a_{23} - a_{22}a_{13})}$$

SpCO=

$$\frac{r_1 (a_{11}a_{22} - a_{12}a_{21}) + r_2(a_{21}a_{13} - a_{23}a_{11}) + r_1r_2(a_{12}a_{23} - a_{22}a_{13})}{r_1 (a_{32}a_{21} - a_{22}a_{31} + a_{12}a_{31} - a_{11}a_{32} + a_{11}a_{22} - a_{12}a_{21}) + r_2(a_{31}a_{23} - a_{21}a_{33} + a_{11}a_{33} - a_{31}a_{13} + a_{21}a_{13} - a_{23}a_{11})} =$$

$$=$$

$$\frac{r_1 (a_{11}a_{22} - a_{12}a_{21}) + r_2(a_{21}a_{13} - a_{23}a_{11}) + r_1r_2(a_{12}a_{23} - a_{22}a_{13})}{+ r_1r_2(a_{22}a_{33} - a_{32}a_{23} + a_{32}a_{13} - a_{12}a_{33} + a_{12}a_{23} - a_{22}a_{13})}$$

$r_1 = A(\lambda_1)/A(\lambda_2)$ and $r_2 = A(\lambda_3)/A(\lambda_1)$

$SpO_2 =$

$$\frac{r_1(a_{32}a_{23} - a_{22}a_{33}) + (a_{31}a_{22} - a_{21}a_{32}) + r_1r_2(a_{21}a_{33} - a_{31}a_{23})}{r_1(a_{32}a_{23} - a_{22}a_{33} + a_{13}a_{22} - a_{12}a_{23} + a_{12}a_{33} - a_{32}a_{13}) + (a_{21}a_{31} - a_{32}a_{21} + a_{11}a_{23} - a_{21}a_{13} + a_{31}a_{13} - a_{33}a_{11})} =$$

$$= \frac{r_1(a_{32}a_{23} - a_{22}a_{33}) + (a_{31}a_{22} - a_{21}a_{32}) + r_1r_2(a_{21}a_{33} - a_{31}a_{23})}{+r_1r_2(a_{22}a_{33} - a_{32}a_{23} + a_{32}a_{13} - a_{12}a_{33} + a_{12}a_{23} - a_{22}a_{13})}$$

SpCO=

$$\frac{r_1(a_{13}a_{22} - a_{12}a_{23}) + (a_{11}a_{23} - a_{21}a_{13}) + r_1r_2(a_{21}a_{12} - a_{22}a_{11})}{r_1(a_{32}a_{23} - a_{22}a_{33} + a_{13}a_{22} - a_{12}a_{23} + a_{12}a_{33} - a_{32}a_{13}) + (a_{21}a_{31} - a_{32}a_{21} + a_{11}a_{23} - a_{21}a_{13} + a_{31}a_{13} - a_{33}a_{11})} =$$

$$= \frac{r_1(a_{13}a_{22} - a_{12}a_{23}) + (a_{11}a_{23} - a_{21}a_{13}) + r_1r_2(a_{21}a_{12} - a_{22}a_{11})}{+r_1r_2(a_{22}a_{33} - a_{32}a_{23} + a_{32}a_{13} - a_{12}a_{33} + a_{12}a_{23} - a_{22}a_{13})}$$

$r_1 = A(\lambda_1)/A(\lambda_2)$ and **$r_2 = A(\lambda_2)/A(\lambda_3)$**

$SpO_2 =$

$$\frac{r_2(a_{31}a_{23} - a_{21}a_{33}) + (a_{21}a_{32} - a_{31}a_{22}) + r_1r_2(a_{22}a_{33} - a_{32}a_{23})}{r_2(a_{31}a_{23} - a_{21}a_{33} + a_{21}a_{13} - a_{32}a_{11} + a_{11}a_{33} - a_{31}a_{13}) + (a_{21}a_{32} - a_{31}a_{22} + a_{11}a_{22} - a_{21}a_{12} + a_{31}a_{12} - a_{11}a_{32})} =$$

$$= \frac{r_2(a_{31}a_{23} - a_{21}a_{33}) + (a_{21}a_{32} - a_{31}a_{22}) + r_1r_2(a_{22}a_{33} - a_{32}a_{23})}{+r_1r_2(a_{22}a_{33} - a_{32}a_{23} + a_{12}a_{23} - a_{22}a_{13} + a_{32}a_{13} - a_{12}a_{33})}$$

SpCO=

$$\frac{r_2(a_{21}a_{13} - a_{32}a_{11}) + (a_{11}a_{22} - a_{21}a_{21}) + r_1r_2(a_{12}a_{23} - a_{22}a_{13})}{r_2(a_{31}a_{23} - a_{21}a_{33} + a_{21}a_{13} - a_{32}a_{11} + a_{11}a_{33} - a_{31}a_{13}) + (a_{21}a_{32} - a_{31}a_{22} + a_{11}a_{22} - a_{21}a_{12} + a_{31}a_{12} - a_{11}a_{32})} =$$

$$= \frac{r_2(a_{21}a_{13} - a_{32}a_{11}) + (a_{11}a_{22} - a_{21}a_{21}) + r_1r_2(a_{12}a_{23} - a_{22}a_{13})}{+r_1r_2(a_{22}a_{33} - a_{32}a_{23} + a_{12}a_{23} - a_{22}a_{13} + a_{32}a_{13} - a_{12}a_{33})}$$

Using these theoretical simulations, wavelength combinations that have high sensitivity to changes in both SpO_2 and SpCO can be obtained. Using the wavelengths identified by the theoretical simulation described above, an algorithm that enables simultaneous measurement of SpO_2 and SpCO can be obtained. Note that a noninvasive device which can measure SpCO alone can be developed. However, at any given point, the derivatives of Hb are in chemical equilibrium with each other. Hence, as the concentrations of HbCO decreases, the relative concentration of HbO_2 increases and vice versa. Therefore, we need a minimum of three wavelengths to measure the concentrations of Hb, HbO_2 and HbCO in order to calculate SpCO. As shown in Eq. 6.21-6.22, using these concentrations of Hb, HbO_2 and HbCO necessary to calculate SpCO, SpO_2 can also be calculated. This makes simultaneous measurement of SpCO and SpO_2 more advantageous commercially because it enables measurement of additional physiological variable using these same concentration values.

6.4. Wavelength ratio selection

As mentioned previously, in the presence of HbCO, a minimum of three wavelengths are required for simultaneous measurement of SpO_2 and SpCO. As shown in Fig. 2.1, the absorption in the wavelength regions between 600 nm and 660 nm increases with increase in SpCO. Between 800 nm to 950 nm, the change in absorption due to changes in SpCO is opposite to the effect observed in the 600-660 nm region. Hence, a ratio of two wavelengths, one from the 600-660 nm region and another from 900-940 nm region will have relatively high sensitivity to changes in SpCO. Two wavelengths (660 nm and 940 nm) that have the highest sensitivity to changes in SpO_2 can be used for simultaneous measurements of SpO_2 and SpCO. Apart from A_{660}/A_{940}, a second ratio of any wavelengths between 600 - 660 nm as well as 940 nm, will have good sensitivity to changes in SpCO. In the sensor used in our lab, there are two LEDs available

in this wavelength region, 610 nm and 643 nm. Therefore, r_1 will correspond to A_{660}/A_{940} and r_2 can be A_{643}/A_{940} or A_{610}/A_{940}. These ratios of r_1 and r_2 will have high sensitivity to changes in SpCO and can be used for simultaneous measurement of SpCO and SpO_2. Although both ratios of A_{643}/A_{940} and A_{610}/A_{940} will have relatively high sensitivity to changes in SpO_2, A_{643}/A_{940} will have a higher sensitivity than A_{610}/A_{940} (Fig. 2.1). Also, the absorption by blood is high around 600 nm and that can cause a low signal to noise ratio at 610 nm. Hence, $r_1 = A_{660}/A_{940}$ and $r_2 = A_{643}/A_{940}$ will have high sensitivity to both SpO_2 and SpCO and can be used for simultaneous measurement of SpO_2 and SpCO. Theoretical simulations were conducted using these wavelengths to confirm the above conclusions.

6.4.1. Validation of the theoretical model for $r_1 = A_{(660/940)}$ and $r_2 = A_{(643/940)}$

In order to validate the theroretical model, theoretical simulation for SpO_2 in the absence of HbCO was obtained at r_1=660/940 and r_2=643/940, by substituting HbCO=0 in Eq. 6.21. When HbCO is absent, SpO_2 value computed by the three-wavelength model and the two-wavelength model (used in commercially available pulse oximeters to measure SpO_2 in the absence of HbCO) should be approximately the same. Hence, SpO_2 calculated from the three wavelength model using $r_1 = A_{(660)/(940)}$ and $r_2 = A_{(643)/(940)}$ was compared to the results obtained for $r_1 = A_{(660)/(940)}$. It was found that SpO_2 calculated from the two and three wavelength model were approximately the same when HbCO=0 (Fig. 6.2-6.3). Therefore, these theoretical simulations, verified that the sensitivity of 660/940 and 643/940 to changes in SpO_2 in the absence of HbCO is approximately the same as the sensitivity of 660/940. Hence, the theoretical model was validated for use of 660 nm, 643 nm and 940 nm as the primary wavelengths.

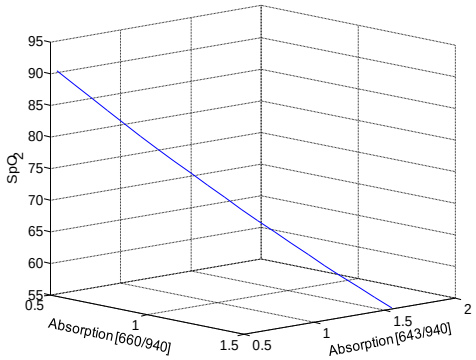

Fig.6.2. Theoretical simulation for $\%SpO_2$ at r_1= 660/940 and r_2=643/940.

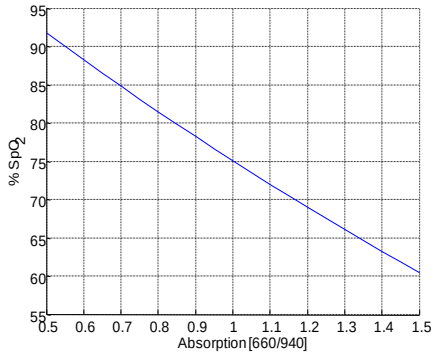

Fig. 6.3. Theoretical simulation for $\%SpO_2$ (HbCO is absent) using two wavelengths (r_1=660/940).

6.5. Theoretical Simulations

SpO_2 and SpCO were theoretically calculated by substituting the absorptivities and absorption ratios in the model. The absorptivity values corresponding to the wavelengths were obtained from the literature [25]. Theoretical absorption ratios for the wavelengths used were approximated based on Fig. 2.1. SpO_2 and SpCO were calculated by substituting these values in the theoretical model. The ratio values were then adjusted to include the clinically significant range of 70 to 100% for SpO_2 and 0-30% for SpCO. Thus, using the models derived for SpCO and SpO_2 for different wavelength ratios, the sensitivity of different wavelength combination to changes in SpO_2 and SpCO were obtained. Five different ratio combinations were obtained from each set of wavelengths considered and theoretical simulations were performed for the different ratios. This was done to verify that all possible combinations that produce high sensitivity were identified. The plots for these theoretical results were generated using Matlab.

6.5.1. Simulations for λ= 660, 610 and 940

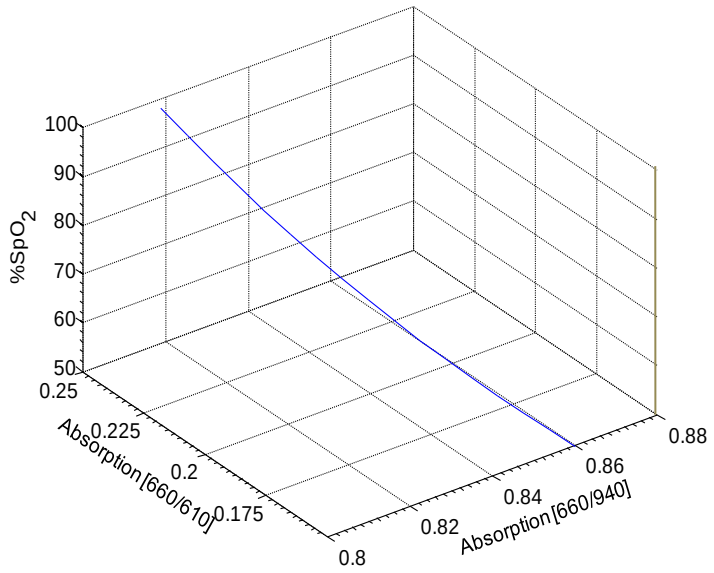

Fig. 6.4. SpO_2 for r_1= 660/940 and r_2=660/610.

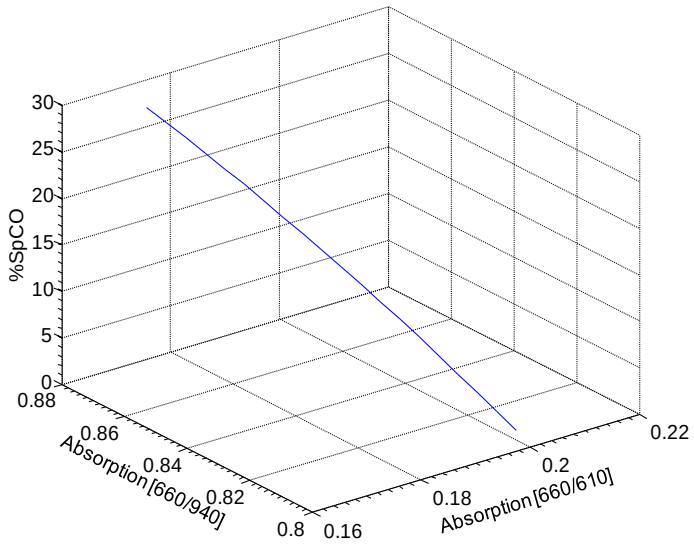

Fig. 6.5. SpCO for r_1= 660/940 and r_2=660/610.

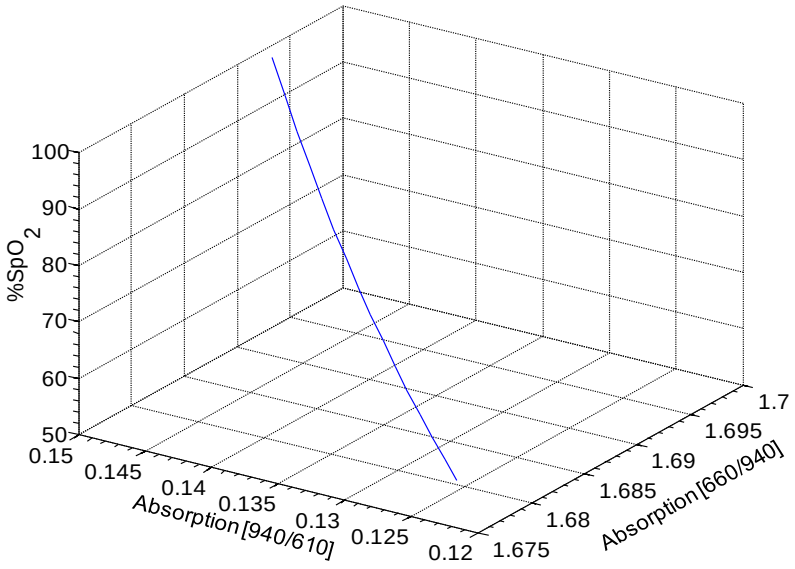

Fig. 6.6. SpO_2 for r_1= 660/940 and r_2=660/610.

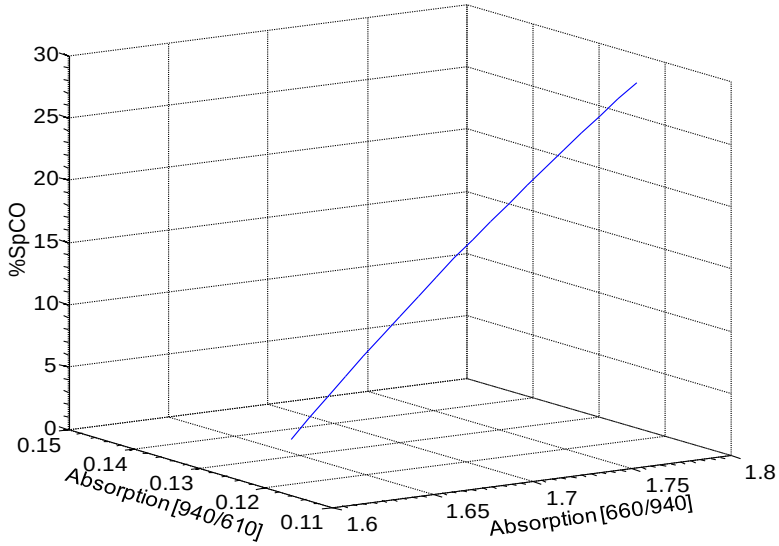

Fig. 6.7. SpCO for r_1= 660/940 and r_2=660/610.

6.5.2. Simulations for λ= 660, 643 and 940

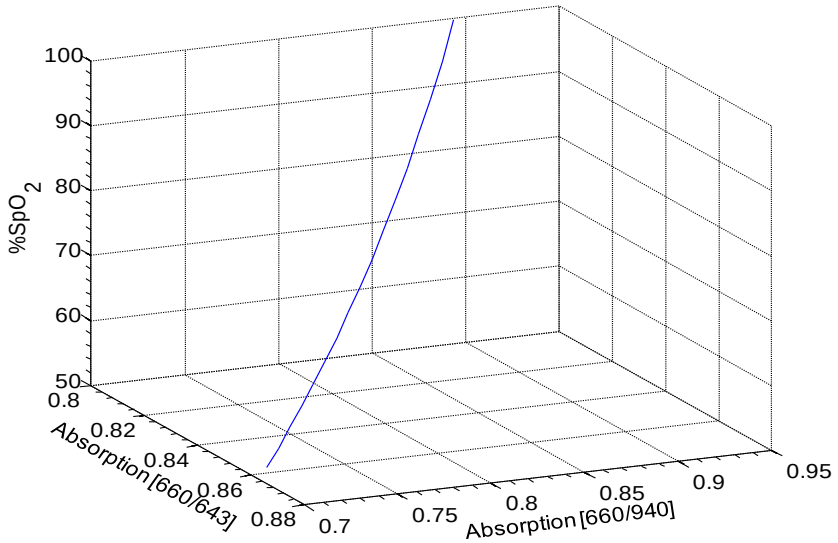

Fig. 6.8. SpO_2 for r_1= 660/643 and r_2=660/940.

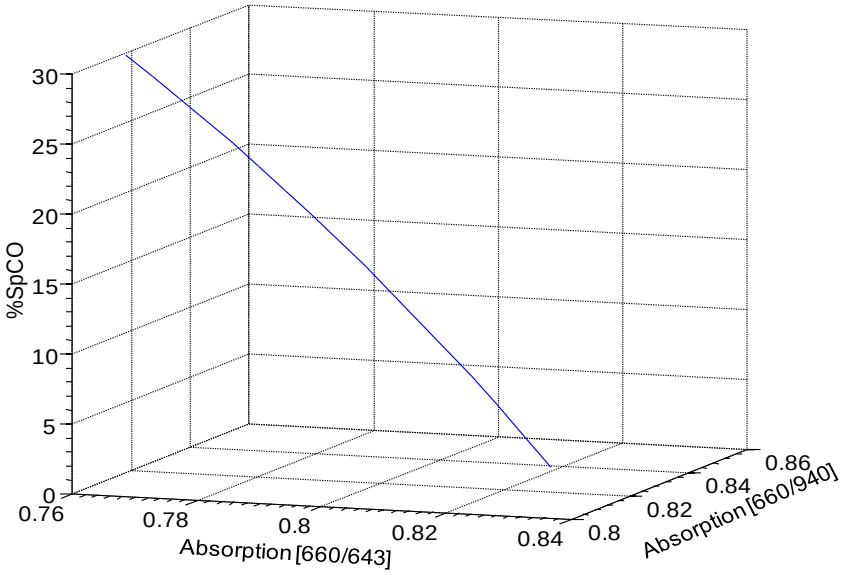

Fig. 6.9. SpCO for r_1= 660/643 and r_2=660/940.

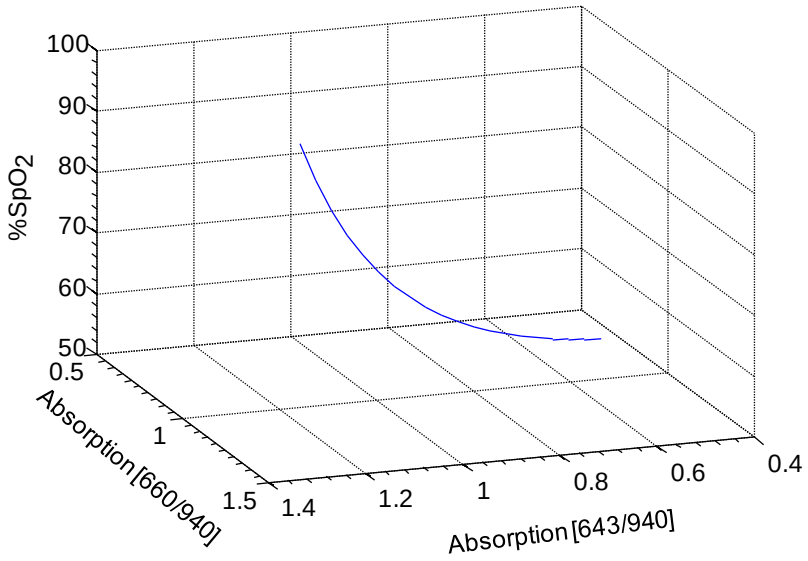

Fig. 6.10. SpO_2 for r_1= 660/940 and r_2=643/940.

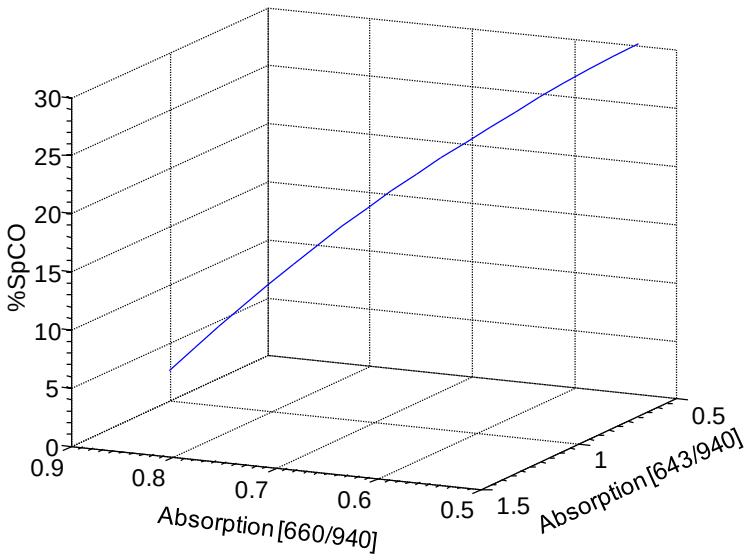

Fig. 6.11. SpCO for r_1= 660/940 and r_2=643/940.

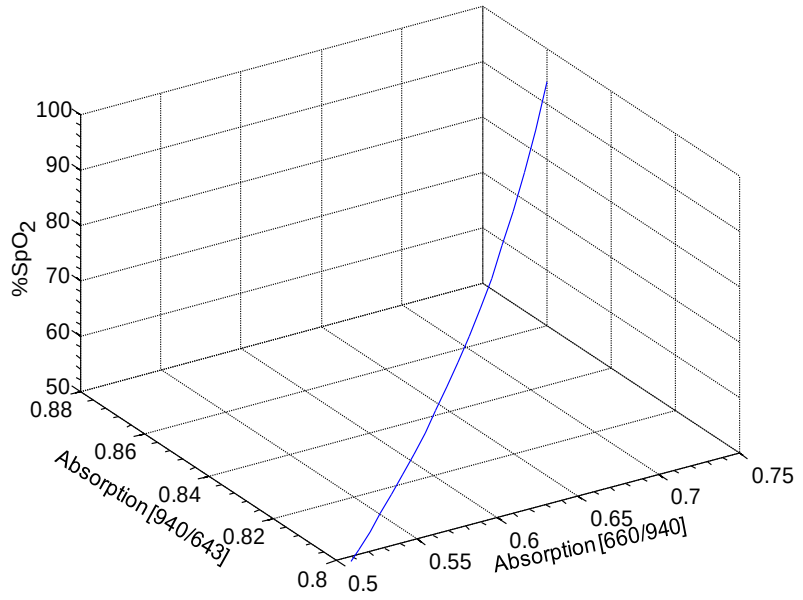

Fig. 6.12. SpO_2 for r_1= 660/940 and r_2=940/643.

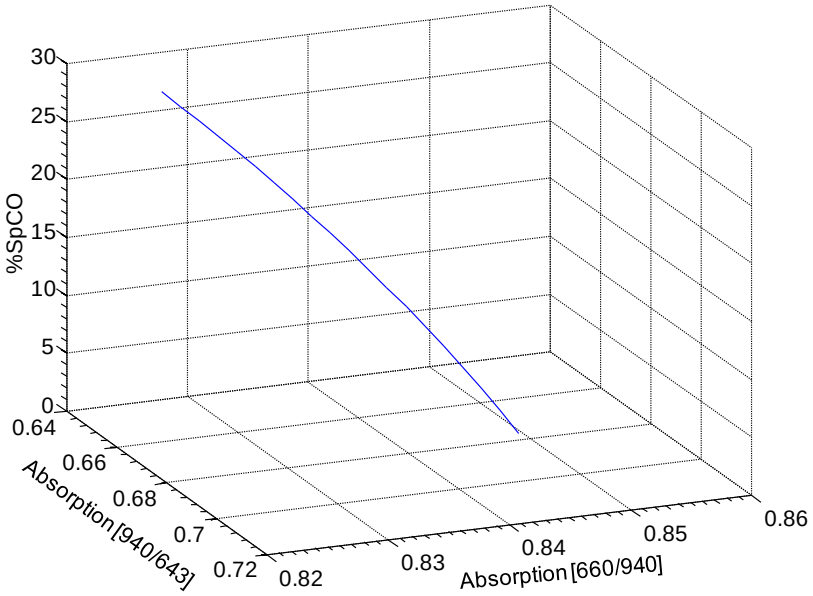

Fig. 6.13. SpCO for r_1= 660/940 and r_2=940/643.

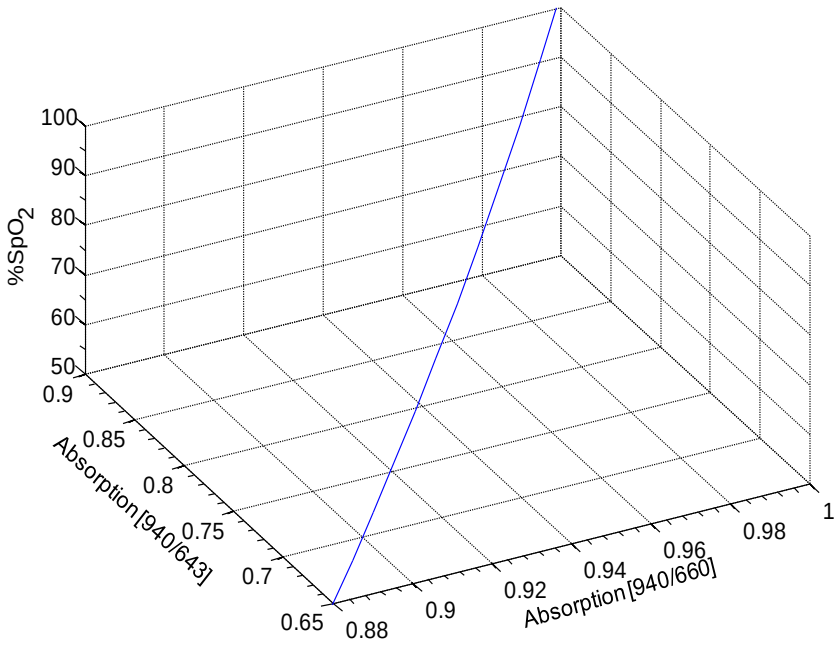

Fig. 6.14. SpO_2 for r_1= 940/643and r_2=940/660.

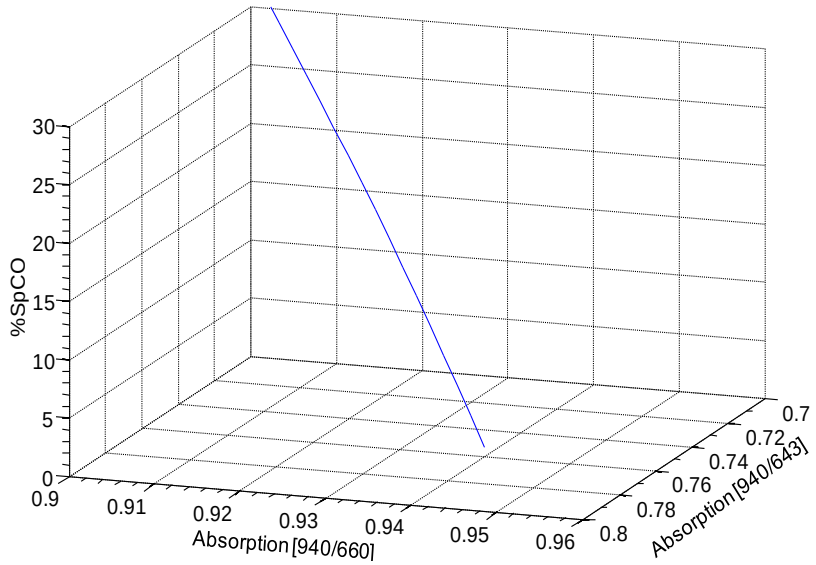

Fig. 6.15. SpCO for r_1= 940/643and r_2=940/660.

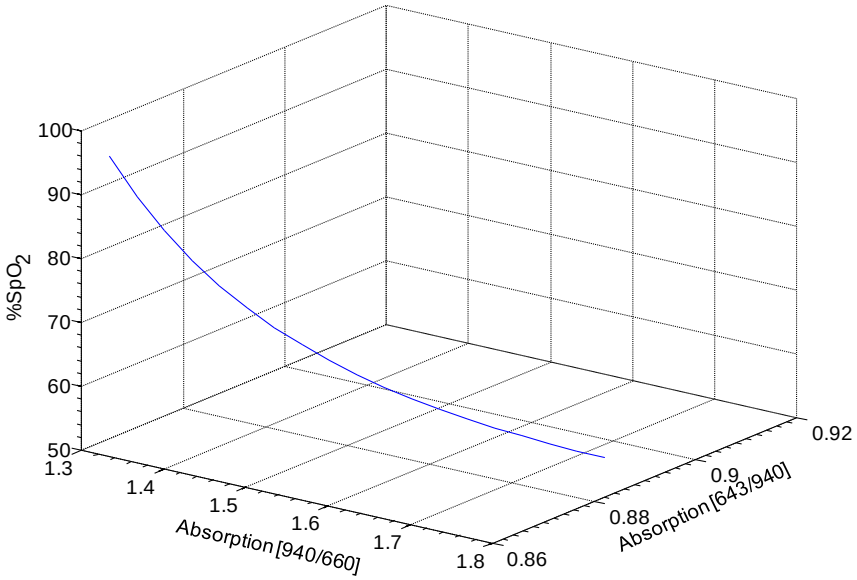

Fig. 6.16. SpO_2 for r_1= 940/660and r_2=643/940.

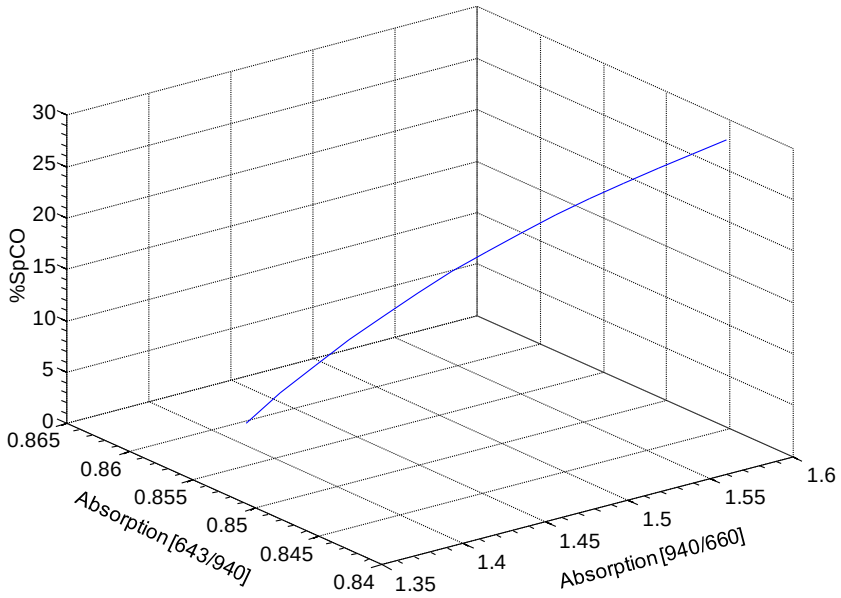

Fig. 6.17. SpCO for r_1= 940/660and r_2=643/940.

6.5.3. Simulations for λ= 660, 740 and 940

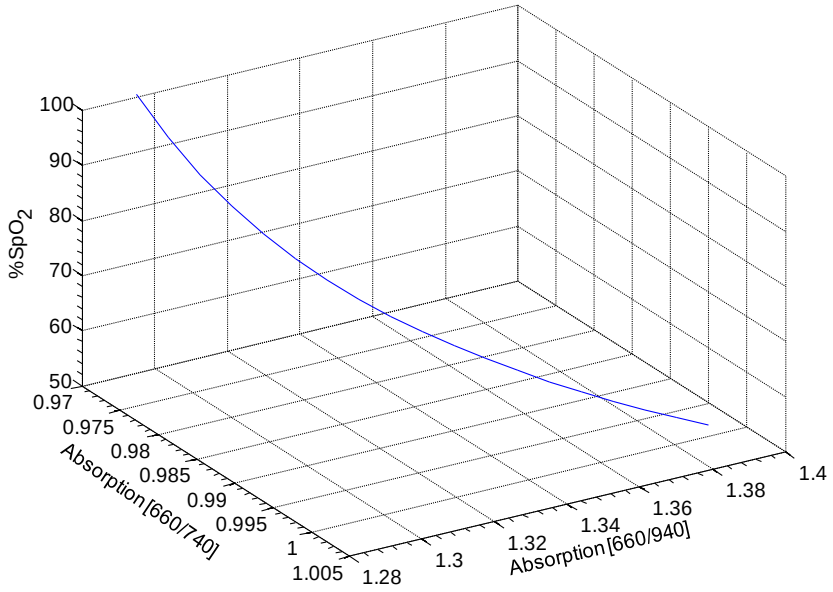

Fig. 6.18. SpO_2 for r_1= 660/740 and r_2=660/940.

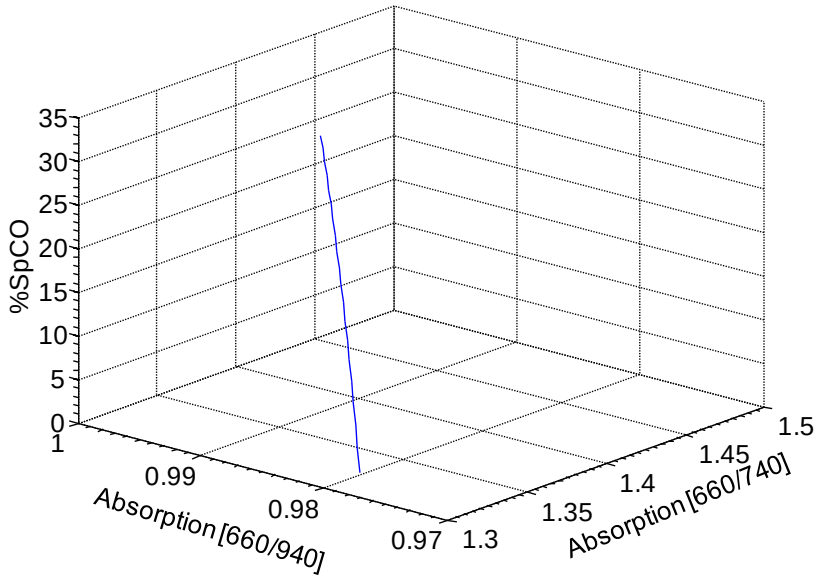

Fig. 6.19. SpCO for r_1= 660/740 and r_2=660/940.

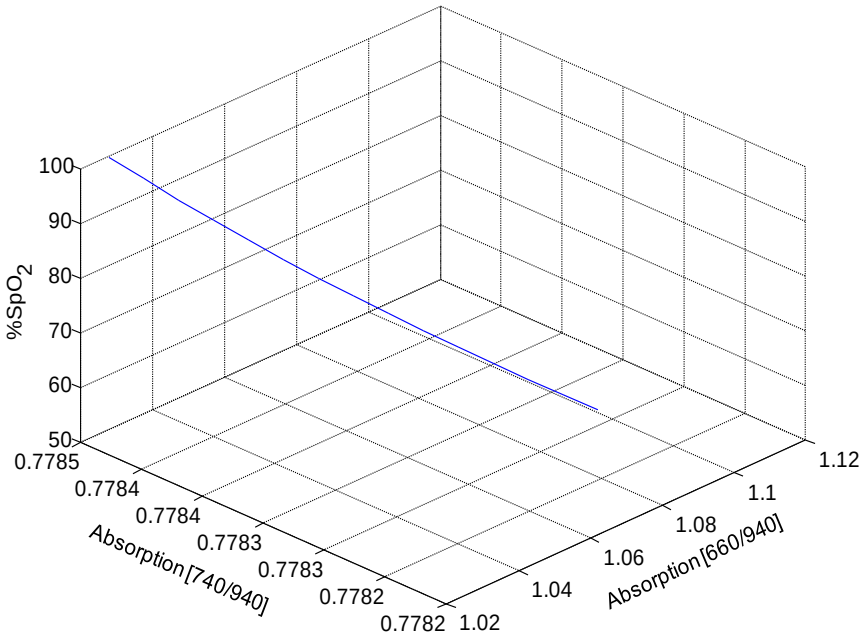

Fig. 6.20. SpO_2 for r_1= 660/940 and r_2=740/940.

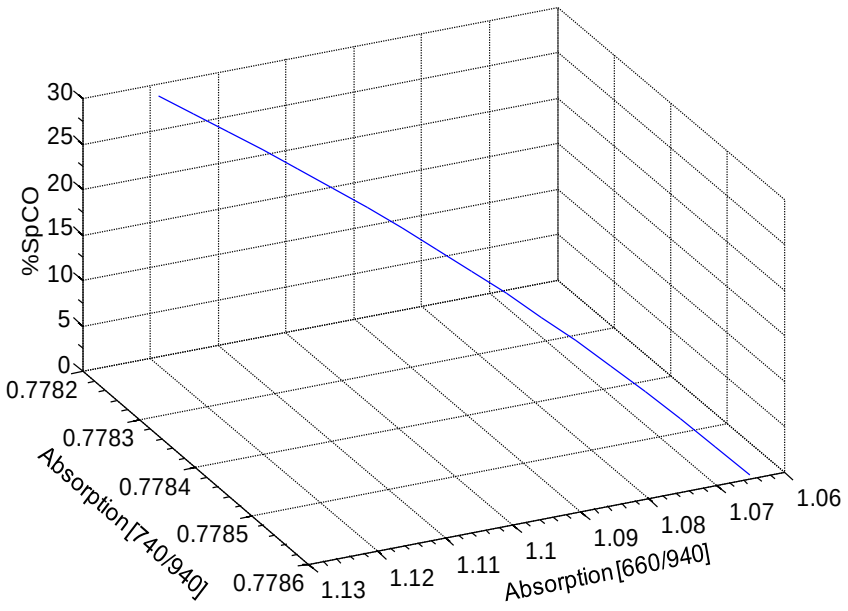

Fig. 6.21. SpCO for r_1= 660/940 and r_2=740/940.

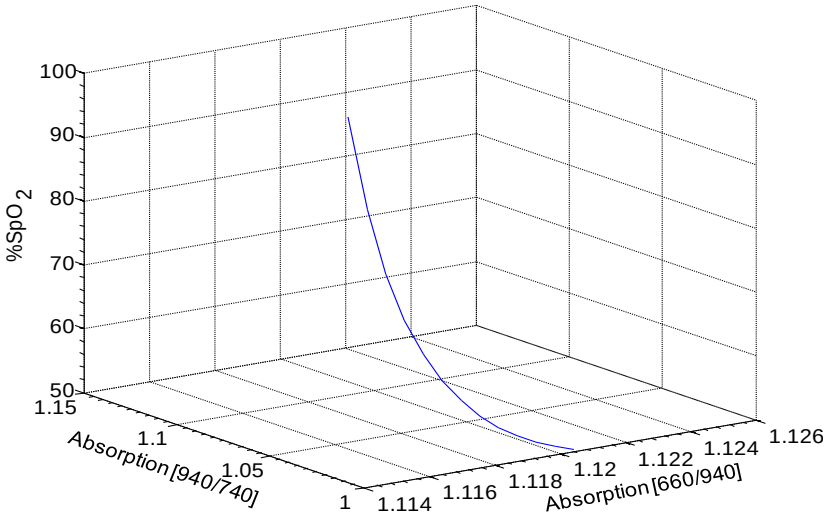

Fig. 6.22. SpO_2 for r_1= 660/940 and r_2=940/740.

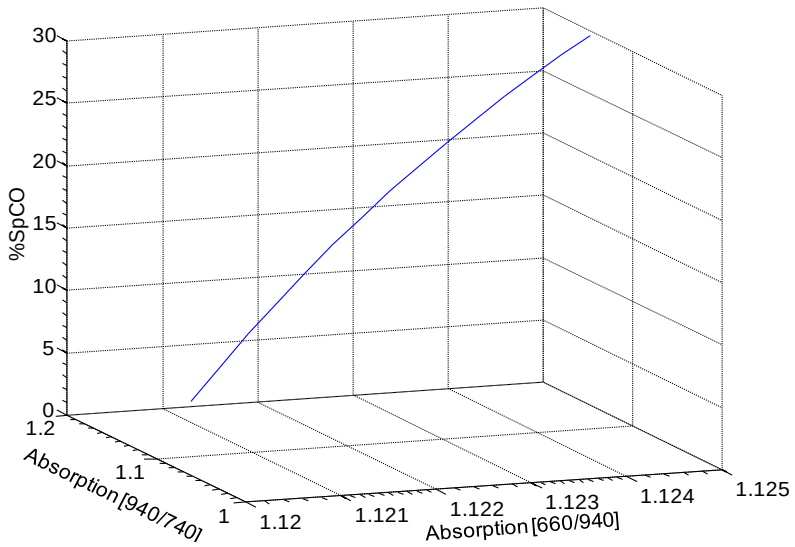

Fig. 6.23. SpCO for r_1= 660/940 and r_2=940/740.

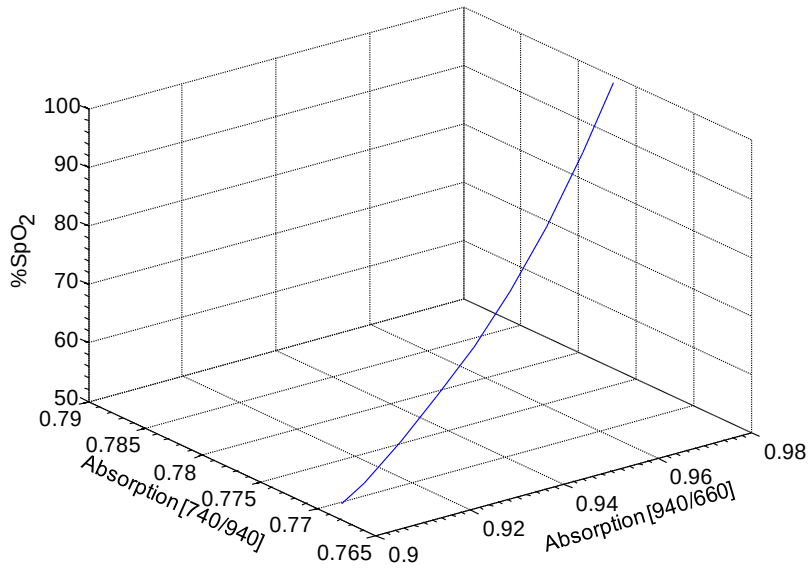

Fig. 6.24. SpO_2 for r_1= 940/660 and r_2=740/940.

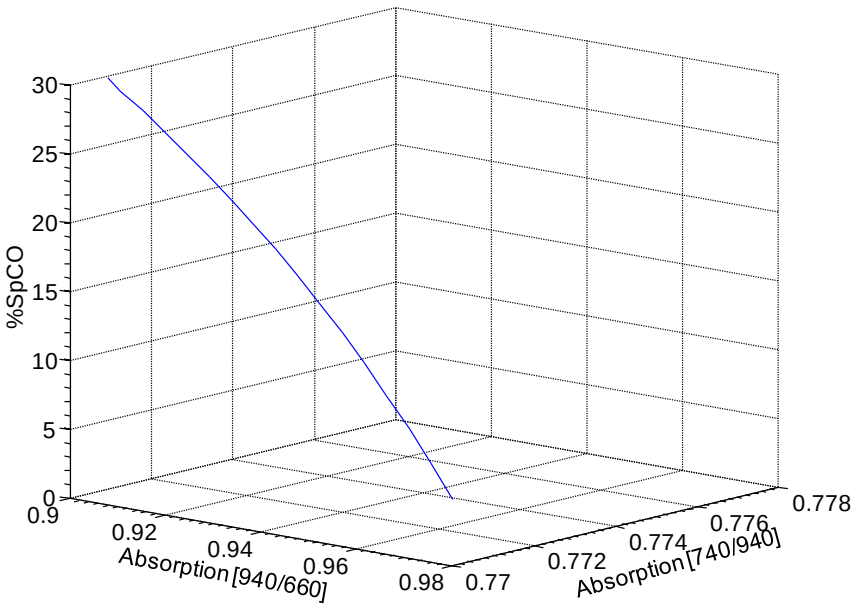

Fig. 6.25. SpCO for r_1= 940/660 and r_2=740/940.

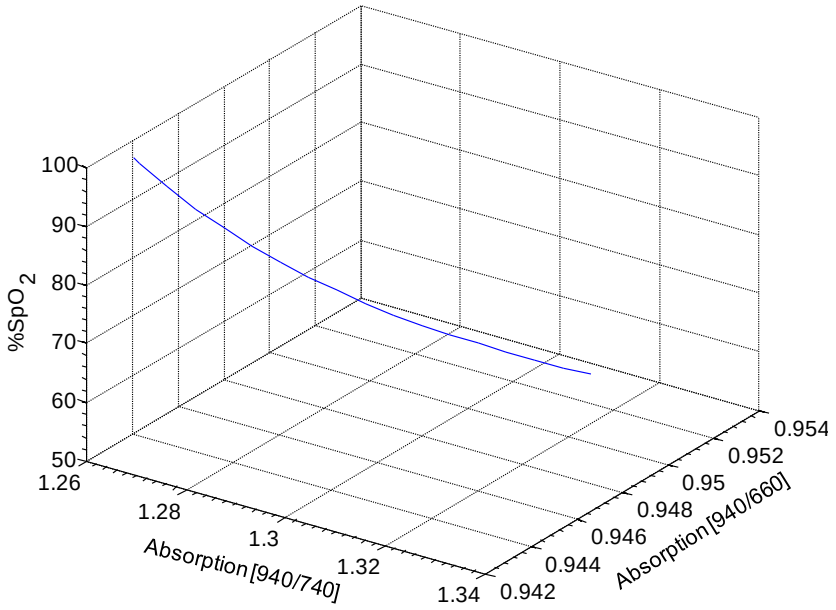

Fig. 6.26. SpO_2 for r_1= 940/660 and r_2=940/740.

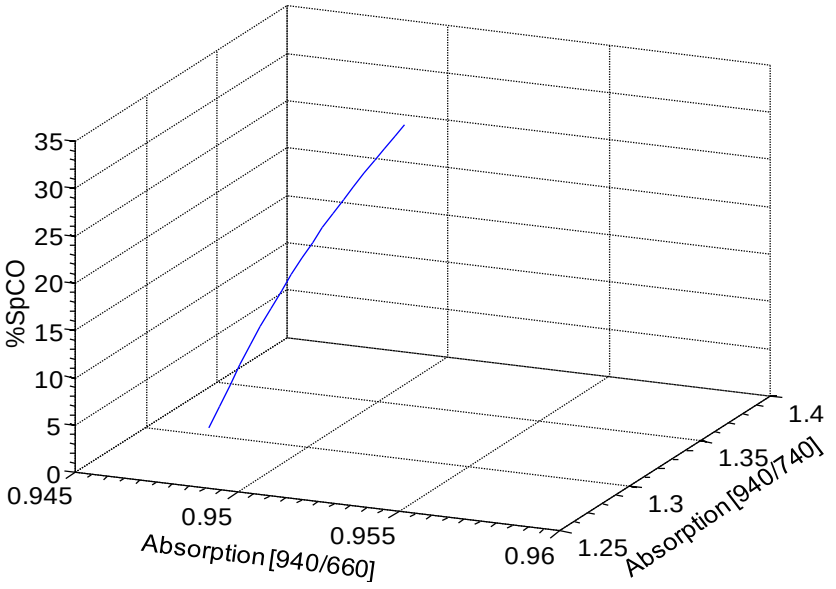

Fig. 6.27. SpCO for r_1= 940/660 and r_2=940/740.

6.5.4. Simulations for λ= 660, 830 and 940

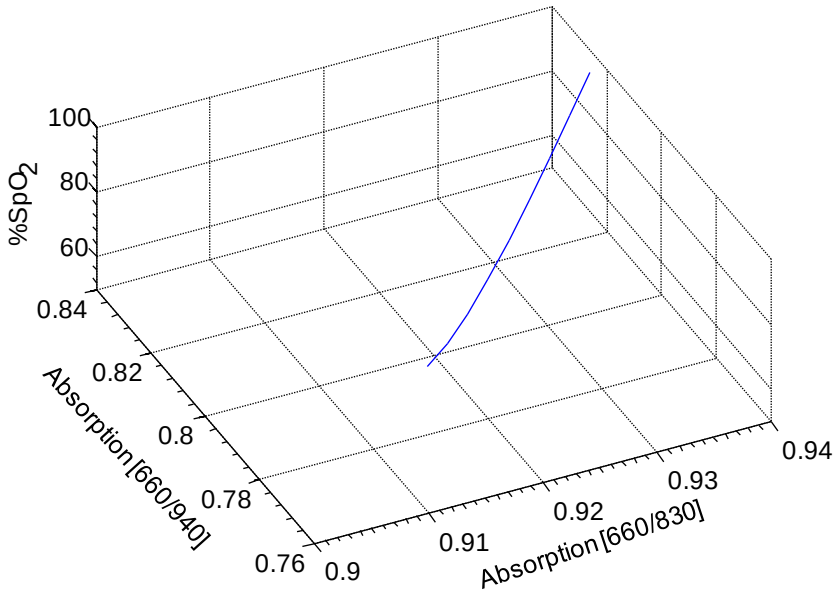

Fig. 6.28. SpO_2 for r_1= 660/940 and r_2=660/830.

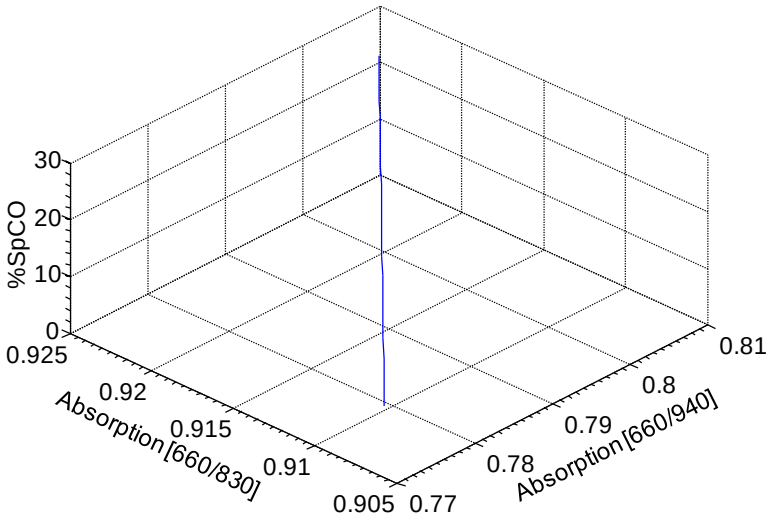

Fig. 6.29. SpCO for r_1= 660/940 and r_2=660/830.

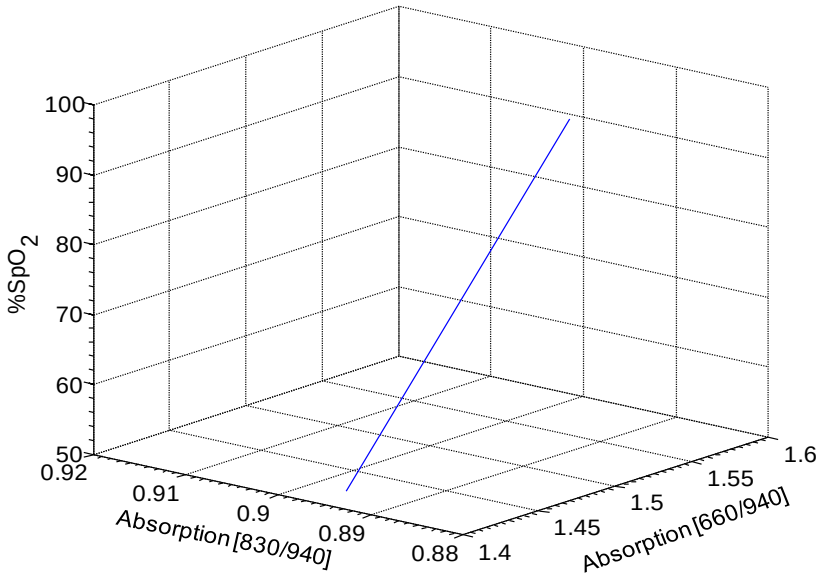

Fig. 6.30. SpO_2 for r_1= 660/940 and r_2=830/940.

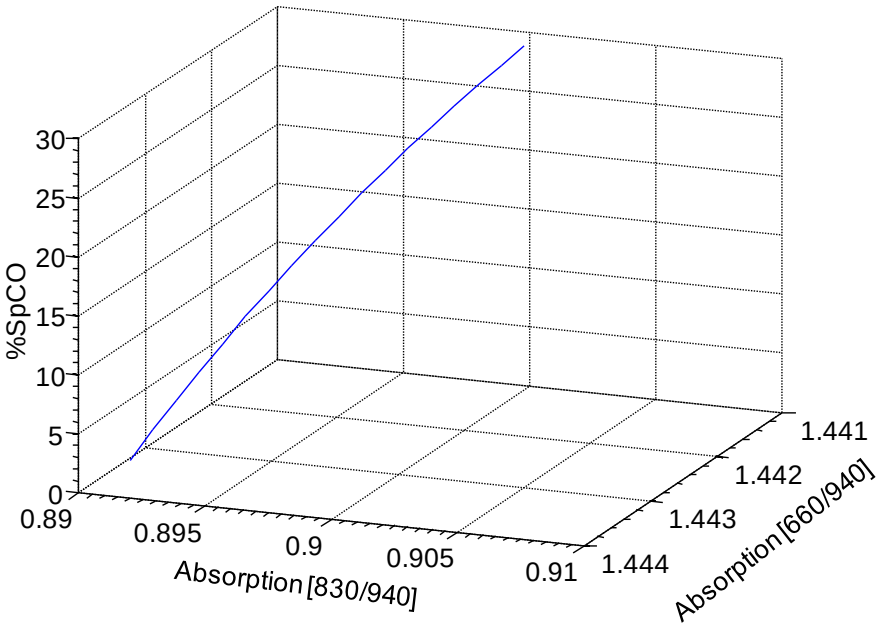

Fig. 6.31. SpCO for r_1= 660/940 and r_2=830/940.

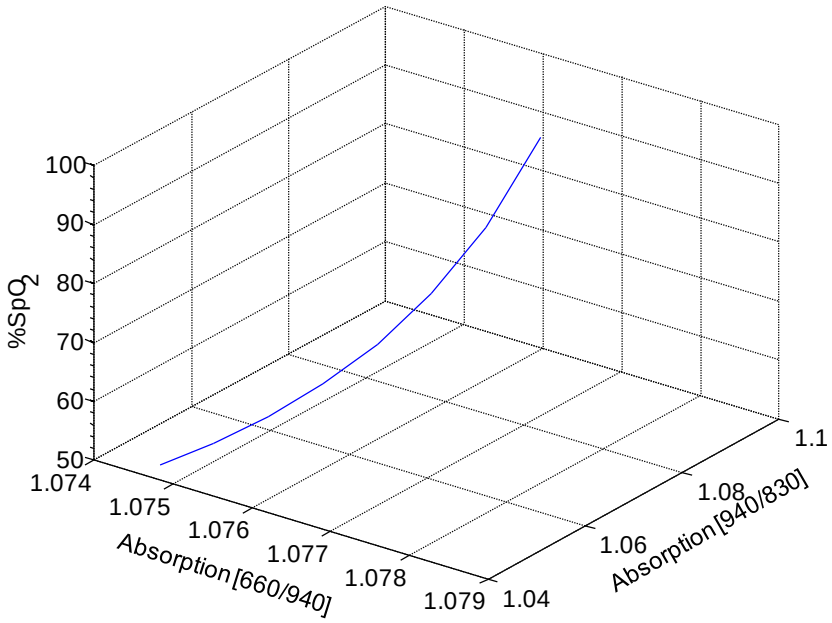

Fig. 6.32. SpO_2 for r_1= 660/940 and r_2=940/830.

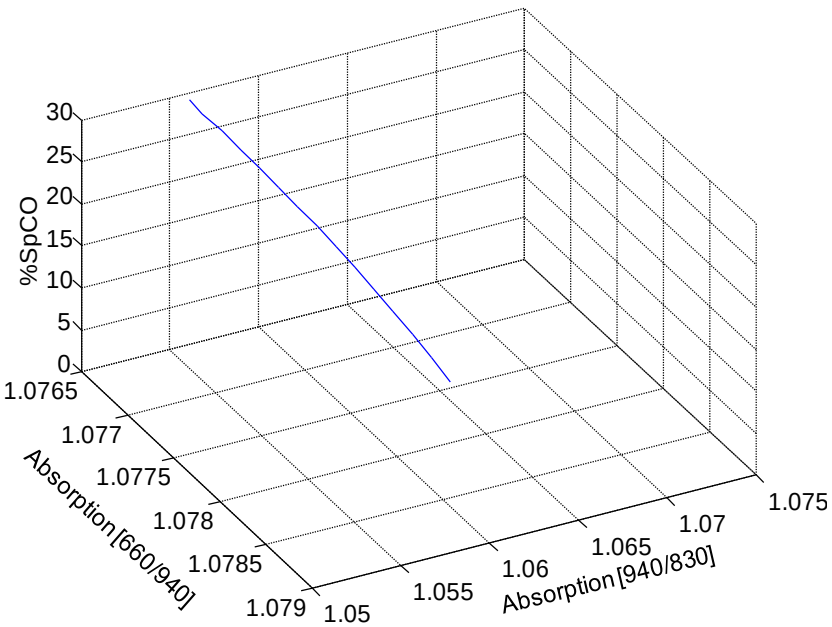

Fig. 6.32. SpCO for r_1= 660/940 and r_2=940/830.

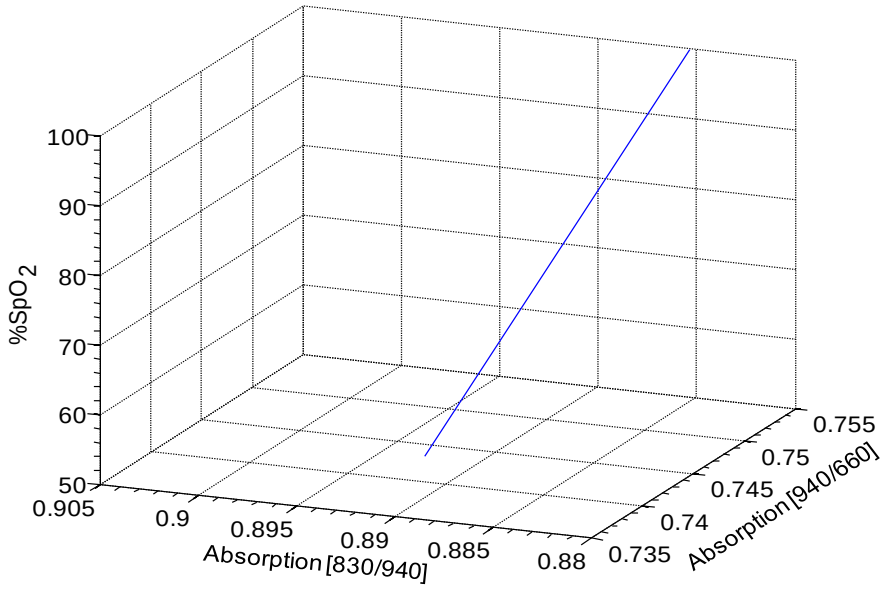

Fig. 6.34. SpO_2 for r_1= 830/940 and r_2=940/660.

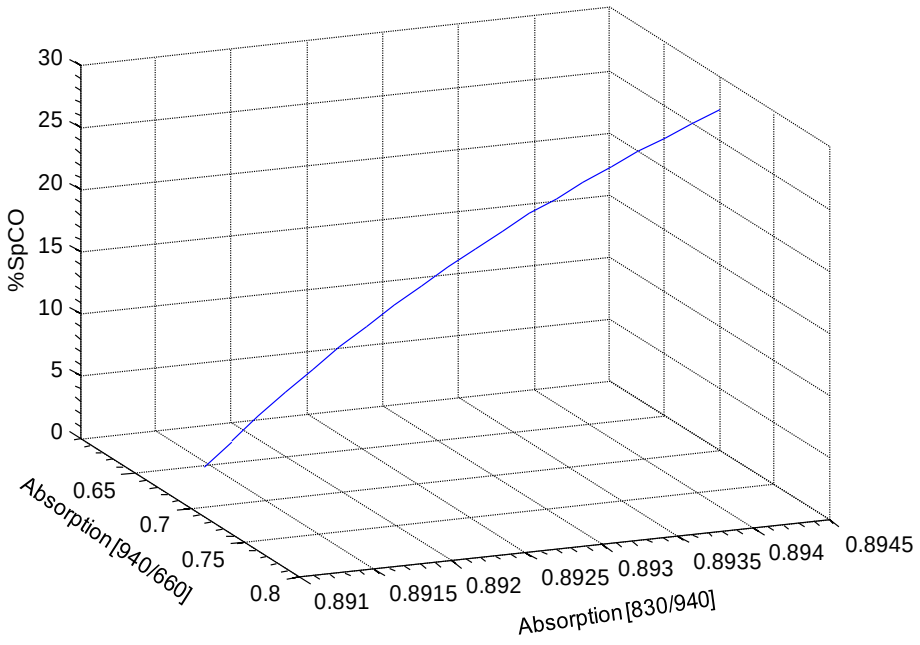

Fig. 6.35. SpCO for r_1= 830/940 and r_2=940/660.

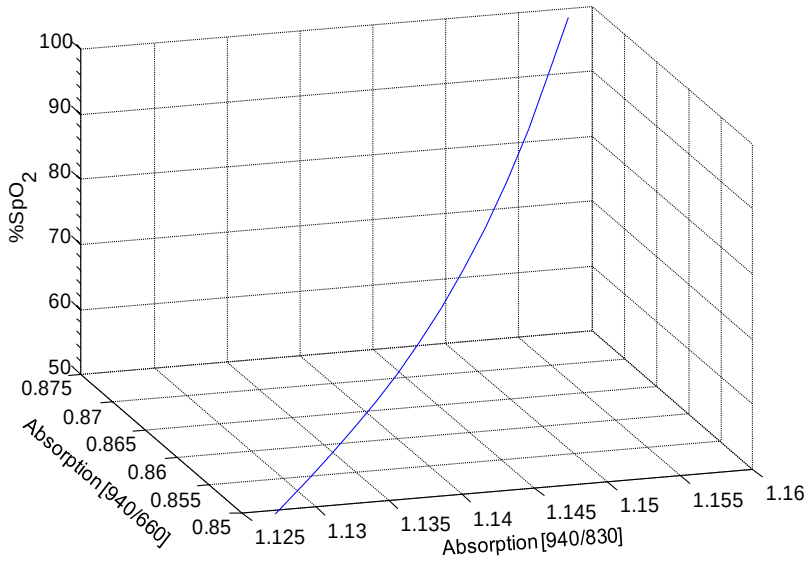

Fig. 6.36. SpO_2 for r_1= 940/660 and r_2=940/830.

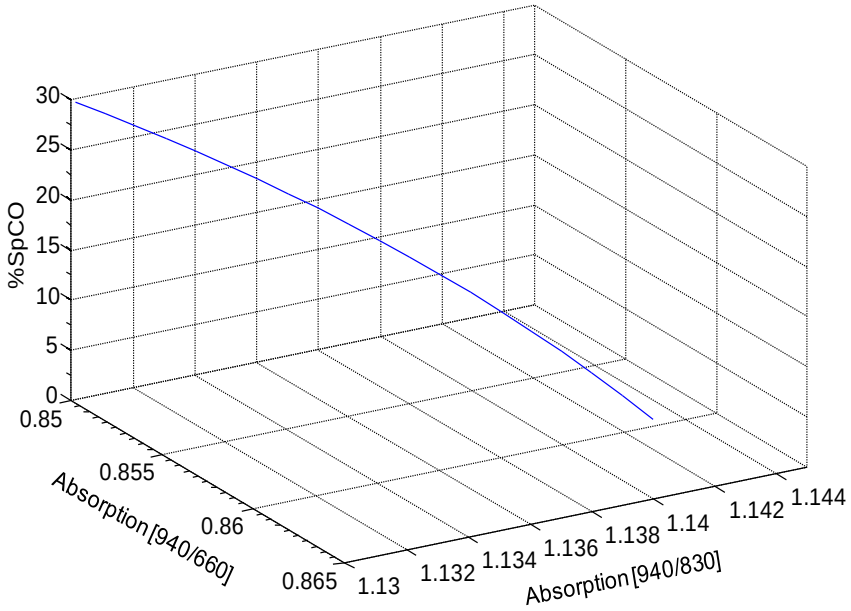

Fig. 6.37. SpCO for r_1= 940/660 and r_2=940/830.

6.5.5. Simulations for λ= 660, 880 and 940

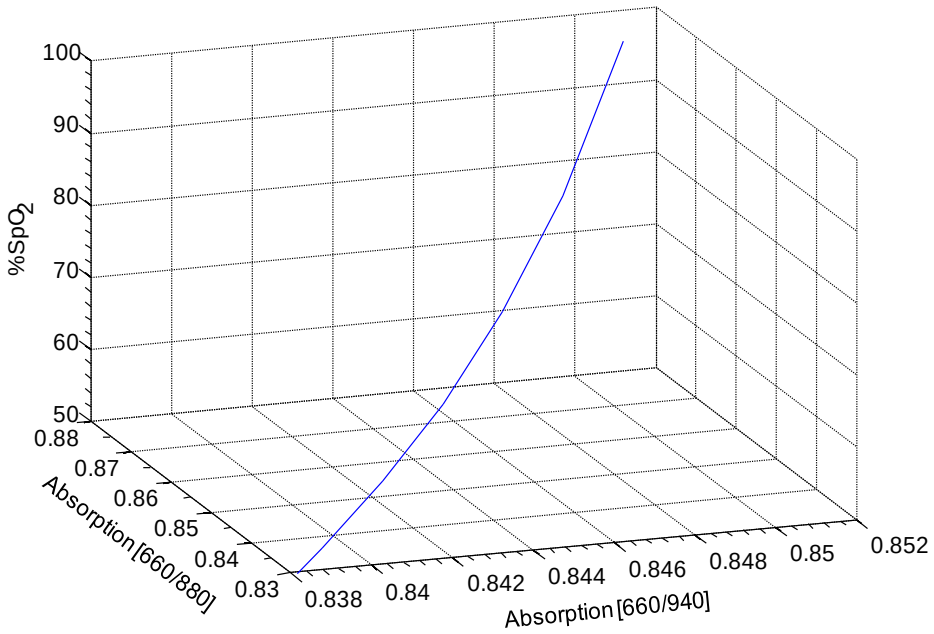

Fig. 6.38. SpO_2 for r_1= 660/880 and r_2=660/940.

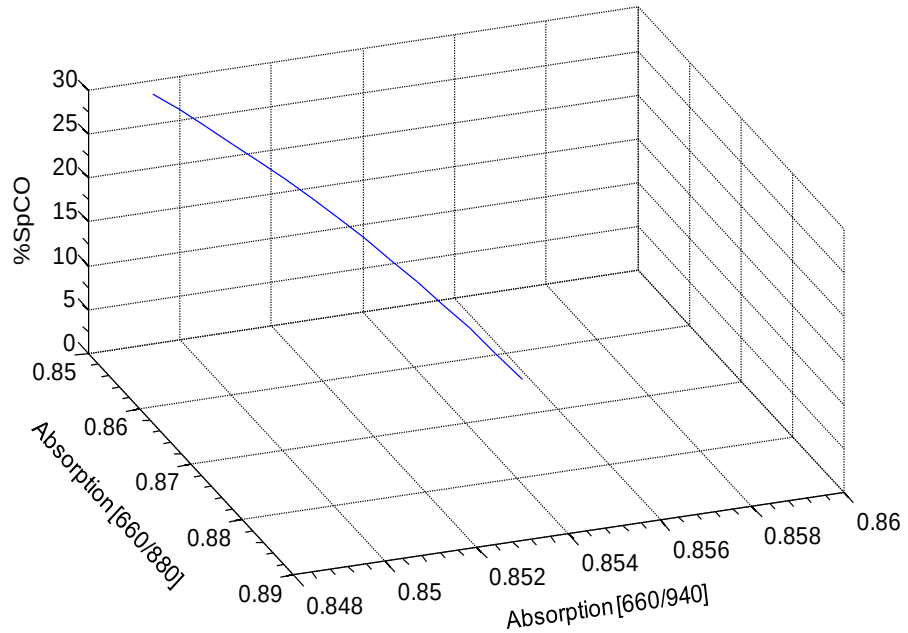

Fig. 6.39. SpCO for r_1= 660/880 and r_2=660/940.

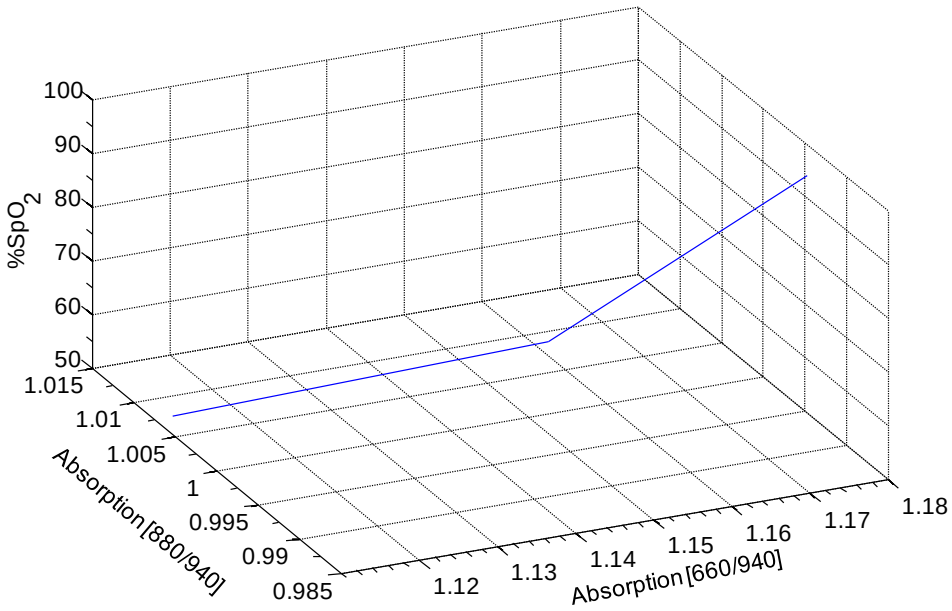

Fig. 6.40. SpO_2 for r_1= 660/940 and r_2=880/940.

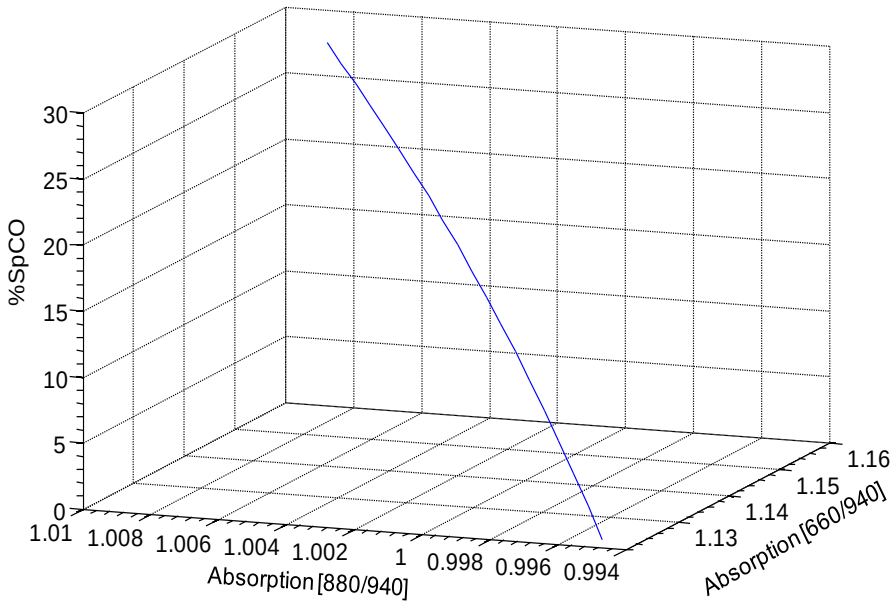

Fig. 6.41. SpCO for r_1= 660/940 and r_2=880/940.

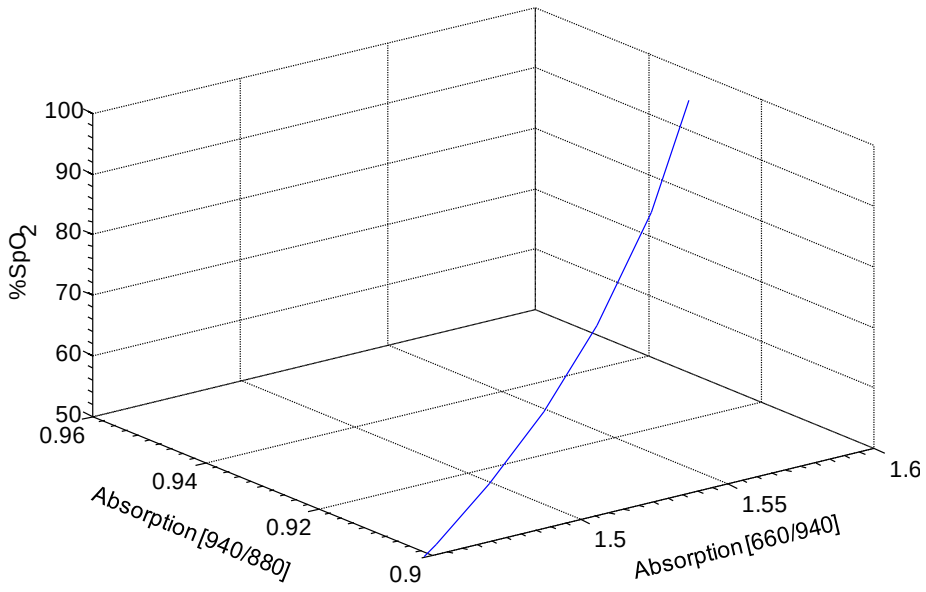

Fig. 6.42. SpO_2 for r_1= 660/940 and r_2=940/880.

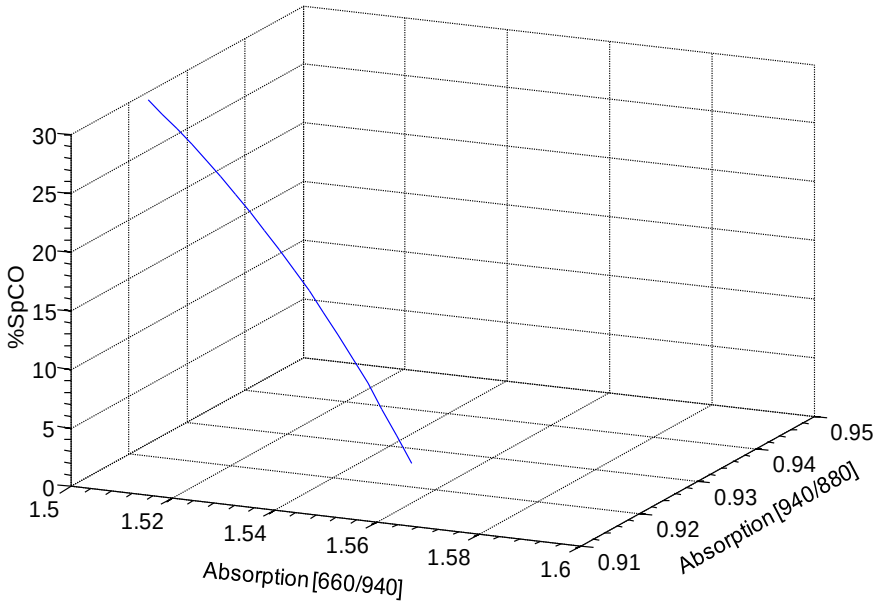

Fig. 6.43. SpCO for r_1= 660/940 and r_2=940/880.

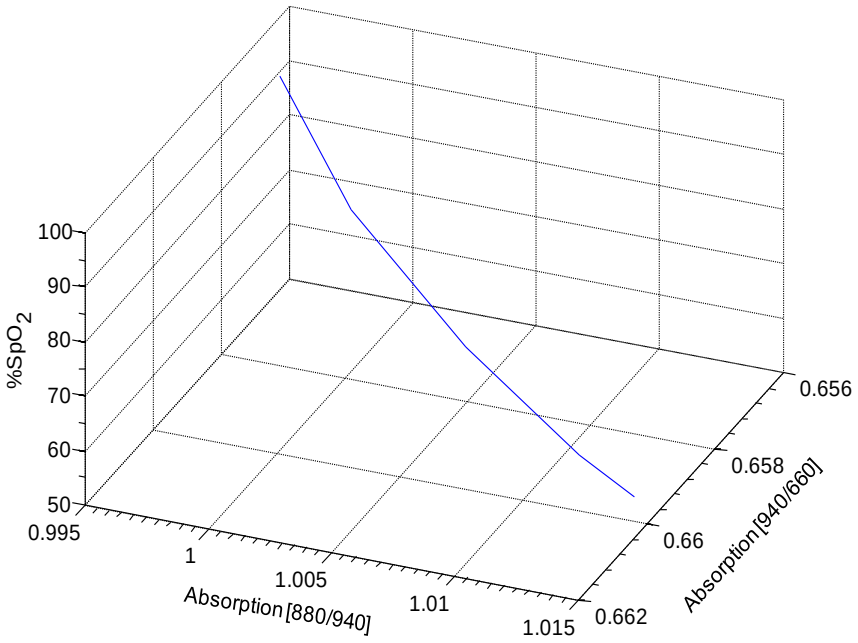

Fig. 6.44. SpO_2 for r_1= 940/660 and r_2=880/940.

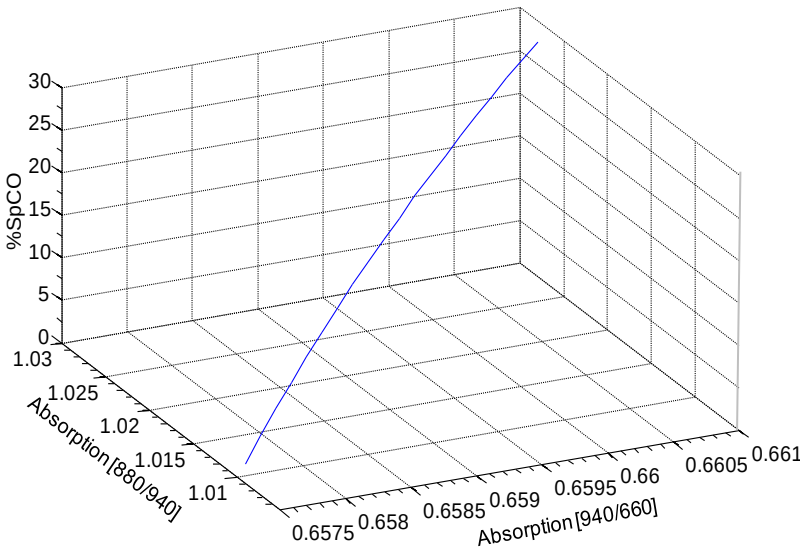

Fig. 6.45. SpCO for r_1= 940/660 and r_2=880/940.

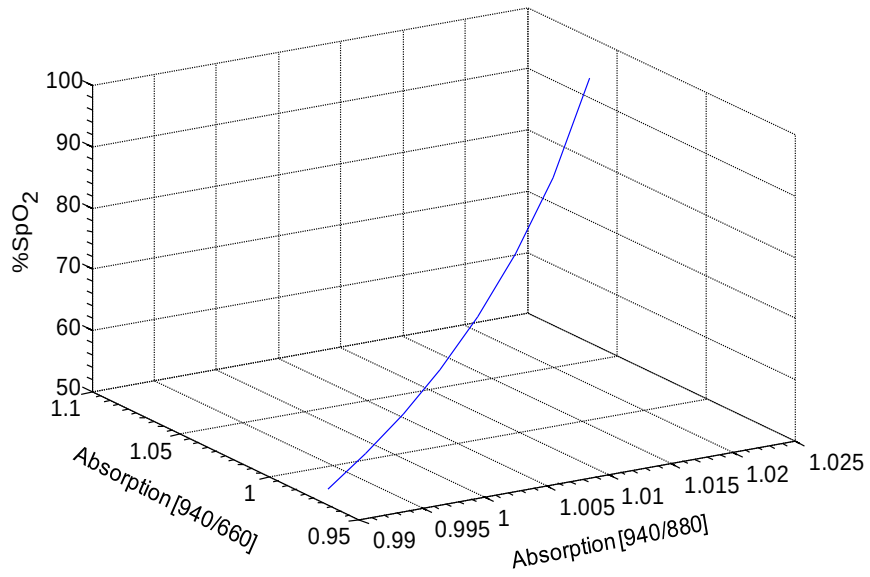

Fig. 6.46. SpO_2 for r_1= 940/660 and r_2=940/880.

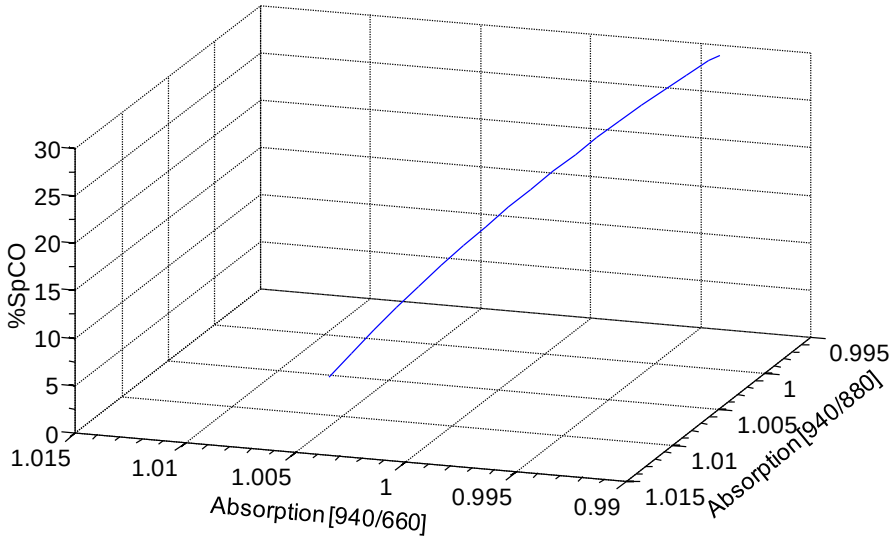

Fig. 6.47. SpCO for r_1= 940/660 and r_2=940/880.

6.6. Discussion

Practically, a small change in the value of SpCO will cause a large change in the absorption value if the wavelength is sensitive to changes in SpCO. Theoretical simulations confirmed that the absorption ratios at 660/940 and 643/940 had the highest sensitivity to changes in SpCO (Fig. 6.10-6.11). Based on the theoretical results shown previously, Table 6.2 was compiled to compare the sensitivities for different wavelength combinations. The table summerizes the differences in the ratio r_1 and r_2 corresponding to a 50% decrease in SpO_2 and an increase in SpCO from 0-30% are calculated. NA in the table indicates those wavelength ratios at which SpO_2 and SpCO could not be obtained within the clinically significant range.

From Table 6.2, it was concluded that the absorption at 643/940 and 660/940 had the highest relative change in absorption corresponding to changes in SpO_2 and SpCO. Therefore, the wavelength ratios 660/940 and 643/940 have relatively high sensitivity to changes in SpO_2 and SpCO as concluded from preliminary experiments.

Table 6.2 showing the wavelengths used categorised according to their sensitivity

Wavelength combinations	Change in SpO_2: 50%		Change in SpCO: 30%	
	Change in r_1	Change in r_2	Change in r_1	Change in r_2
r_1=660/940;r_2=610/940	NA	NA	NA	NA
r_1=660/610;r_2=660/940	0.0789	-0.0474	0.0330	-0.0480
r_1=660/940;r_2=940/610	-0.5089	0.0245	-0.1080	0.0198
r_1=940/610;r_2=940/660	NA	NA	NA	NA
r_1=940/660;r_2=610/940	NA	NA	NA	NA
r_1=660/940;r_2=643/940	0.8710	0.7080	0.3889	0.3590
r_1=660/643;r_2=660/940	0.1579	0.0450	0.0864	-0.0114
r_1=660/940;r_2=940/643	0.1853	0.0379	0.0430	0.0206
r_1=940/643;r_2=940/660	0.1895	0.0953	0.0997	0.0499
r_1=940/660;r_2=643/940	-0.4200	-0.0350	-0.2580	0.0181
r_1=660/940;r_2=740/940	-0.0360	0.0030	-0.0640	0.0040
r_1=660/740;r_2=660/940	-0.0930	-0.0177	-0.0510	-0.0097
r_1=660/940;r_2=940/740	-0.0050	-0.0330	-0.0060	-0.0340
r_1=940/660;r_2=740/940	0.0698	0.0063	0.0420	0.0038
r_1=940/660;r_2=940/740	-0.0089	-0.0067	-0.0042	-0.0430
r_1=660/940;r_2=830/940	0.0530	-0.0166	0.0030	0.0096
r_1=660/940;r_2=660/830	-0.0110	-0.0044	-0.0188	-0.0092
r_1=660/940;r_2=940/830	0.0030	0.0250	0.0020	0.0100
r_1=940/660;r_2=830/940	-0.0071	-0.0171	-0.0550	-0.0030
r_1=940/660;r_2=940/830	0.0137	0.0240	0.0076	0.0130
r_1=660/940; r_2=880/940	0.0360	-0.0113	-0.028	-0.0123
r_1=660/880; r_2=660/940	0.0311	0.0105	0.0207	0.0086
r_1=660/940;r_2=940/880	0.4510	0.0168	0.0420	0.0087
r_1=940/660;r_2=880/940	-0.0020	-0.0163	-0.0031	-0.0130
r_1=940/660; r_2=940/880	0.0240	0.0215	0.0140	0.0125

6.7. Experimental verification

A series of six *in-vitro* experiments were conducted in order to verify the theoretical assumptions that 643nm, 660nm and 940nm are the most sensitive wavelengths to measure simultaneously changes in SpO_2 and SpCO. The data from these six experiments were averaged and substituted in the respective theoretical model according to the ratios considered. SpO_2 and SpCO values calculated for these averaged data were plotted against the corresponding ratios as shown below.

6.7.1. λ= 660, 610 and 940

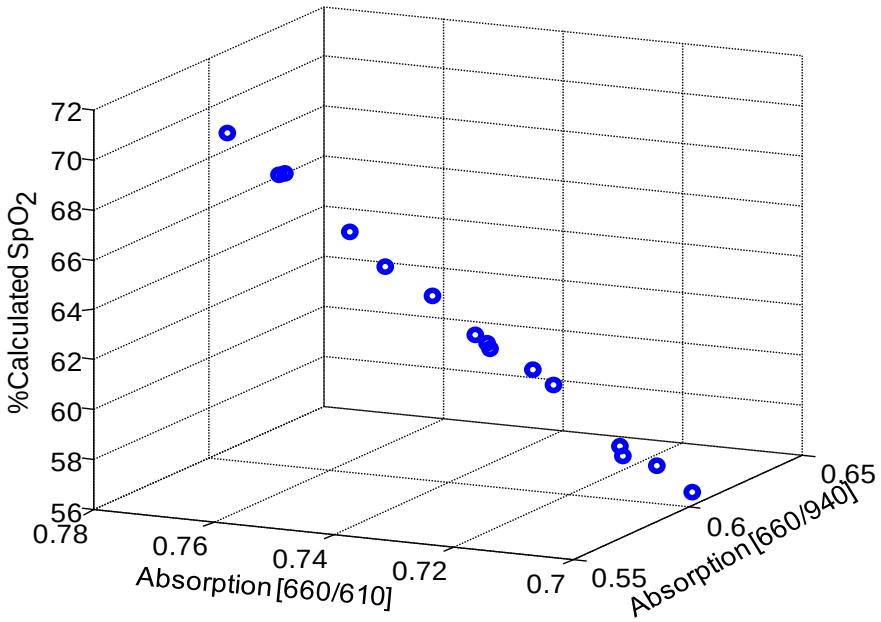

Fig. 6.48. SpO_2 at r_1= 660/940 and r_2=660/610 for an average of six experiments.

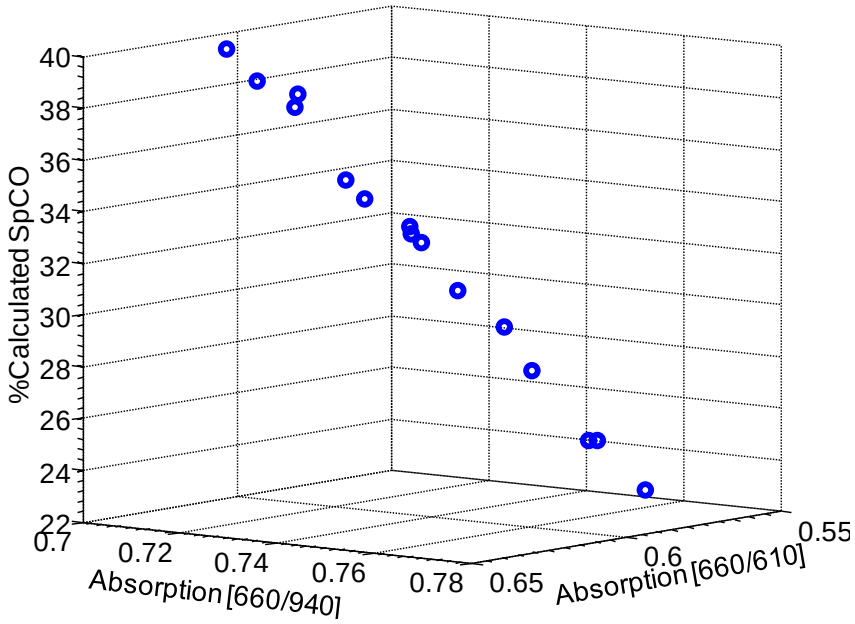

Fig. 6.49. SpCO at r_1= 660/940 and r_2=660/610 for an average of six experiments.

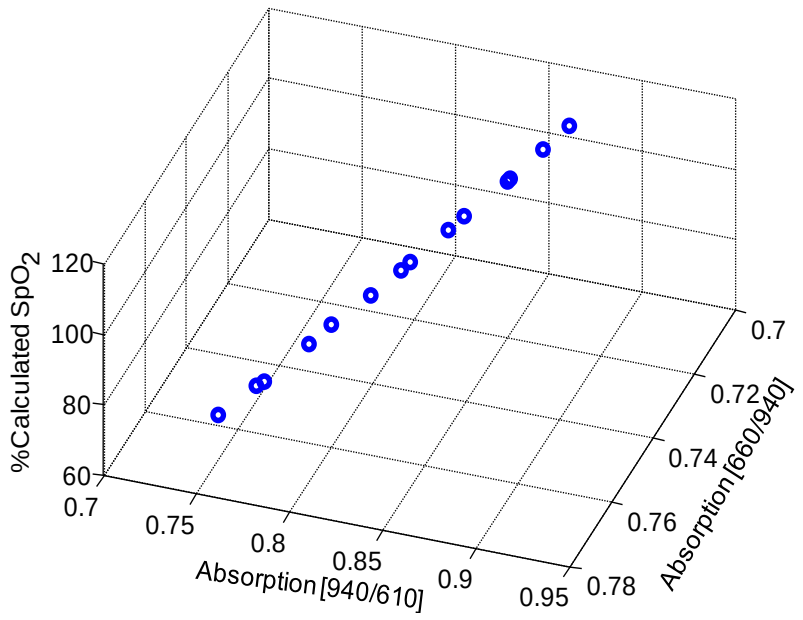

Fig. 6.50. SpO_2 at r_1= 660/940 and r_2=940/610 for an average of six experiments.

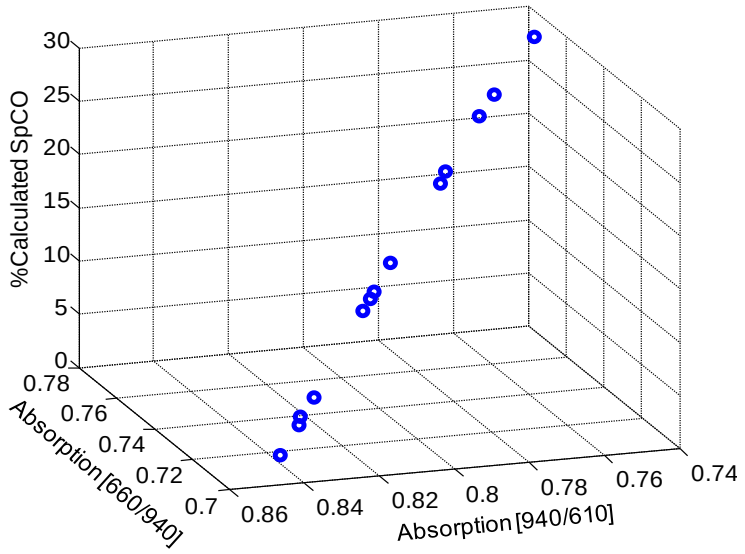

Fig. 6.51. SpCO at r_1= 660/940 and r_2=940/610 for an average of six experiments.

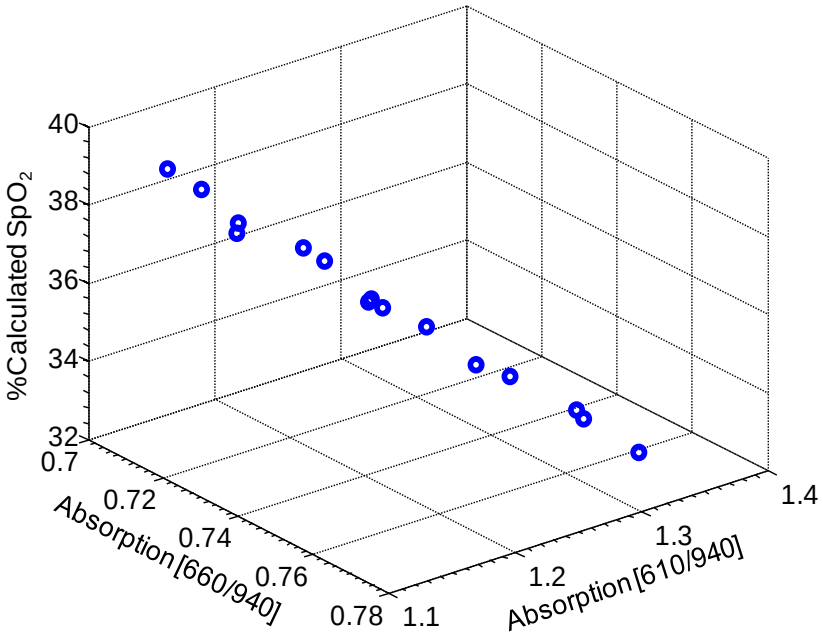

Fig. 6.52. SpO_2 at r_1= 660/940 and r_2=610/940 for an average of six experiments.

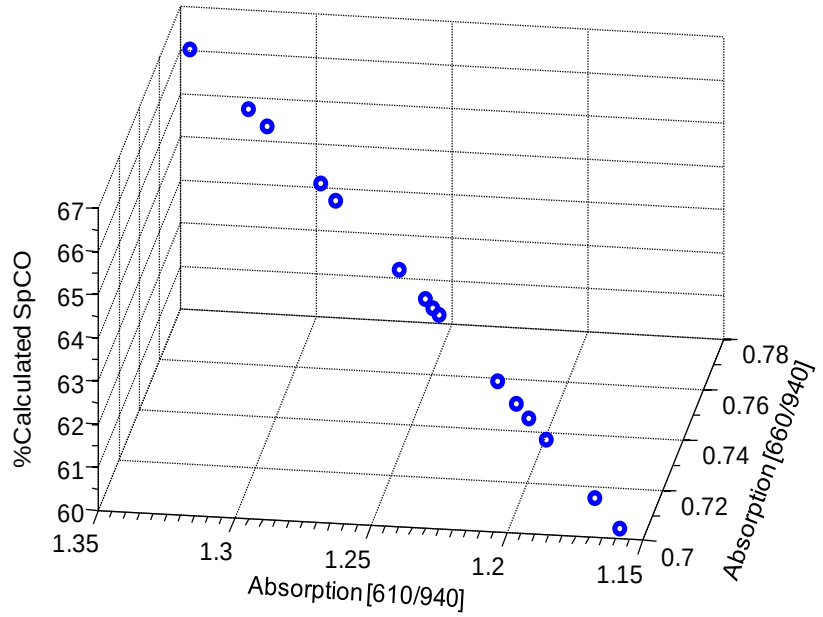

Fig. 6.53. SpCO at r_1= 660/940 and r_2=610/940 for an average of six experiments.

6.7.2. λ= 660, 643 and 940

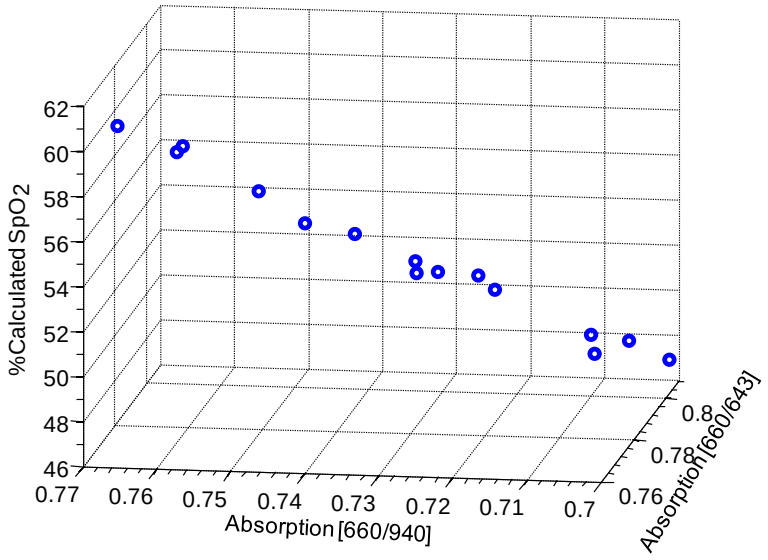

Fig. 6.54. SpO_2 at r_1= 660/940 and r_2=660/643 for an average of six experiments.

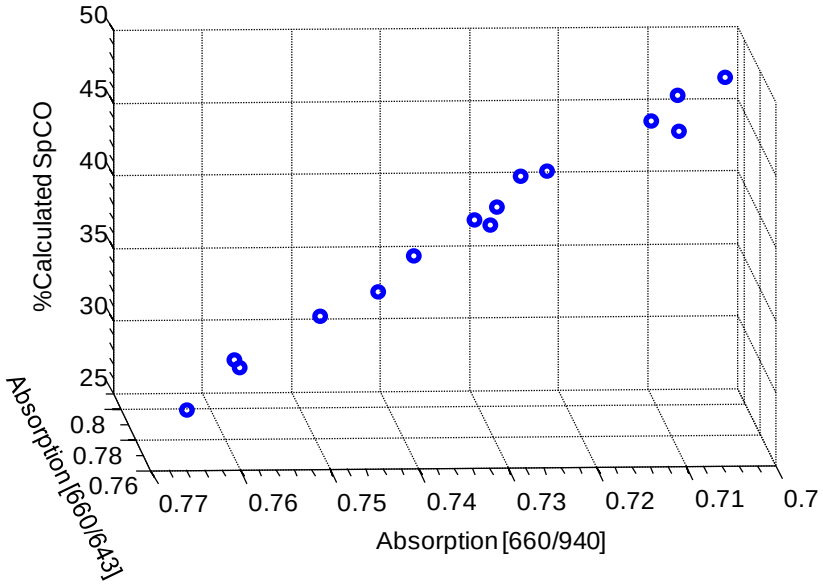

Fig. 6.55. SpCO at r_1= 660/940 and r_2=660/643 for an average of six experiments.

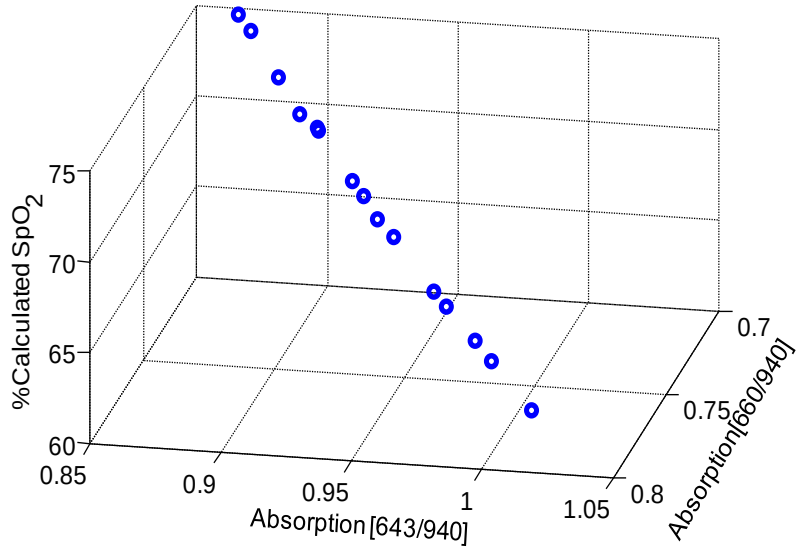

Fig. 6.56. SpO_2 at r_1= 660/940 and r_2=643/940 for an average of six experiments.

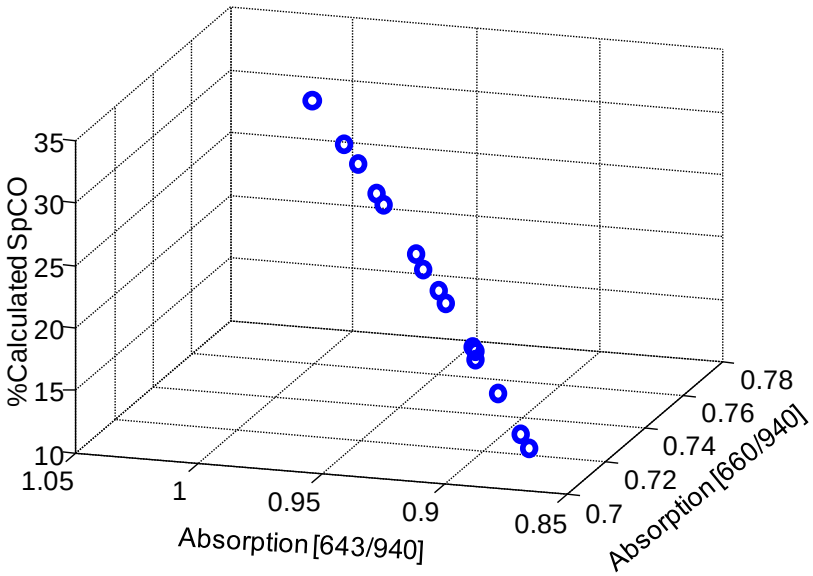

Fig. 6.57. SpCO at r_1= 660/940 and r_2=643/940 for an average of six experiments.

6.7.3. λ= 660, 740 and 940

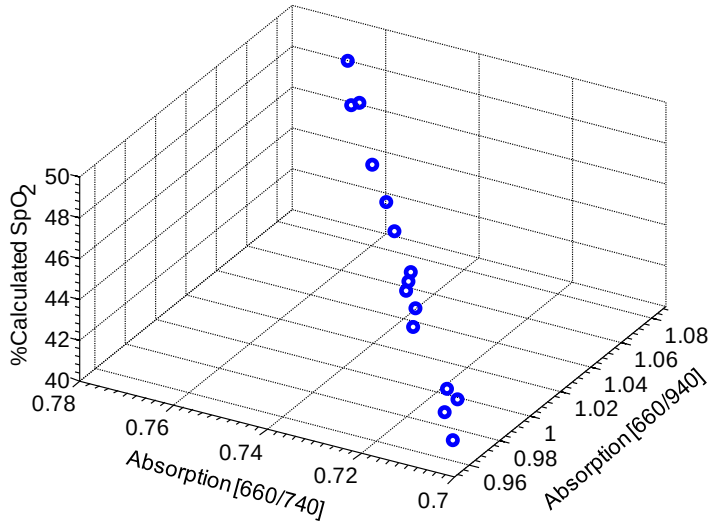

Fig. 6.58. SpO_2 at r_1= 660/740 and r_2=660/940 for an average of six experiments.

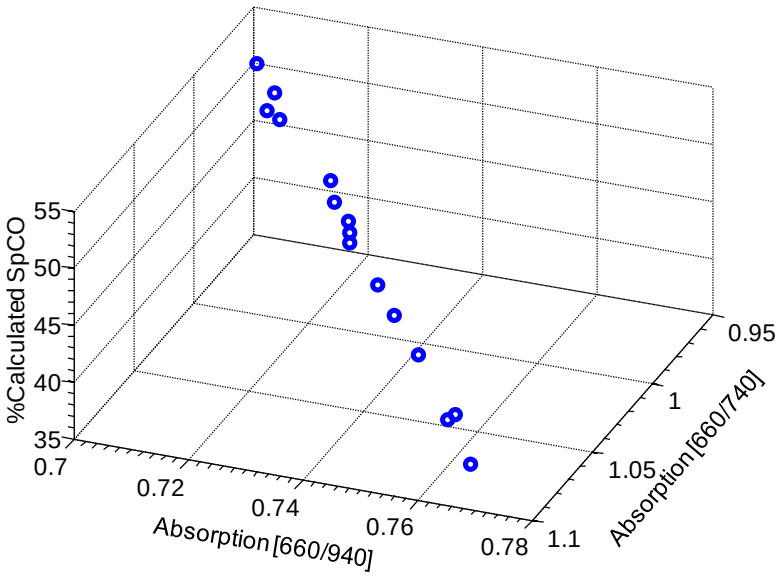

Fig. 6.59. SpCO at r_1= 660/740 and r_2=660/940 for an average of six experiments.

6.7.4. λ= 660, 830 and 940

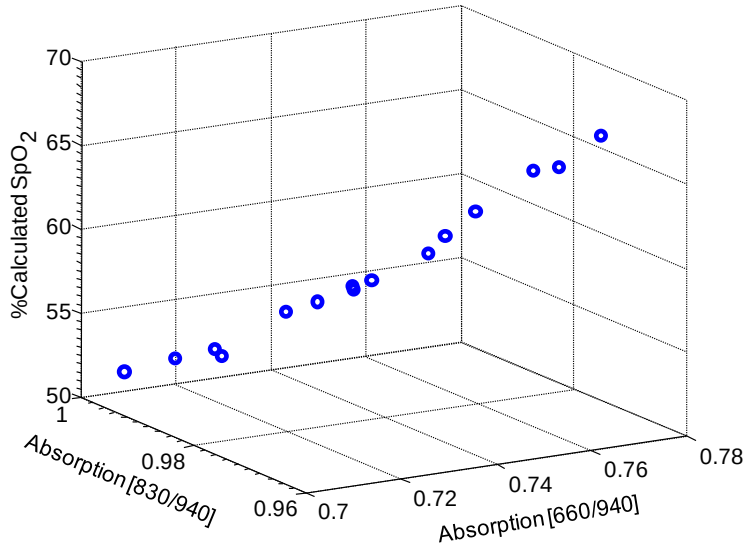

Fig. 6.60. SpO_2 at r_1=660/940 and r_2=830/740 for an average of six experiments.

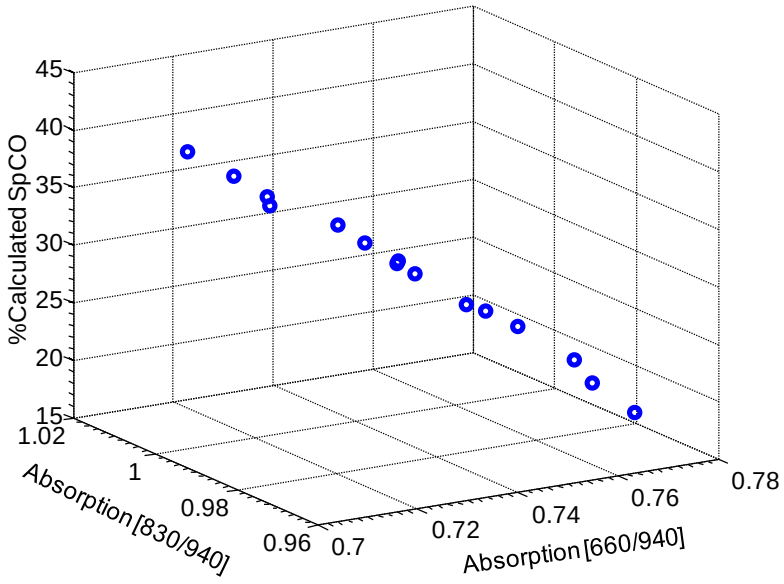

Fig. 6.61. SpCO at r_1=660/940 and r_2=830/740 for an average of six experiments.

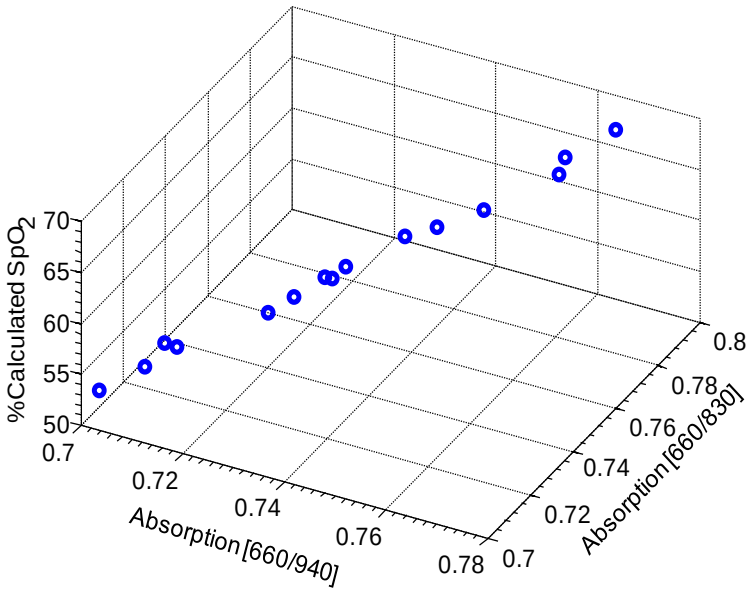

Fig. 6.62. SpO_2 at r_1=660/940 and r_2=660/830 for an average of six experiments.

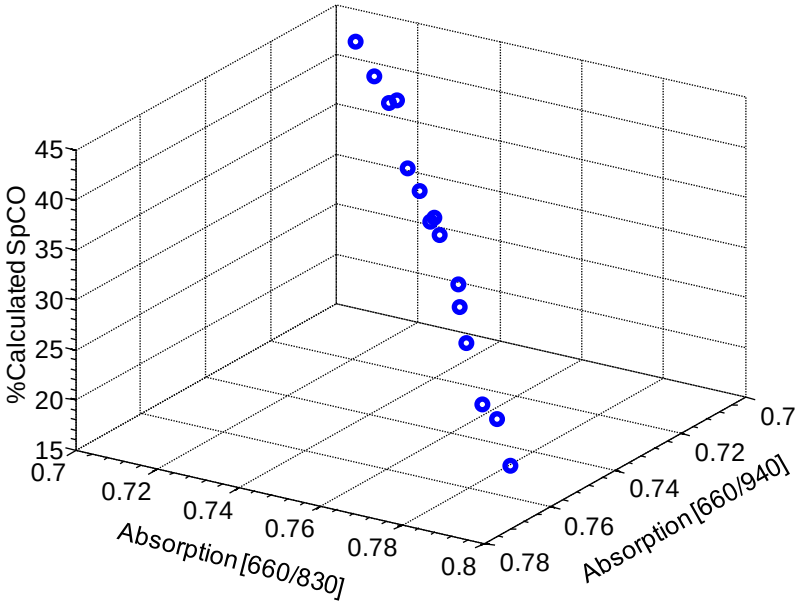

Fig. 6.63. SpCO at r_1=660/940 and r_2=660/830 for an average of six experiments.

6.7.5. λ= 660, 880 and 940

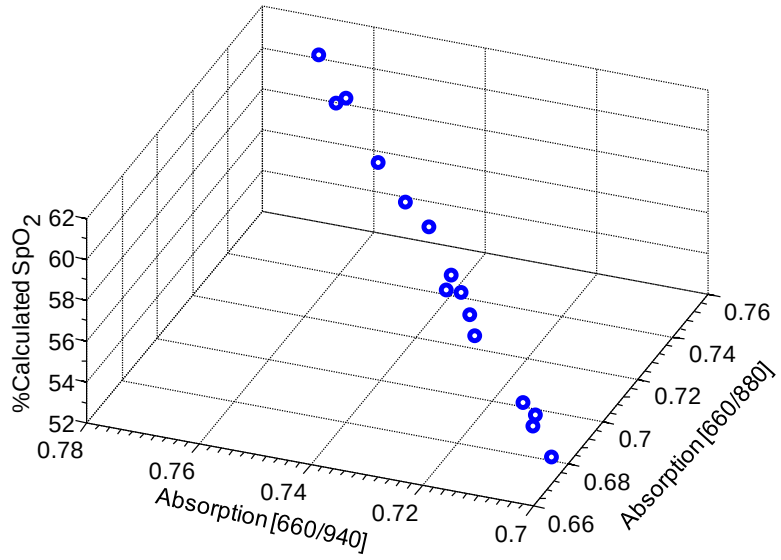

Fig. 6.64. SpO_2 at r_1=660/880 and r_2=660/940 for an average of six experiments.

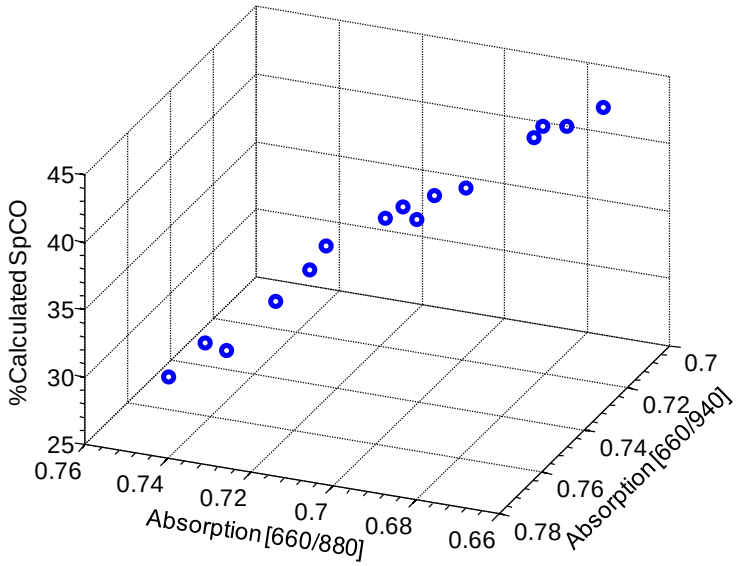

Fig. 6.65. SpCO at r_1=660/880 and r_2=660/940 for an average of six experiments.

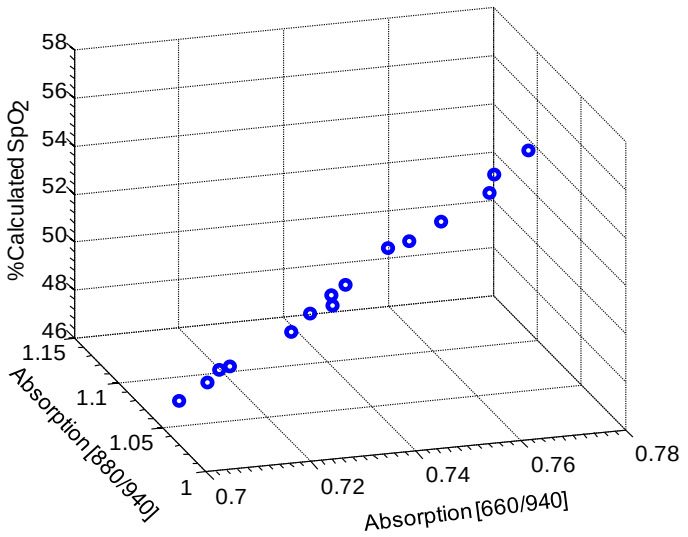

Fig. 6.66. SpO_2 at r_1=660/940 and r_2=880/940 for an average of six experiments.

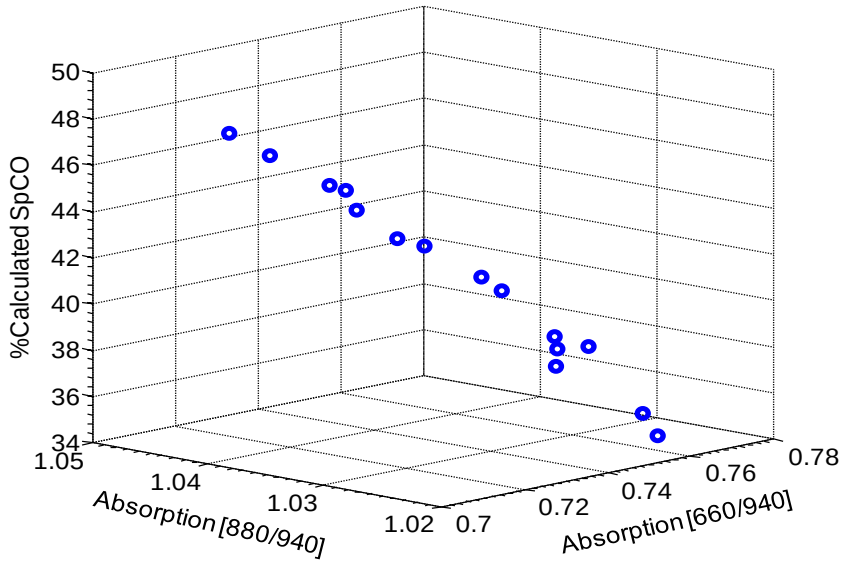

Fig. 6.67. SpCO at r_1=660/940 and r_2=880/940 for an average of six experiments.

On comparing the SpO_2 and SpCO experimental plots obtained at different wavelength ratios (Figs. 6.47-6.64), it was shown that, similar to the theoretical results, changes in SpCO and

SpO_2 (in the presence of HbCO) causes a relatively larger change in the absorption ratios of 660/940 and 643/940 (Fig. 6.53-6.54). Hence, from the theoretical and experimental results, it was concluded that among the different wavelength ratios considered, absorption ratios at 660/940 and 643/940 has relatively high sensitivity to SpCO and SpO_2. Therefore, 660 nm, 643 nm, 940 nm were used to simultaneously measure SpO_2 and SpCO.

Chapter 7. Algorithm for simultaneous measurement of SpO_2 and SpCO

After the specific wavelengths that can be used to measure SpO_2 and SpCO have been identified, the next step was to formulate the algorithm to differentiate between the presence and absence of HbCO in blood.

To determine HbCO, it is necessary to differentiate between the absorption of blood when HbCO is present or absent. Hence, the absorptions obtained by our sensor were analyzed in a series of *in-vitro* experiments. The absorptions values obtained when HbCO was present were compared to the absorptions when HbCO was absent. From the results of this comparison, it was found that apart from 660 nm, 643 nm and 940 nm, the absorption ratios obtained at 740 nm had a significant change in absorption depending on the presence or absence of HbCO. This can be explained based on Fig. 2.1, which shows that the absorption in the region between 700 nm to 750 nm decreases when HbCO is present, while the absorption increases when HbCO is absent. Hence, in addition to 660 nm, 643 nm and 940 nm, the absorption at 740 nm was also included in the computation to increase the overall selectivity of the device.

These changes in absorption were used in the algorithm to differentiate between the presence and absence of HbCO. A series of 20 *in-vitro* experiments with elevated HbCO resulted in approximately 350 data points at each of the four wavelengths (643 nm, 660 nm, 740 nm, 940 nm). Similarly, a series of 20 *in-vitro* experiments conducted in the absence of HbCO resulted in approximately 350 data points at each of the four wavelengths. Based on the absorption values that were observed from these results, thresholds were set to differentiate between the presence and absence of HbCO. These thresholds were incorporated into the algorithm to differentiate between the presence or absence of HbCO.

7.1. Thresholds used in the algorithm

The thresholds for r_1, r_2 and r_3 shown in Table 7.1 were incorporated in the algorithm and based on the presence or absence of HbCO the algorithm would choose the appropriate formula, derived in chapter 6, to calculate SpO_2 and SpCO, respectively.

Table 7.1. Thresholds used in the algorithm to differentiate the presence and absence of HbCO.

$r_1(A_{660/940})$	$r_2(A_{643/940})$	$r_3(A_{740/940})$	Present	Absent
Greater than or equal to 1	Greater than or equal to 1	NA	SpO_2	SpCO
Greater than 0.84	Greater than 1	Greater than 0.73	SpO_2	SpCO
Greater than 0.54 and less than 0.82	Less than or equal to 1.025	Greater than 0.6 and less than 0.82	SpO_2 and SpCO	NA

Chapter 8. Algorithm to calculate SpO_2 and SpCO

A series of 19 *in-vitro* SpO_2 and SpCO experiments were conducted resulting in 285 and 271 data points, respectively. The absorption values obtained at 643nm, 660nm, 740nm, and 940 nm were averaged and substituted in the algorithm. SpO_2 and SpCO calculated by the algorithm were plotted against the actual values of SpO_2 and SpCO obtained from the IL 682 CO-Oximeter, respectively. The regression equations obtained for SpO_2 and SpCO are shown in Fig. 8.1 and Fig. 8.4. To validate the regression equations, another series of 5 experiments were conducted resulting in 120 and 117 data points for SpO_2 and SpCO, respectively. These data points were averaged and then calibrated using the regression line obtained from Fig. 8.1 and 8.4. The calibrated results were plotted against the actual values obtained from the IL 682 CO-Oximeter as shown in Fig. 8.2 and 8.5. Variations in the absorption values were noted, at all wavelengths, between different experiments even for the same value of SpCO. To compensate for these variations, which were later determined to be caused by changes in light coupling between the sensor and tissue simulator, the data points used to calculate and validate the regression equation were averaged.

8.1. Results

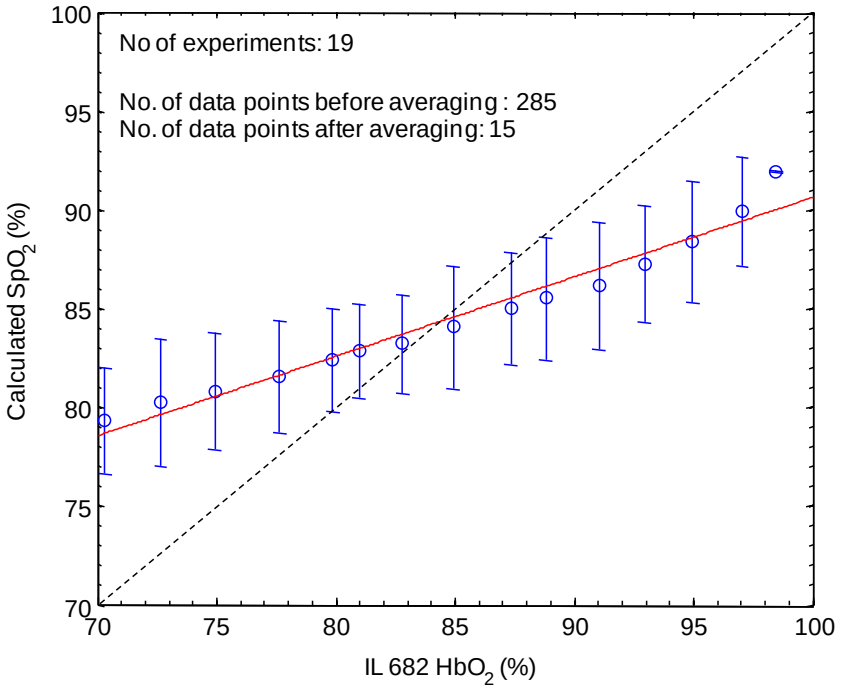

Fig. 8.1.Calculated SpO_2 versus IL 682 HbO_2 values. Dashed line is the line of identity. Regression equation: (Calculated SpO_2)= 0.4 (IL-682 HbO_2) + 50.

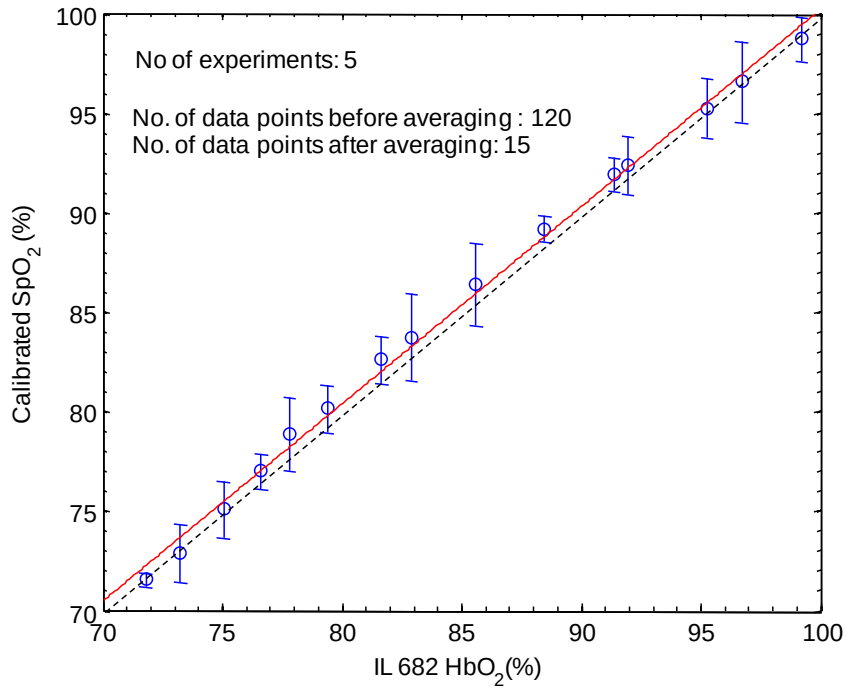

Fig. 8.2.Calibrated SpO_2 versus IL 682 HbO_2 values. Dashed line is the line of identity. Regression equation: Calibrated SpO_2=0.99*(IL-682 HbO_2) +1.1.

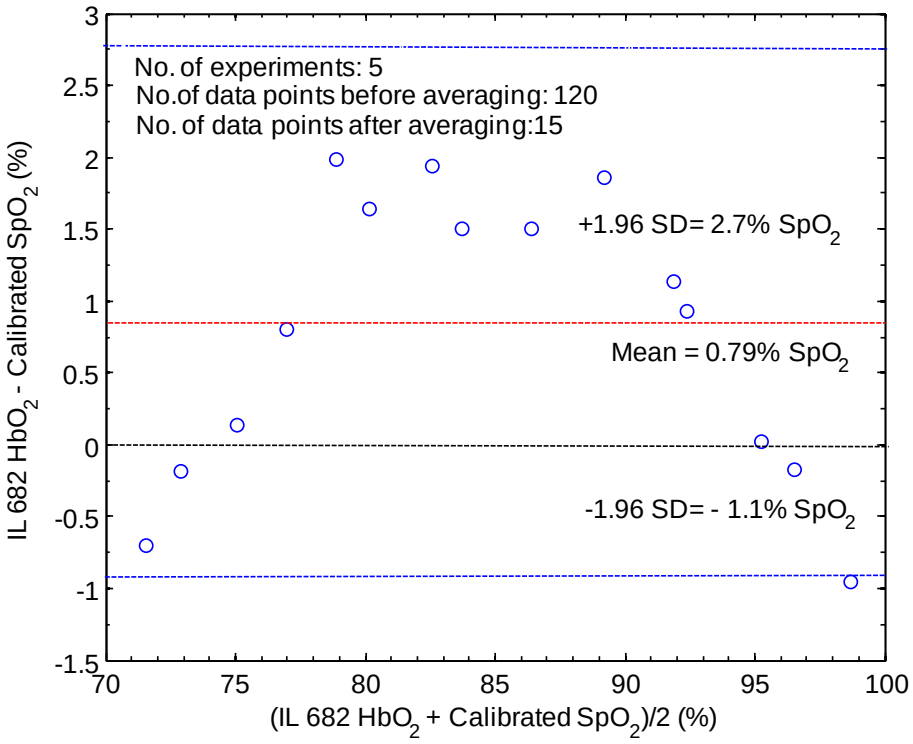

Fig. 8.3. Residual plot for data points shown in Fig. 8.2.

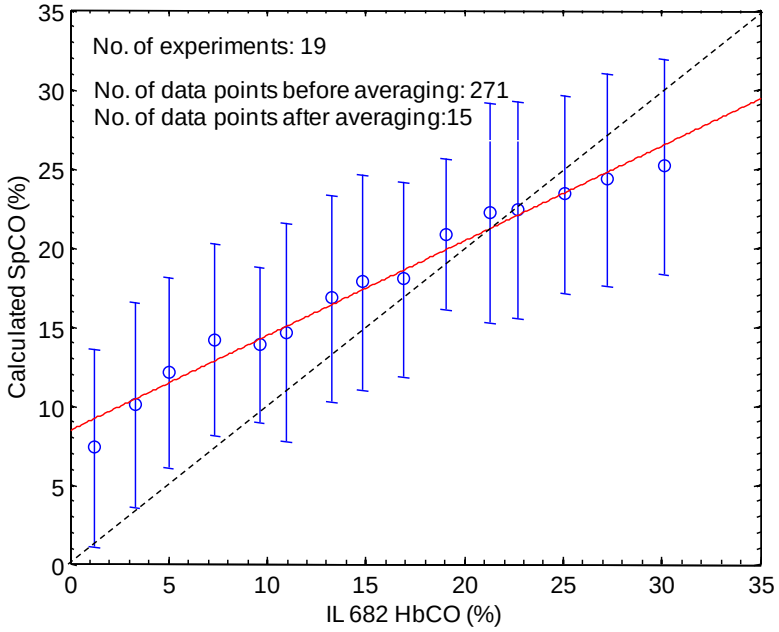

Fig. 8.4. Calculated SpCO versus IL 682 HbCO values. Dashed line is the line of identity. Regression equation: (Calculated SpCO)= 0.6*(IL 682 HbCO) + 8.4.

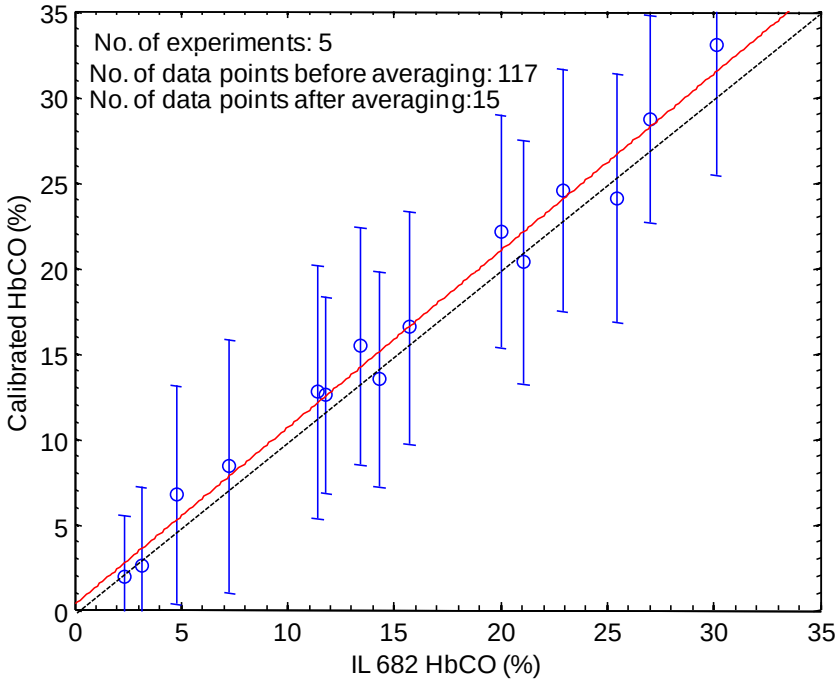

Fig. 8.5. Calibrated SpCO versus IL 682 HbCO values. Dashed line is the line of identity. Regression equation: (Calibrated SpCO) = (IL 682 HbCO) + 0.28).

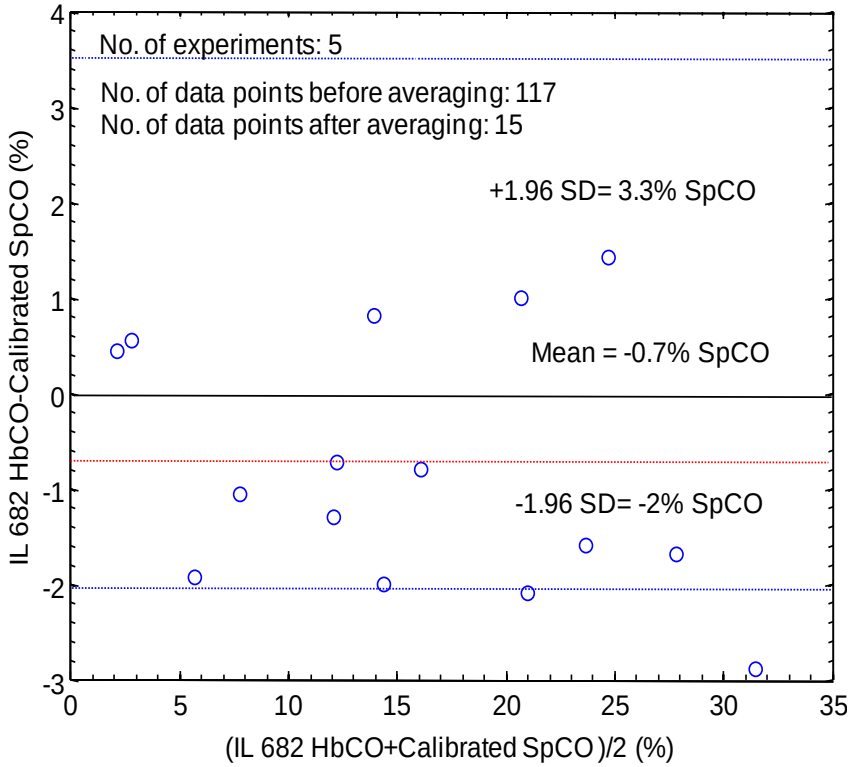

Fig.8.6. Residual plot for data shown in Fig. 8.5.

8.2. Discussion

Comparing Fig. 8.1 to Fig. 8.2, it is evident that the variation between the calibrated SpO_2 and IL-682 reference values were much smaller compared to the variation between the calculated SpO_2 and IL-682 reference readings. Similarly, the variation between the calibrated SpCO and IL 682 CO-oximeter readings (Fig. 8.5) was smaller than the variation between the calculated SpCO and IL 682 HbCO (Fig. 8.4). From Fig. 8.1 and Fig. 8.2, it is also evident that the variations observed between individual experiments, indicated by the error bars, were approximately ±3% for SpO_2 before calibration, but was smaller for the calibrated SpO_2 values. From Fig. 8.4 and 8.5, it was observed that the variations between individual experiments were more pronounced in SpCO experiments, at approximately ±6%, for both calculated and calibrated values.

Results from SpCO experiments were analyzed to determine if blood hematocrit (HCT) levels caused the variations observed between the experiments. It was observed that calculated values from two SpCO experiments with the same HCT level at approximately 30% had a standard deviation of ± 2% and ± 7%, respectively. Similarly, it was also observed that results from another set of two SpCO experiments with different HCT levels at approximately 40% and 30% had a similar standard deviation of ± 2.9% and ± 3.1%, respectively. Hence, it was concluded that changes in HCT levels did not have a significant effect on the results. Hence, steady state SpCO experiments were conducted to determine if changes in light coupling caused large variations between the SpCO obtained from different experiments. These experiments were conducted by maintaining HbCO level at a steady state value. Other variables like the blood hematocrit were also held constant and readings from our sensor were obtained along with

simultaneous sampling using the IL 682 CO-Oximeter. The sensor position was changed four times during the experiment and 5 readings were taken at each position for comparison.

From Table 8.1 and 8.2, it is clear that, the changes in light coupling between the sensor and the simulator did contribute to variations between the experiments although the variations within each set were small. The variations between the mean SpCO values obtained at different sensor position for the same value of HbCO were approximately 7.4%.

Table 8.1. Calculated SpCO corresponding to steady state HbCO at 26.3-27.1% obtained at four different sensor positions.

Position 1	Position 2	Position 3	Position 4
30.5	22.1	22.1	33.7
31.0	17.6	18.6	32.2
30.8	21.6	17.1	38.6
33.4	21.1	17.0	35.9
30.8	21.8	17.1	37.6

Table 8.2. Mean and standard deviation between the calculated values for SpCO at different sensor positions.

	Position 1 (%)	Position 2 (%)	Position 3 (%)	Position 4 (%)	Mean (%)	Standard deviation (%)
Mean	31.2	20.8	18.4	35.6	26.7	7.4
Standard deviation	1.1	1.8	2.1	2.6		
Coefficient of variation	3.5	8.6	11.4	7.3		

Similar steady-state experiments were conducted for different ranges of SpCO. Even at lower ranges of SpCO, the data from different experiments had a variation of approximately ±7%. These were approximately the same variations that were observed between the calculated and calibrated SpCO readings. Hence, it was concluded that changes in light coupling between the sensor and the tissue simulator did affect the *in-vitro* readings. When the sensor is placed too close to the model, the amount of light that reaches the blood will be large and will result in larger absorption values which would affect the ratios. Similarly, if the sensor is placed far from the tissue simulator, the light that reaches the blood will be relatively small and cause a corresponding decrease in absorption. Such increase or decrease in absorption will cause a corresponding change in the ratio values computed thereby affecting the SpCO values computed. The effect that these variations, observed *in-vitro*, will have on *in-vivo* measurements is not clear. *In-vivo*, the maximum ratio of blood volume to tissue is estimated to be approximately 5% [28, 33]. Hence, only a very small fraction of the incident light reaches the blood. In contrast, in our *in-vitro* model, the blood to tissue is ratio is relatively much higher and can be estimated to be more than approximately 80%. Hence, most of the incident light in the model reaches the blood compartment. Therefore, sensor positions that may not affect pulse oximeters *in-vivo* can have a more pronounced effect on the readings obtained *in-vitro*. The ultimate effect of this factor can be assessed only after conducting extensive *in-vivo* tests.

After identifying the cause of variation between the individual experiments, the calibrated data for both SpO_2 and SpCO were used to the plot of mean difference between the Il 682 CO-Oximeter values and the calibrated data. The mean of difference between the IL-682 CO-oximeter HbO_2 and calibrated SpO_2 ±1.96 SD were computed and plotted in Fig. 8.3. Similarly, Fig. 8.6 compares the mean difference between the HbCO measured IL-682 CO-oximeter and

calibrated % SpCO ±1.96 SD values. A SD value of ±1.96 was chosen because 95% of the readings will fall within this range. In the absence of HbCO, 95% of the readings fell within 2.7 to -1.1 for SpO_2 between 70-100% (Fig. 8.3). From Fig. 8.6, 95% of the readings fell within a variation of 3.3 to -2 % for SpCO between 0-30%. The plot of mean against difference was used because, Bland et al. [34] reports that the commonly used plot of difference against reference value would give misleading results. The paper shows that, in cases where there is no association between the magnitude of the reference and difference between the test and reference values, the commonly used plot of difference against reference values will give a positive correlation whereas, the plot of difference against the test measurement will show a negative correlation for the same case. Hence, any of these plots can be misleading as the association shown between the test and reference device will depend on the method of analysis. Hence, the study shows that the plot of difference versus the mean of the reference and test measurement as a better way of determining the agreement between two device measurements. The results from our SpCO experiments (Fig. 8.6) were compared to the accuracy reported by the Masimo Rad-57 pulse oximeter which reports an accuracy of ±3% (±1 SD) for SpCO between 0-45 % [35].

The specificity and sensitivity of the results were then calculated and tabulated as shown below in Table 8.3-8.4. Sensitivity is a measure of probability of the test correctly identifying a person with disease and specificity is a measure of probability of the test correctly identifying a person who does not have a disease. Sensitivity and specificity are given by Eq. 8.1-8.2.

Sensitivity= No. of true positives/ (No. of true positives + No. of false negatives) (8.1)

Specificity= No. of true negatives/ (No. of true negatives + No. of false positives) (8.2)

where, *true positives* are cases the device correctly identifies a disease;

true negatives are cases the device correctly identifies a lack of disease;

false positives are the cases the device wrongly identifies a healthy person as having a disease;

false negatives are the cases the device fails to identify a disease and wrongly identifies a person with a disease as being healthy [36].

In our case, sensitivity would mean the probability of the device correctly detecting CO poisoning and specificity is the ability of the device to correctly identify persons who do not suffer from CO poisoning. For the calculation of SpO_2 sensitivity and specificity for, 90% was considered the threshold for mild hypoxia [37]. In case of SpCO, 12% was considered as the threshold for calculating specificity and sensitivity because the treatment for carbon monoxide poisoning is the same for values of SpCO less than 12%. Concentration of SpCO higher than 12% requires specific treatment like 100% oxygen therapy [38].

Table 8.3. Performance characteristics for SpO_2 measurements obtained from the *in-vitro* model and our sensor using our algorithm.

SpO_2	Laboratory value <90	Laboratory value >90	Total	Negative Test	Positive Test	Specificity	Sensitivity
Tissue simulator <90	9	1	10	True negative 5	True positive 9	83.3%	100%
Tissue simulator >90	0	5	5	False negative 0	False positive 1		
Total	9	6	15				

In the experiments we conducted, SpO_2 in blood was less than 90% in nine readings and the algorithm correctly identified all nine cases. Hence, in Table 8.3, the number of true positives is

9. Similarly, the algorithm correctly identified five cases where SpO_2 was greater than 90%. So, the number of false negatives in Table 8.3 is 5. But, the algorithm wrongly identified one reading as being less than 90%, which requires treatment, when the actual SpO_2 was greater than 90%. So, the false positive is 1. There were no cases when the algorithm wrongly identified the values as being greater than 90% when it was actually less than 90%. Hence, the false negative in Table 8.3 is 0. Using these values specificity and sensitivity was calculated from the formula shown in Eq. 8.1 and 8.2.

Table 8.4. Performance characteristics for SpCO measurements obtained from the *in-vitro* model and our sensor using our algorithm.

SpCO	Laboratory value >12	Laboratory value <12	Total	Negative test	Positive Test	Specificity	Sensitivity
Tissue simulator >12	9	1	10	True negative 5	True positive 9	83.3%	100%
Tissue simulator <12	0	5	5	False Negative 0	False positive 1		
Total	9	6	15				

In the experiments we conducted, SpCO in blood was greater than 12% in nine readings and the algorithm correctly identified all nine cases. Hence, in Table 8.4, the number of true positives is 9. Similarly, the algorithm correctly identified five cases where SpCO was less than 12%. So, the number of false negatives in Table 8.4 is 5. But, the algorithm wrongly identified one reading as being greater than 12%, which requires treatment, when the actual SpCO was greater than 12%. So, the false positive is 1. There were no cases when the algorithm wrongly identified the SpCO value as being less than 12% when it was actually greater than 12%. Hence, the false negative in

Table 8.4 is 0. Using these values specificity and sensitivity was calculated from the formula shown in Eq. 8.1 and 8.2.

As summarized in Tables 8.3 and 8.4, SpCO and SpO_2 measurements obtained from our senor *in*-vitro have high sensitivity, thereby ensuring that patients with carbon monoxide poisoning will be correctly identified. Although the specificity was slightly lower and lead to few false positives, 83% of the data were correctly identified. The results obtained from our experiments were compared with the results of the Masimo Rad-57 pulse oximeter published in the literature as shown in Table 8.5.

Table 8.5. Comparison of SpCO with HbCO measured by a CO-Oximeter [39].

Author	Year	Setting	No. of subjects	Limits of agreement for SpCO vs HbCO (%)	Bias (%)
Mottram et al	2005	Respiratory Dept.	31	-1.5 to +5.5	2.0
Barker et al	2006	Laboratory	10	-5.5 to +3.1	-1.2
Coulange et al	2008	Emergency Dept.	12	-6.4 to +3.4	-1.5
Suner et al	2008	Emergency	64	-2.8 to +5.6	-4.2
Kot et al	2008	Hyperbaric chamber	49	-7.9 to +8.9	0.5
Piatkowski et al	2009	Burn center	20	-1.5 to +7.8	3.2
Tougher et al	2010	Emergency	120	-11.6 to +14.4	1.4
Our i*n-vitro*-tissue simulator	2011	Laboratory	15	-2 to +3.3	-0.7

Although, it was shown from table 8.5, that the accuracy range obtained from our *in-vitro* model is close to the accuracy ranges reported by Masimo, the results reported by Masimo were

obtained *in-vivo* whereas our results were obtained from an *in-vitro* model. Various physiological parameters like skin color, amount of tissue, vasoconstriction that were not simulated in our *in-vitro* model may affect *in-vivo* measurements. Similarly, factors that are more pronounced in the model may or may not affect *in-vivo* measurements. Hence, the results obtained from our model cannot be ascertained without further *in-vivo* verifications. Conducting human studies to simultaneously calculate SpO_2 and SpCO using our algorithm is a part of future work. This would involve identifying the factors that affect the measurement of SpCO and SpO_2 *in-vivo* and compensating for those variations in order to produce accurate *in-vivo* measurements using a pulse oximeter.

Chapter 9. Conclusions and future work

Measurement of vital physiological conditions from patients is important to provide effective triage and medical care in the field. Developments in remote non-invasive monitoring of physiological parameters could provide a possibility of immediate medical care for firefighters, army personnel and other people working in dangerous environment. SpCO measurement using a wireless wearable pulse oximeter that measures SpO_2, HR and RR would have a significant advantage and could find potential applications for people who are exposed to CO in their line of duty. Pulse oximeters are unable to detect HbCO in blood and give erroneous SpO_2 values in the presence of HbCO. This research therefore, was aimed at developing an algorithm for simultaneous measurement of SpO_2 and SpCO using a wireless wearable pulse oximeter developed in our laboratory.

To simultaneously measure SpO_2 and SpCO, a minimum of three wavelengths were required since it involves computing three unknown variables which includes the concentration of HbO_2, HbCO and Hb. From the absorption spectra of Hb and its derivatives at wavelengths between 600 nm and 1000 nm, several specific wavelengths at which changes in SpO_2 and SpCO can be measured with relatively high sensitivity and specificity were identified. Based on the availability of LEDs used in the prototype sensor developed in our laboratory, a set of three wavelengths (643 nm, 660 nm, 940 nm) were identified. To verify this choice of wavelengths, a theoretical model was developed using the Beer-Lambert's law. From theoretical simulations, it was found that absorption ratios of 660 nm/940 nm and 643 nm/940 nm can be used for simultaneous measurement of SpO_2 and SpCO with relatively high sensitivity. Additionally, an algorithm was formulated to calculate SpO_2 and SpCO simultaneously. Hence, based on the *in-vitro* experiments conducted, in addition to 660 nm, 643 nm and 940 nm, absorption at 740 nm

was also included to increase the selectivity of the device. Based on a series of *in-vitro* preliminary experiments, in addition to 660 nm, 643 nm, and 940 nm, the absorption at 740 nm was included to increase the selectivity of the device. Based on the results of the *in- vitro* experiments, thresholds for the absorption ratios at 660/940. 643/940 and 740/940 were incorporated to differentiate the presence and absence of HbCO. The last objective of the thesis was to verify this algorithm using *in-vitro* experimental results. From a series of *in-vitro* experiments conducted, SpO_2 and SpCO were calculated using the algorithm. The preliminary results from our device reports an accuracy of 2.7 to -1.1 for 70-100% SpO_2 and 3.3 to -2 % for 0-30% SpCO with a specificity of 83.3% and a sensitivity of 100% for both SpO_2 and SpCO, respectively.

Although the performance characteristics obtained from the *in-vitro* measurements are within the clinically acceptable range, we observed variations in SpCO between the experiments. This was identified to be caused by changes in the coupling of light between the optical reflectance sensor and the *in vitro* tissue simulator. The effect that these variations will have on *in-vivo* measurements is not clear. Hence, the algorithm developed *in-vitro* will need to be evaluated *in-vivo* by conducting human validation studies. This would involve identifying the factors that could potentially affect *in-vivo* measurement of SpCO and SpO_2 and compensate for those variations in order to produce accurate measurements using a wearable pulse oximeter.

In a clinical setting, monitoring of SpO_2 is vital for following physiological trends during surgical procedures, post surgery, in emergency rooms and in intensive care units. On the contrary, the ability to measure SpCO is more vital for spot checking to diagnose CO poisoning rather than to monitor a trend. Typically, the presence of SpCO at values greater than 25% can cause permanent neurological damage. The Masimo Rad 57 pulse oximeter measures SpCO with

an accuracy of ±3% (1SD). Hence, 1.96 SD which would include 95% of the measurements will have an accuracy of approximately ±6%. Although this is not a high accuracy value, the indication of HbCO in blood will enable screening of patients with CO poisoning and enable clinicians to decide on an appropriate course of action. Hence, from a clinical standpoint, spot checking for SpCO is more critical than the need to monitor the trend in SpCO measurement. Although, results from our algorithm using data points obtained from an *in-vitro* simulator have been shown to have an accuracy of 2.7 to -1.1, variations up to ±7% have been observed due to changes in the coupling of light between the sensor and the simulator. If the coupling of light between the sensor and the skin is not found to affect the readings *in-vivo*, and if we can identify and compensate for other factors that could potentially affect SpCO measurement *in-vivo*, then the accuracy rate that can be obtained from our algorithm can potentially be better than the accuracy of currently available devices.

In-vivo testing of our algorithm can be done in the future similar to the *in-vivo* testing reported by Tougher et al. [39] in trauma and burn center of a hospital. People suspected of CO poisoning were tested using the Masimo device with simultaneous blood sampling using a CO-Oximeter (Siemens Rapidlab 1200 blood gas analyzer) to obtain the true HbCO values. The results from both the methods were then compared to assess the accuracy of the Masimo Rad 57 pulse oximeter. Testing can also be conducted in a laboratory setting using volunteers breathing safe levels of SpCO. Testing of the Masimo pulse oximeter reported by Barker et al. [40] was conducted in a laboratory where 10 volunteers breathed 500 ppm of CO until HbCO levels reached 15%. As the readings from the Masimo device was obtained, blood samples from arterial cannulas were obtained simultaneously to test for true HbCO values. The readings from the two devices were compared to establish the accuracy of the Masimo Rad 57 oximeter.

Appendix A: Bandwidth of wavelengths used in our prototype sensor

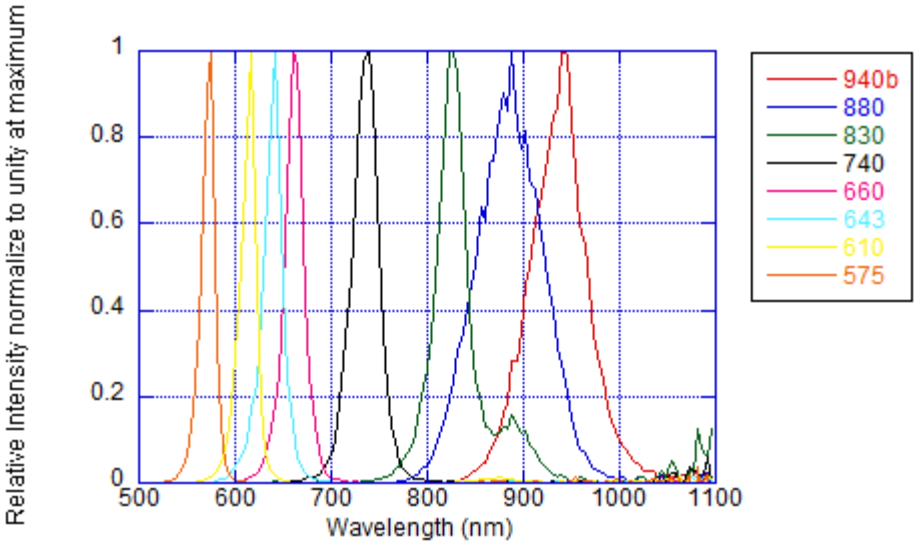

Fig. A1. Bandwidth of the wavelengths used in our prototype sensor.

Table A1: Full width at half maximum for wavelengths used in our prototype sensor

Data (nm)	Max (nm)	FWHM (nm)
940b	940	59
880	888	73
830	823	32 (40)
740	739	30
660	660	22
643	641	20
610	618	16
575	576	15

Appendix B: Flowchart for the algorithm used for SpO_2 and SpCO determination

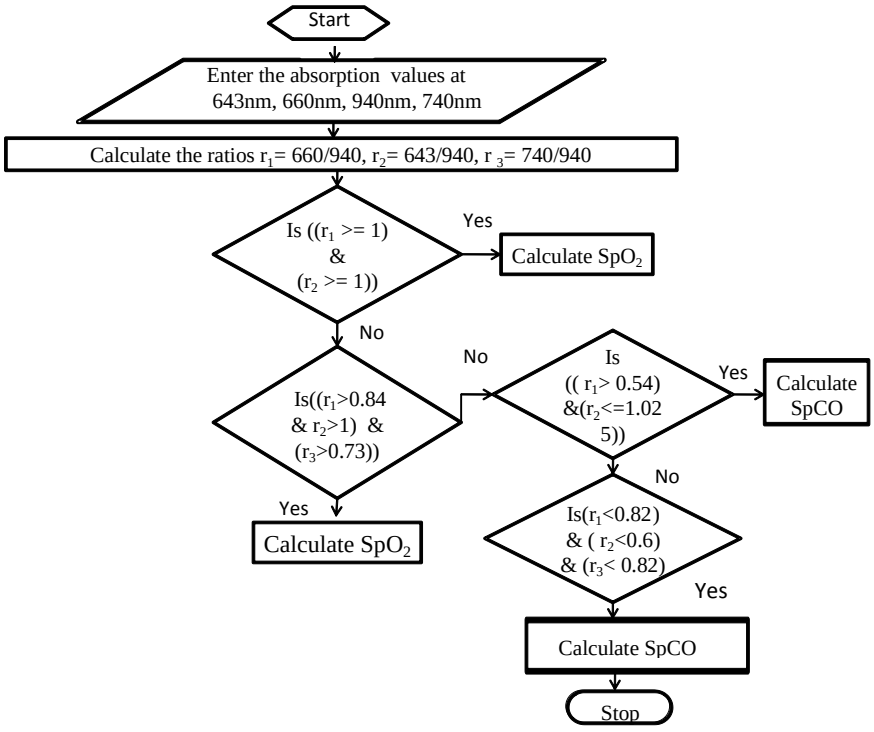

REFERENCES:

1. J. G. Webster (Editor), "Design of pulse oximeter", S. A. Clark (Author), " Normal Oxygen Transport", IOP publishing Ltd, pp.1-13, 1997.
2. A. C. Guyton and J. E. Hall. "Textbook of Medical Physiology", W.B. Saunders Company, pp 516-517, 1996.
3. M. F. Perutz. "Hemoglobin structure and respiratory transport", Sci Am., Vol. 239(6), pg. 92-125, 1978.
4. J. P. Payne and J. W. Servinghaus, "Pulse oximetry", Springer-Verlag, pp21-22, 1986.
5. J. G. Webster (Editor), "Design of pulse oximeter," O. Wieben (author), "Light absorbance in pulse oximetry," IOP publishing Ltd, pp. 40-55, 1997.
6. J. G. Webster (Editor), "Design of pulse oximeter", Joanna B Ruchala (author), "Applications of pulse oximetry", IOP publishing Ltd, pp. 214-220, 1997.
7. L. W. Kao, K. A. Nanagas, " Carbon monoxide poisoning", Medical Clinics of North America, Vol. 89, pp. 1161-1194, 2005.
8. M.Micheal, R.E.Zumwalt, "Fatal carbon monoxide poisoning after the detonation of explosives in an underground mine: A case report", American Journal of Forensic Medicine & Pathology, Vol. 22, pp 387-390, 2001.
9. H. Mathew, A. A. H. Lawson, "Carbon monoxide poisoning in a former mining community", Britsh medical journal, Vol. 286, pp:18-19, 1983.
10. A. Ernst, J. D. Zibrak, "Carbon monoxide poisoning", The New England Journal of Medicine, Vol. 339, pp. 1603-1609, 2004.
11. D. G. Penny, "Hemodynamic response to carbon monoxide", Environmental Health Perspectives, Vol(77), pp. 121-30, 1978.
12. B. W. Timothy, C. D. Ridgeley, "Carbon monoxide", R. Zajtchuk, (Editor), "Occupational health, the soldier and the industrial base", pp, 397-429, 1993.
13. Y. Mendelson, "Pulse oximetry: Theory and applications for noninvasive monitoring," Clinical Chemistry, Vol. 38, pp. 1801-1807, 1992.
14. J. Sola and O. Chetelat, "Combination of multiple paths in pulse oximetry: The finger ring example," Proceedings of the 29th Annual International Conference of IEEE EMBS, pp. 6697-6698, 2007.
15. J. T. B. Moyle, "Pulse Oximetry", BMJ books, Second edition, pp35-36, 1994.

16. N. Stabile, K. Reynolds, “Technological review of pulse oximeter simulators”, Journal of Clinical Engineering, pp 287-297, 2002.
17. J. H. Sammons, R. L. Coleman, " Journal of occupational medicine; official publication of industrial medical association, Vol.16, pp. 543-546, 1974.
18. T. Edrich, M. Flaig, R. Knitza, G. Rall, “ Pulse Oximtery: An improved *in-vitro* model that reduces blood flow-related artifacts”, IEEE transactions on biomedical engineering, Vol. 47(3), pp. 338-343, 2000.
19. R. Nijland, H. W. Jongsma, J. G. Nijhuis, B. Oeseburg, “Accuracy of fetal pulse oximetry and pitfalls in measurements”, European Journal of Obstetrics and Gynecolog and Reproductive Biology, Vol. 72 Suppl. 1, pp. S21-S27, 1997.
20. P. B. Batchelder, D. M. Raley, “Maximizing the laboratory setting for test devices and understanding statistical output in pulse oximeter”, Anesthesia and Analgesia, Vol. 105, pp S85- S94, 2007.
21. M. Vegfors et. al., “Accuracy of pulse oximetry at various hematocrits and during haemolysis in an *in vitro* model”, Medical and Biological Engineering and computing, Vol. 31, pp. 135-141, 1993.
22. K. J. Reynolds, J. T. B. Moyle, M. K. Sykes, C. E. W. Hahn, “Response of 10 pulse oximeters to an *in-vitro* test system”, British journal of anaesthesia, Vol. 68, pp 365-369, 1992.
23. M. Oura, N, Kobayashi, S. Yamamori, S. Takeda,”Calibration System for pulse spectrophotometer using a double-layer pulsation flow cell”, 31st Annula International Conference of IEEE EMBS, pp 896-899, 2009.
24. L. J. Brown, “A new instrument for simultaneous measurement of total hemoglobin, %oxyhemoglobin, % carboxyhemoglobin , %methemoglobin and oxygen content in whole blood”, IEEE transactions on biomedical engineering, Vol. 27, pp. 132-138, 1980.
25. W. G. Zijlstra, A. Buursma and W. P. Meeuwsen-der Roest, “ Absorption spectra of human fetal and adult oxyhemoglobin, carboxyhemoglobin and methemoglobin,” Clinical Chemistry, Vol. 39, pp 1633-1638, 1991
26. V.Twersky, “Absorption and multiple scattering by biological suspensions”, Journal of the opical society of America, Vol. 60, pp. 1084-1093, 1970.

27. J. L. Reuss, “Multilayer modeling of reflectance pulse oximetry”, IEEE transactions on biomedical engineering, Vol. 52, pp 153-160, 2005.
28. J. M. Schmitt, “Simple photon diffusion analysis of the effects of multiple scattering on pulse oximetry”, IEEE transactions on biomedical engineering, Vol. 38, pp. 1191-1203, 1991.
29. V. O. Rybnyok, P. A. Kyriacon. “Beer-Lambert law along non-linear mean light pathways for the rational analysis of photoplethysmography”, Journal of physics: Conference series 238, pp. 1-7, 2010.
30. P. D. Mannheimer, “The light interaction of pulse oximetry”, Anesthesia and Analgesia, Vol. 105, pp.10-17, 2006.
31. J. C. S. Lee, P. W. Cheung, D. R. Marble, M. A. Kenny and D. Landicho, “Simultaneous measurement of percent carboxyhemoglobin and functional oxygen saturation”, IEEE Engineering in Medicine and Biological Society 11th Annual International Conference, pp. 1092 – 1093, 1989.
32. C. Pieralli, R. Devillers, G. Tribillon, “Three wavelength optical oximetry including the measurement of carboxyhemoglobin concentration,” Medical Sensors II and fiber optical sensors, SPIE Vol. 2331, pp. 80-88, 1994.
33. D. R. Marble, D. H. Burns, “Diffusion-based model of pulse oximetry: *in vitro* and *in vivo* comparisons”, Journal of Applied Optics, Vol. 33, pp. 1279-1285, 1994.
34. J. M. Bland, D. G. Altman, “Comparing methods of measurements: why plotting difference against standard method is misleading”, Lancet, Vol. 346, pp. 1085-7, 1986.
35. Masimo Corporation website. Rad-57 Pulse CO-oximeter.
36. T. W. Loong, “Understanding sensitivity and specificity with the right side of the brain”, British Medical Journal, Vol 327, pp. 716, 2003.
37. W. W. Lee, K. Mayberry, R. Crapo, R. L. Jensen, “ The accuracy of pulse oximetry in the emergency department”, American Journal of Emergency Medicine, Volume 18 (4), pp. 427-431, 2000.
38. N. Hampson (Author), D. G. Penny (Editor) “Carbon monoxide poisoning, CRC press, Chapter 33, pp-739-745, 2008.

39. M. Touger, A. Birnbaum, J. Wang, K. Chou, D. Pearson, P. Bijur, “Performance of the RAD-57 Pulse Co-Oximeter compared with standard laboratory carboxyhemoglobin measurement”, Annals of emergency medicine, Vol 56(4), pp. 382-388, 2010.
40. S. J. Barker, J. Curry, D. Redford, S. Morgan, “Measurement of carboxyhemoglobin and methemoglobin in pulse oximetry”, Anesthesiology, Vol. 105, pp 892-897, 2006.